Mesoproterozoic Basement From The Central And Southern Appalachians Reveal High-temperature Magmatic Conditions And Non-laurentian Origin Of Earth's Most Zircon Fertile Magmas

Kyle Makovsky
Syracuse University, kmak4.6ga@gmail.com

Abstract

The Mesoproterozoic (1.4-0.9 Ga) Grenville Orogeny led to the formation of the supercontinent Rodinia. One unique characteristic of the Grenville Orogeny is that it produced a volumetrically significant amount of zirconium- (Zr) enriched granitoids, evidently more than any period both prior to and after the Grenville. To investigate this further, Mesoproterozoic basement rocks were sampled along the axis of the current Appalachian Mountains from western North Carolina north to southern New York, as well as from the northern Andes in southern Colombia. Zircon was extracted from these rocks to exploit its propensity to incorporate several isotopic tracers useful in determining age, petrogenesis, and thermal conditions during crystallization. These include Uranium-Lead (U-Pb), Hafnium (Hf), the rare earth elements (REE), stable isotopes of Oxygen (O), and Titanium (Ti). Using these isotope systems together, the main goal of the research presented here is to better our understanding of the tectonic history of southeastern Laurentia during the Mesoproterozoic (Chapter 1), to investigate the potential link between Laurentia and Amazonia during the formation of Rodinia (Chapter 2), and to elucidate the tectonic processes responsible for creating Zr-enriched magmas (Chapter 3).

Mesoproterozoic Basement from the Central and Southern Appalachians Reveal High-Temperature Magmatic Conditions and Non-Laurentian Origin of Earth's most Zircon Fertile Magmas

by

Kyle Aaron Makovsky

B.S. Earth Science, Minnesota State University, Mankato, 2010

M.S. Geology, Boise State University, 2013

Dissertation

Submitted in partial fulfillment of the requirements for the degree of Doctor of

Philosophy in Earth Sciences

Syracuse University

May 2021

Acknowledgements

There are so many people that have encouraged, supported, and inspired me to this point. I first would like to acknowledge the mentors that have been such a monumental part of my life. Beginning at my undergraduate institution, Professors Steven Losh and Chap Wittkop encouraged my enthusiasm for Geology and fostered an environment for me to successfully think critically. My Masters advisor Professor Walter Snyder, who gave me a chance when most people did not. I would not be the geologist I am today without your mentorship. Also, thanks Walt for the many "therapy" sessions at the golf course. Lastly, and not least, Professor Scott Samson for giving me the opportunity to work on an amazing set of projects for my Dissertation, thank you.

For me the journey has been ameliorated by the friends I have made along the way. Having attended three different institutions for my degrees has afforded me the opportunity to meet people from all over the country, all with different and unique backgrounds and experiences. My life has been greatly enriched by your friendships, thank you.

Lastly, I must thank my family. Your unwavering support throughout my schooling and other life-events goes beyond words or expression. My parents especially encouraged my academic pursuits. Although my late father is not able to read this document, I still hope it will finally convince you that I am smarter than you!

Table of Contents

List of figures

Chapter 1

Chapter 2

Chapter 3

List of tables

Chapter 1

Chapter 2

Chapter 3

Chapter 1: Timing of Grenville Magmatism in the French Broad Massif, Southern Blue Ridge, North Carolina, USA: New in situ Zircon U-Pb Geochronology and Implications for Timing of Rodinian Orogenesis in Eastern Laurentia

In preparation for submission to:

Precambrian Research

Abstract

Mesoproterozoic metaplutonic rocks from the southern French Broad massif in southwestern North Carolina preserve Grenville magmatic and metamorphic ages (1.28-1.0 Ga).   New in-situ zircon U-Pb measurements from eight basement lithologies, produced by laser ablation and ion-probe techniques, delineate Elzevirian (1283-1250 Ma), Shawinigan (1191-1126 Ma), and Ottawan (1034-1008 Ma) magmatism and metamorphism. Magmatism produced dominantly calc-alkaline plutons with normative compositions of quartz gabbro, quartz diorite, quartz monzodiorite, granodiorite, and monzogranite. Major and trace element geochemistry suggests the plutons are not the result of fractional crystallization of a shared parental magma source, but instead are more likely the result of melting of multiple unique sources. Elevated concentrations of high field strength elements (e.g., Nb, Zr) along with moderate Ga/Al ratios show the plutons are transitional between I- and A-type granites. Concentrations of Ta, Rb, Yb, Y, and Nb suggest these rocks were produced in a tectonic environment transitional from a volcanic arc (older, Shawinigan-aged units) to within plate (Ottawan-aged unit-Max Patch granite) settings. The emplacement of Elzevirian plutons prior to 1.2 Ga suggests they may not be of Laurentian affinity and are instead part of the greater Mars Hill terrane, which has been shown to be exotic to Laurentia and ultimately of Amazonian heritage. The majority of magmatism in the field area occurred between ca. 1190 and 1125 Ma, a period correlative to the Shawinigan phase of the Grenville Orogeny. Syn- to post-emplacement metamorphism of these units is evidenced by complex zircon U-Pb systematics in all Shawinigan age plutons. Ottawan magmatism, expressed as the Max Patch granite and protoliths of the Earlies Gap granitoid gneiss,

is less voluminous than Shawinigan magmatism, a difference that mirrors their relative proportions elsewhere in the orogen. Ottawan metamorphism is expressed by growth of new zircon rims around magmatic core domains in several samples and spans a period of ca. 25 m.y. from ca. 1035 to 1010 Ma. The timing of the older and younger magmatic suites from the southern French Broad massif correlate to well-established times of Shawinigan and Ottawan magmatism and metamorphism in other Grenville terranes within the U.S. (e.g., Appalachian inliers, Adirondacks).

1. Introduction

Mesoproterozoic growth of easternmost Laurentia occurred by successive tectonomagmatic phases of the Grenville Orogeny, leading to the assembly of the supercontinent Rodinia, and has been argued to be Earth's longest-lived, hottest, and largest orogen (Beaumont et al., 2006, Rivers, 2008). In North America most rocks related to the Grenville orogen are exposed in eastern Canada. Exposures of Grenville aged rocks also occur in the Adirondack Mountains (NY, USA) and constitute the southernmost extent of the main Grenville Province (Fig. 1; McLelland et al., 2013). Within the main Grenville Province, several lithotectonic domains exist consisting of belts of reworked Archean and Paleoproterozoic Laurentian crust, accreted allochthonous belts, arc rocks, large regions of anorthosite, mangerite, charnockite, and granite (AMCG), and shear zones associated with collision followed by orogenic collapse (Rivers et al., 2012).

Rivers (1997) defined the Grenville Orogeny as a series of compressional events lasting from 1190 Ma to 980 Ma, and differentiated three unique events: Shawinigan,

Ottawan, and Rigolet orogenic phases at ca. 1190-1140 Ma, 1080-1020 Ma, and 1000-

980 Ma, respectively. Gowers and Krogh (2002) argued that the most appropriate

definition for the Grenville Orogeny relates to tectonothermal events leading to the

current observed structural configuration, i.e., the Grenville Orogeny is defined by the

final stages of continent-continent collision between Laurentia and (purportedly)

Amazonia. However, for the purposes of this study, the chronologic framework of the

Grenville Orogeny (sensu lato) follows the proposal of McLelland et al. (2013). This

framework expands upon Gowers and Krogh (2002) and includes additional orogenic

phases collectively known as the Grenville Orogenic Cycle, which spans ~420 m.y. from

1400-980 Ma (Fig. 2). To summarize, these phases include the Pre-Elzeverian (1400-

1300 Ma), Elzeverian, (1250-1220 Ma), Shawinigan (1190-1140 Ma), Ottawan (1080-

1020 Ma), and the Rigolet orogenic phases (1000-980 Ma; McLelland et al., 2013). A

detailed review of these events is beyond the scope of this paper but the reader is

referred to McLelland et al. (2013) for such a review. The Pre-Elzeverian phase

consists of volumetrically minor, yet geographically extensive magmatism occurring

from ~1350-1300 Ma in which a presumably segmented oceanic island arc was

accreted to the Laurentian margin (McLelland et al., 2013). Evidence of this

magmatism (in the USA) exists primarily in the Adirondacks (McLelland et al., 1996) and

northern Appalachians (e.g., Mt. Holly complex; Ratcliffe et al., 1991); however, recent

evidence from Moecher et al. (2020) from the southern Appalachians demonstrates a

southern extension of this magmatic episode. The Elzeverian orogenic phase saw

continued closure of the Trans-Adirondack basin and the emplacement of calc-alkaline

plutons in the Adirondacks of New York (McLelland et al., 1996; 2013). The Shawinigan

Orogeny is delineated by the existence of accreted material to the Laurentian margin and also by widespread magmatism and continued contraction throughout the Grenville Province. Shawinigan-age plutons exist in all major Grenville provinces (e.g., Canadian, Adirondacks, and Appalachian Inliers). The Ottawan orogenic phase is evidenced by widespread, high-grade metamorphism in all Grenville Provinces (Rivers, 2008; McLelland et al., 2013; Moecher et al., 2020). The Rigolet phase represents the final phase of the Grenville orogenic cycle, marking the foreland-ward migration of orogenesis following the collapse of the Ottawan orogenic plateau and development of the Grenville front, as currently configured (Rivers, 2009; Rivers et al., 2012).

Mesoproterozoic rocks exposed along the axis of the Appalachian orogen in the USA (the Grenville Appalachian Inliers of Hatcher, 1987) extend from central Vermont to Alabama (Fig. 1). Exposure of Mesoproterozoic rocks within the inliers is not continuous and thus direct geologic correlation with the main Grenville Province has remained a challenge. However, recent studies utilizing high spatial resolution zircon U-Pb dating of Mesoproterozoic rocks of the Appalachian Inliers demonstrate the timing of magmatism and tectonism between these two major tectonic provinces to be similar (Southworth et al., 2010; McLelland et al., 2013; Tollo et al., 2017; Moecher et al., 2020). These studies have thus begun to close the gap in our understanding between these two regions of Grenville crust. This study aims to build upon previous work to better establish better the timing and nature of Grenville magmatism in the southern Appalachians, specifically in the French Broad Massif of Tennessee and North Carolina, the largest region of exposed Grenville crust in the southernmost Appalachians. In this study, the progression of tectonic events occurring in the Appalachian Inliers will be

correlated to those in the Adirondacks (and by extension, the main Canadian Grenville Province), given the geographic proximity between the two.

2. Orogen-Scale Tectonic Setting

The evolution of the Grenville orogen in eastern Laurentia is reviewed to place the results of this study in the context of type Grenville events. The Adirondacks are separated into the Adirondack Highlands terrane (AHT) and the Adirondack Lowlands terrane (ALT), separated by the northeast-striking, northwest-dipping, Carthage-Colton shear zone (CCSZ; Fig. 3; McLelland et al., 2013). AHT rocks consist predominantly of orthogneisses with minor paragneisses whereas the ALT consists primarily of paragneiss and marble. Zircon U-Pb geochronology from the AHT defines three major Mesoproterozoic tectonomagmatic events: the Elzevirian Orogeny (1.25-1.22 Ga), the Shawinigan Orogeny (1.16-1.14 Ga), and the Ottawan Orogeny (1.09-1.03 Ga) (McLelland et al., 2013). A major magmatic episode at 1.15 Ga, associated with the Shawinigan tectonic phase, produced the voluminous Anorthosite-Mangerite-Charnockite-Granite (AMCG) rocks within the AHT.

Metamorphism is pervasive within both the ALT and AHT; however, differences in metamorphic grade exist. Coeval metamorphism of the AHT and ALT during the Shawinigan Orogeny reached granulite and amphibolite facies conditions, respectively. The ALT exhibits only a weak Ottawan overprint, whereas the AHT juxtaposed across the CCSZ exhibits Ottawan granulite facies assemblages, suggesting the two terranes were at different structural levels during the Ottawan.

Mesoproterozoic plutons in the Mt. Holly complex of the Green Mountain massif in Vermont share similar emplacement ages as those in the nearby Adirondacks (Ratcliffe et al., 1991). A protracted history of contractional tectonic events lasting nearly 100 m.y. is evidenced by calcalkaline rocks in both the Mt. Holly complex and the adjacent Adirondacks ranging in age from ~1350 Ma to 1257 Ma (Ratcliffe et al., 1991). Thus, there is evidence of a similar tectonic history shared at least through the Elzevirian Orogeny (Fig. 2). Magmatic rocks of Shawinigan age also occur in the Green Mountain massif and share similar age and composition to rocks occurring farther south in the Berkshire massif and as far south as the Baltimore Gneiss domes in Maryland (Ratcliffe et al., 1991; Aleinikoff et al., 2004; McLelland et al., 2013). Evidence for Ottawan-age plutonism in the Mt. Holly complex is scarce. However, U-Pb dates of 1060-1070 Ma from zircon rims indicate that some Ottawan-age anatexis occurred (Ratcliffe et al., 1991; McLelland et al., 2013). Ottawan metamorphism and plutonism is well documented in other Appalachian inliers (New Jersey Highlands, Shenandoah massif). This led previous workers to suggest that the Mt. Holly complex and the Berkshire massif were part of the orogenic lid during the Ottowan Orogeny and therefore did not reach *P—T* conditions necessary for anatexis (McLelland et al., 2013). With some minor local deviations, the majority of events recorded in the Adirondacks (and by extension the main Grenville province) are also recorded in many of the Appalachian inliers.

3. Petrogenesis of Grenville Lithologies in the southern Blue Ridge

Tollo et al. (2006, 2017) and Southworth et al. (2010) delineated two major episodes of magmatism in the Shenandoah and northern French Broad massifs from 1190-1130 (Early Magmatic Suite) and 1075-1030 Ma (Late Magmatic Suite), both of which generally correlate to timing of Shawinigan and Ottawan events in the Adirondacks and Canada. The extent to which these events occur within the southern French Broad Massif, the largest and most southernly expanse of Grenville basement in eastern Laurentia, warrants investigation. Recent 1:100,000 scale bedrock geologic mapping by Merschat and Cattanach (2008) in the French Broad Massif in western North Carolina identified major exposures of basement rocks of broadly Grenvillian age. Geochronology and geochemistry presented in this study contribute to our understanding of the timing and nature of magmatism and metamorphism associated with the Grenville Orogeny south of the Blue Ridge Province in Virginia.

Tollo et al. (2006, 2010, 2017) characterized suites of Mesoproterozoic igneous and meta-igneous rocks related to Grenville magmatism. In the Shenandoah massif, these rocks exhibit highly variable SiO_2 contents ranging nearly 30 wt%, high TiO_2 and P_2O_5 contents, and low CaO, leading them to interpret these rocks as igneous charnockites (Tollo et al., 2006). Most of the rocks studied by Tollo et al. (2006) are subalkaline, strongly tholeiitic, enriched in K, and have aluminum saturation indices (ASI) suggesting the melts were peraluminous to strongly metaluminous. Further south in the Mt. Rogers area, there are Mesoproterozoic meta-igneous basement rocks with a similar spectrum of SiO_2 and alkali contents as those from the Shenandoah massif, with SiO_2 values ranging from 53 to 76 wt% (Tollo et al., 2010, 2017). Unlike the highly ferroan and tholeiitic Mesoproterozoic rocks from the Shenandoah massif,

Mesoproterozoic rocks from the Mt. Rogers area (northern French Broad massif) are magnesian in composition (Tollo et al., 2010). Two other suites of Mesoproterozoic plutonic rocks, also from the Mt Rogers area, exhibit a more limited range in SiO_2 contents compared to those from Virginia, varying from 63-77 wt% SiO_2. These rocks are subalkaline, variably magnesian, calc-alkalic to alkali-calcic, peraluminous to metaluminous, and all exhibiting K-enrichment (Tollo et al., 2017).

Trace element characteristics of Mesoproterozoic rocks from the northern Blue Ridge reveal variable petrogenetic sources, consistent with collisional and volcanic-arc sources to syn- to post-collisional granitoids (Tollo et al., 2006). Despite the complexity revealed by rocks of this area, Tollo et al. (2006) concluded that the majority of Mesoproterozoic rocks exposed in their field area were derived from crustal sources. Specifically, they posited the source material was most likely calc-alkaline, with high degrees of melting to produce the geochemical signatures they observed.

Trace element characteristics of Mesoproterozoic rocks from the northern French Broad massif vary according to their age and petrogenetic source. Tollo et al. (2017) noted that most rocks from their study area are enriched in high field strength elements (HFSE) and this enrichment is stronger in the younger, Ottawan age rocks. Based on several lines of evidence, they suggest the older units from their field area were produced in a subduction-related magmatic arc setting (Tollo et al., 2017; Hildreth and Moorbath, 1988; Davidson et al., 1990). In contrast, the younger, Ottawan-age units from their field area exhibit trace-element characteristics common to within-plate sources.

4. Study Area and Sample Descriptions

Six of eight Mesoproterozoic rocks for this study were collected from the French Broad massif of western North Carolina, ranging from 16-45 Km northwest of Asheville, NC in the southern Blue Ridge Mountains. Lithologies sampled for this study are all map-scale units at the 1:100k scale and all but two lie wholly within the West Asheville 1:100k quadrangle. Detailed mapping by Merschat and Cattanach (2008) identified several moderately to strongly metamorphosed igneous Mesoproterozoic basement lithologies in this area (Fig. 4a). Sample NC17-10 (Toxaway Gneiss) was collected from a more southwesterly location (Fig. 4b). Sample NC17-1 (Great Smoky Mountains augen gneiss) was collected at its type-locality within the Dellwood Quadrangle (Fig. 4c). Collectively, the exposure of Mesoproterozoic crystalline basement rocks in this area is one of the most aerially extensive within all of the Appalachians and therefore represents an important magmatic component of the Grenville orogen.

4.1 Sample Descriptions

Mesoproterozoic basement rocks from the Asheville area consist of K-feldspar augen gneiss, mafic granulites, pyroxene granulites, charnockites (opx-bearing granites), quartz monzonites, and granites. In addition to Grenville metamorphism, most rocks experienced amphibolite to granulite facies Middle Ordovician (Taconian) metamorphism (Merschat and Cattanach, 2008; Moecher et al., 2011, 2020), resulting in widespread development of migmatites in many of the dated lithologies. Taconic deformation is non-penetrative, such that relict Grenville assemblages and fabrics are preserved within foliated orthogneiss formed during the Taconian orogeny (Moecher et

al., 2020). Late Paleozoic deformation under greenschist facies conditions is expressed mainly as high strain zones and late folding. The Max Patch Granite occurs within the region of lowest grade Taconic overprinting and is the only unit that displays greenschist facies mineral assemblages. The eight units sampled for this study are listed in Table 1, which includes lithologic descriptions, references for nomenclature, and a key to map symbols.

5. Analytical Methods

5.1 Sample Preparation

Approximately 20 kg of material was collected from each of the eight rock units sampled in order to prepare powders and mineral separates. Whole-rock geochemical data were collected by X-ray fluorescence spectrometry. Powders were created from fresh fragments of rock using a ceramic-crucible shatterbox. Powders were weighed to 3.5 g and mixed with 7 g of Lithium Tetraborate flux. The 10.5 g mixture was then heated in a furnace to 1000° C for ~1 hour. The resulting glass beads were then recrushed using a tungsten-carbide crucible shatterbox. This powder was remelted at 1000° C for ~1 hour. The mechanical crushing and remelting process outlined here ensures a final glass bead that is chemically homogenous. The measurements were made at the Hamilton Analytical Laboratory located at Hamilton College (NY, USA) using a Thermo ARL Perform'X XRF spectrometer. Analytical conditions and data reduction follow Johnson et al. (1999). All geochemical plots were created using IgPet software (Carr and Gazel, 2017).

Rare Earth Element (REE) concentrations were measured employing a technique described by Conrey et al. (2019) using a pellet cut from the same glass bead as XRF analyses described above. This piece is then mounted in epoxy resin, polished, and analyzed using a Photon Machines Analyte 193 (G1) UV excimer laser coupled to a Varian 820 laser ablation inductively coupled plasma mass spectrometer (LA-ICPMS) at Rennselaer Polytechnic Institute (Troy, NY, USA). Analytical conditions for measurement are described in Conrey et al. (2019).

To investigate the timing of Mesoproterozoic plutonism and metamorphism within the North Carolina Blue Ridge zircon was separated from the eight basement rocks. Standard separation protocols used to extract zircon included pulverization in a jaw crusher and disk mill. Milled samples were then sieved for size fractions between 30 and 250 microns. Single use nylon mesh sieves were used to significantly minimize the likelihood of cross-contamination. The resulting material was passed through a magnetic field via a Frantz Isodynamic Magnetic Separator at 0.25 A and 0.5 A, both at a 15° side-tilt. Heavy mineral separation was performed on the non-magnetic fraction using both Bromoform and Methylene Iodide. The final heavy mineral separates were again introduced to the Frantz Magnetic Separator at 1.0 A at 20° side-tilt and 1.4 A at 10° side-tilt. The final separate was in all cases nearly 100% zircon. To better assess the complete zircon growth history for each sample, grains of all sizes, shapes, and varying degrees of optical clarity were mounted in epoxy. Obvious metamict grains were avoided. All epoxy mounts were first ground with 1200 carbide-grit sandpaper to expose the grains, followed by 1-micron alumina and colloidal silica polishing. Cathodoluminescence (CL) and back-scattered electron (BSE) images were collected

using either the Cameca SX-5 electron microprobe at Syracuse University, with beam conditions of 15 nA and 15 KeV, or the Joel JSM-IT100 scanning electron microscope at the University of Kentucky.

The results presented here include 1,209 U/Pb measurements using four geochronologic methods collected from multiple laboratories including (1) the Thermo Element2 laser ablation inductively coupled plasma mass spectrometer (LA-ICPMS) at the University of Arizona LaserChron Center following the methods of Pullen et al. (2018); (2) the ThermoFisher iCap LA-ICPMS at Middlebury College (VT, USA), following the methods of Cartwright et al. (2019); (3) the Nu Plasma II LA-ICP in split stream mode at Curtin University in Perth, Australia, following the methods of Spencer et al. (2019); and (4) the Sensitive High-Resolution Ion Microprobe Reverse Geometry (SHRIMP-RG) located at Stanford University (CA, USA) following the methods of Coble et al. (2018). Table 1 summarizes the samples analyzed by each technique. Zircon U/Pb standards used for analyses at the LaserChron Center were FC1, SL, and R33. The primary age standard used at Curtin was FC1; secondary standards used were MUN, 530, GJ1, MUD, OGC, Plesovice, P1, and R33. The primary standard FC1 was measured at Middlebury College; secondary standards measured were R33, 91500, and Plesovice. The primary age standard at Stanford was Temora-1; secondary standards measured at Stanford were MAD and MADDER. Details of dates obtained for all of the standards are given in the Supplementary Material.

Important to geological age interpretation derived from zircon U-Pb measurements is the post-analysis characterization of data based on CL textures. This is particularly true when dealing with large-n data sets (i.e., >30 analyses per igneous

sample). The texture of each grain was characterized via CL and categorized as the following: bright-cores, light-cores, dark-cores, textural rims, and edges. The measured isotope ratios for each grain were then placed into their respective CL categories. The goal of this approach is to parse potential age domains across cores and textural rims and intra-core CL textural variability permitting more robust interpretations of potential xenocryst populations within any sample.

To adequately characterize all potential age domains contained within one zircon grain, we analyzed the outer edges of several zircon grains per sample. If the edge of the grain did not appear to exhibit a substantially different CL response compared to the core we characterized it as an "edge". If, however, the edge of the grain appeared to be clearly distinct in CL compared to the grain's core we characterized it as a "textural rim". In some cases, there was a detectable age difference between these two categories, where edges shared similar ages to core domains and CL rims were quantifiably younger.

An additional screening tactic was to use the measured $^{206}Pb/^{204}Pb$, when possible, as a way to filter out zircon grains with excessive common lead. Note that these measurements were only made at LaserChron and by SHRIMP-RG. Once filtered by CL texture and $^{206}Pb/^{204}Pb$, all resulting data were plotted using IsoPlotR (Vermeesch, 2018).

6. Results and Interpretations

6.1 Zircon U-Pb Geochronology

Geochronologic data presented in the following section include 1,209 new U/Pb measurements from four analytical laboratories. In order to establish the viability of comparing results across laboratories and analytical methods, all primary standards were compared to their accepted values. U/Pb standards used for analyses at LaserChron were FC1, SL, and R33; 236 analyses of FC1 produced a concordia weighted mean age within 2σ of the accepted age of 1099 ± 1 Ma (Paces and Miller, 1993; Schmitz et al., 2003). The primary age standard used at Curtin was FC1, where 17 analyses produced a weighted mean $^{207}Pb/^{206}Pb$ age within 2σ of the accepted age of 1099 ± 1 Ma (Paces and Miller, 1993; Schmitz et al., 2003); secondary standards used were MUN, 530, GJ1, MUD, OGC, Plesovice, P1, and R33. A weighted mean concordia age of 24 FC1 measurements at Middlebury College were also within 2σ of the accepted age of 1099 ± 1 Ma (Paces and Miller, 1993; Schmitz et al., 2003); secondary standards measured were R33, 91500, and Plesovice. The primary age standard at Stanford was Temora-1, for which 35 analyses yielded a weighted mean $^{206}Pb/^{238}U$ age of 420 ± 0.9 Ma, slightly older than the accepted age of 416.8 ± 1.1 Ma (Black et al., 2003); secondary standards measured at Stanford were MAD and MADDER. Data and weighted mean plots/concordia diagrams for standards can be found in the supplementary files.

Only concordant analyses are used to determine ages from the core domains of zircon for sampled units in this study. However, due to the limited number of rim analyses, both concordant and slightly discordant grains were used to determine their ages. For cores, this was established by first plotting all analyses on a concordia diagram, then visually inspecting whether or not error ellipses for an individual analysis

intersected the concordia line. If it did not, it was considered discordant and was separated out from the concordant analyses. Two tables containing these data can be found in the Supplementary Material, which lists the concordant and discordant analyses, respectively. For some units, there were nearly 100 analyses that were discordant; however, one major advantage of producing large-n datasets is that despite having a very strict rejection criterion, a high number of concordant analyses remained to determine the geologic age of the unit.

The U-Pb systematics for the rocks presented in this study are complex. Evidence of at least one event leading to varying degrees of lead-loss is present in all units sampled (Except NC17-5; Max Patch Granite) (also see Moecher et al., 2020). As such, the method used to make age interpretations of these rocks is dynamic and is not necessarily identical from sample to sample. In an attempt to be as transparent as possible, geologic dates are presented from more than one method for each sample (except NC17-5; Max Patch Granite, which is geochronologically simpler). All concordia diagrams present dates determined either by concordia (maximum likelihood method) or model-1 discordia regressions (following Ludwig, 1998). All concordia plots contain insets of probability density plots (PDP) showing $^{207}Pb/^{206}Pb$ age distributions for concordant and discordant analyses. All weighted mean plots present $^{207}Pb/^{206}Pb$ dates.

Geochronologic data from the study area for each unit sampled are presented from oldest to youngest and categorized within accepted age ranges for the Shawinigan and Ottawan orogenies, the latter representing a part of the broader Grenville orogenic cycle. Table 2 is a summary of the preferred ages for each unit. Representative CL

images of zircon textures are presented for each sample (Fig. 5); however, all CL

images for each grain analyzed are available in the Supplementary Data. Additionally,

concordia plots and ^{207}Pb/^{206}Pb weighted mean plots illustrate both the complexity of

the U-Pb systematics for the rocks sampled in the field area in addition to providing

context into which age interpretations were made.

6.1.1 NC17-6 (Yepg- pyroxene granulite of Earlies Gap granitoid gneiss)

6.1.1.1 Results

Zircon from NC17-6 are typically rounded to slightly elongate and are 75-250 μm

in length. Backscattered electron images show that grains contain very few fractures

and mineral inclusions; however, some grains contain apatite and quartz inclusions.

Cores vary in their CL intensity from dark to bright, but all show oscillatory zoning (Fig.

5). Cores are often truncated by bright rims. As was explained in the methods section

regarding the classification of cores by their CL intensity, this sample contained bright,

dark, and light cores. However, they have indistinguishable U and Th, with the bright,

dark, and light cores containing average Th/U ratios of 0.47, 0.5, and 0.52, respectively.

Although the U-Pb systematics for most of the units sampled are complex, this sample

is the most complex. Concordant analyses (within 2σ) range from 1394 Ma to 968 Ma,

with no systematic trend related to CL intensity. The phenomenon of concordant zircon

U-Pb analyses spread across concordia over a range of several hundred million years

has been observed in other Grenville-aged granitoid gneisses in Antarctica (Halpin et

al., 2012). It is believed that zircon from high-grade (i.e., granulite facies) meta-igneous

rocks will experience Pb-loss in such a way that any given analysis will still plot along

the chord. The ^{207}Pb/^{206}Pb weighed mean (n = 78) for this sample is 1218 ± 1.8 Ma, but has an MSWD of 143 (Fig. 6b). A model-1 discordia line was fit to the data to calculate upper and lower intercept dates (MSWD 3.1; n=84), resulting in dates of 1283 ± 9.4 Ma and 1018 ± 15 Ma respectively (Fig. 6a).

Two crystal edges, interpreted as textural rims based on CL imaging, from this sample were analyzed and yield a concordia date of 1008 ± 14 Ma (MSWD 3.7; n=2; Fig. 6c), which overlaps within error the lower intercept date of the cores (1018 ± 15 Ma).

6.1.1.2 Interpretation

The upper intercept date of the cores (1283 ± 9 Ma) is taken as the best estimate of the emplacement age of the protolith. The age does not fit neatly into events defining the Grenville cycle (sensu stricto; Fig. 2), It is older than the Elzevirian orogeny (1245-1220 Ma) and slightly younger than the pre-Elzivirian magmatic event (1.35-1.31 Ga) recognized elsewhere in the southern Blue Ridge (Moecher et al., 2020). The lower intercept date of the cores (1018 ± 15 Ma) is interpreted as the approximate time of significant Pb* loss and/or a re-equilibration of zircon. This is reinforced by the mean date of the two zircon rims (1008 ± 14 Ma) suggesting Pb* loss/new zircon formation between ca. 1018-1008 Ma, a time corresponding (within error) with the younger age of Ottawan orogenic events in the Grenville Province in Canada (e.g. Rivers, 2008), e.g., Ottawan metamorphism.

6.1.2 NC19-9 (Yegpg- pyroxene granulite of Earlies Gap granitoid gneiss)

6.1.2.1 Results

Zircon grains from NC19-9 are euhedral to subhedral, exhibit high length/width aspect ratios, and are typically 100-300 μm in size along the c-axis. In BSE the grains are commonly fractured and contain very few inclusions; however, when present, apatite is the most common inclusion mineral. Cathodoluminescence textures are complex and consist of three distinct types. All grains exhibit cores with very dark CL intensities, although oscillatory zoning is evident (Fig. 5). Lighter mantles are either gradational or truncate dark cores. In all cases, however, both light and dark cores are truncated by bright rims. The U and Th concentrations were not measured for most analyses and therefore geochemical comparison between dark and bright cores is not possible. Using the CL intensity as a guide, there is a clear difference in dates between them. Similar to sample NC17-6 (which is a subunit of the Earlies Gap granitoid gneiss), dark cores from sample NC19-9 display a large spread in dates along concordia. Thus for dark cores, a model-1 discordia upper intercept date was determined to be 1250 $\pm$ 54 Ma (Fig. 6a; MSWD 2.1; n=21) whereas a weighted $^{207}Pb/^{206}Pb$ date of 1200 $\pm$ 10 Ma (Fig. 7b; MSWD 10, n=20) was calculated. Concordant analyses from light cores yield a concordia date of 1087 $\pm$ 9.2 Ma (Fig. 7c; MSWD 8.5; n=9) and a $^{207}Pb/^{206}Pb$ weighted mean date of 1126 $\pm$ 23 Ma (Fig. 7b; MSWD 1.0, n=8).

Twenty-nine grain edges were analyzed for NC19-9. Four analyses were originally defined as simple edges, all others were categorized as true textural rims. Despite this attempt, no difference in dates are readily apparent. A concordia date is 1024 $\pm$ 3.5 Ma (Fig. 7d; MSWD 220; n=29) and a $^{207}Pb/^{206}Pb$ weighted mean date is 1112 $\pm$ 12 Ma (Fig. 7e).

6.1.2.2 Interpretation

The model-1 discordia date of 1250 ± 54 Ma is interpreted to be the best estimate of the crystallization age for the dark core domain. The weighted mean $^{207}Pb/^{206}Pb$ date of 1126 ± 23 Ma is in turn the best estimate for the light core domain. The latter age is interpreted to represent the thermal event responsible for the *Pb-loss of the dark core domain. The $^{207}Pb/^{206}Pb$ date of 1112 ± 12 Ma is interpreted as the best estimate for the age of the textural rim domain as the MSWD is extremely high (220) for the concordia date of 1024 ± 3.5 Ma. The age of the textural rim domain is similar (within error) to that of the light core domain. This is interpreted to represent the growth of new zircon at 1126 Ma within either a long-lived igneous system or post-crystallization metamorphism lasting 14 m.y. spanning from 1126 to 1112 Ma. In the northern Blue Ridge, VA, Tollo et al. (2006) recognized a magmatic event at 1120-1111 Ma (their magmatic group 2). Evidence provided here suggests this magmatic event may stretch southward into the southern French Broad Massif, although it may be non-existent in the northern French Broad Massif (e.g., Tollo et al., 2017).

6.1.3 NC19-7 (Ygdc- Dogget Gap protomylonitic granitoid gneiss- coarse)

6.1.3.1 Results

Zircon grains from NC19-7 are generally blocky to slightly elongate, subhedral to rounded, and typically 75-250 μm in longest dimension. In BSE, grains contain small fractures and are inclusion-rich. Mineral inclusions (in order of abundance) are apatite, K-feldspar, and quartz. Cathodoluminescence textures in this sample are generally simple but some can be complex. Most grains show either oscillatory or sector zoning

in the core, rimmed with, and sometimes truncated by, bright rims (Fig. 5). In some cases the bright CL zones are mottled with an irregular contact with the dark core. Based on CL intensity, two age populations are evident. Bright/light cores yield a concordia date of 1187 $\pm$ 3.2 Ma (Fig. 8a; MSWD 2.8; n=54) and a ^{207}Pb/^{206}Pb weighted mean date of 1191 $\pm$ 8.1 Ma (Fig. 8b; MSWD 1.8; n=49). Dark cores have a calculated concordia date of 1034 $\pm$ 5.7 Ma (Fig. 8c; MSWD 0.5; n=18) and a ^{207}Pb/^{206}Pb weighted mean date of 1031 $\pm$ 13 Ma (Fig. 8b; MSWD 1.3; n=18).

Five total crystal edges were analyzed for NC19-7, and all but one was characterized as true textural rims. No discernable difference is apparent in their age. A concordia date of 1186 $\pm$ 13 Ma (Fig. 8d; MSWD 4; n=5; Fig. 8c) and a ^{207}Pb/^{206}Pb weighted mean date of 1208 $\pm$ 36 Ma (Fig. 8e; MSWD 1.5) was determined for this domain.

6.1.3.2 Interpretation

NC19-9 is interpreted to represent a Shawinigan magmatic pluton overprinted by Ottawan metamorphism and recrystallization. The weighted ^{207}Pb/^{206}Pb date of 1191 $\pm$ 8.1 Ma is interpreted to be the crystallization age of this unit. The interpreted age of the textural rim domain is the concordia date of 1186 $\pm$ 13 Ma and suggests the four textural rims and one edge are most likely the result of continued growth of the light/bright core domains. Importantly, these "rims" are for grains with light or bright cores, and therefore are crucial evidence to support this interpretation. Ottawan-age growth of new zircon is represented by the dark core domain, having an interpreted concordia age of 1034 $\pm$ 5.7 Ma.

6.1.4 NC17-3 (Ymg- mafic granulite of the Fines Creek Gneiss)

6.1.4.1 Results

Zircon grains from NC17-3 are elongate and euhedral, and typically in the 75-150 μm size range. In BSE grains are generally fracture-free and contain scattered apatite and quartz inclusions. Cathodoluminescence textures are simple, typically showing dark oscillatory zoned cores surrounded by a bright rim, which in some cases can be 20-40 μm thick (Fig. 5). Despite small differences in CL intensity, no evidence was found to support a hypothesis that CL intensity in cores was related to changing magma compositions (with respect to Th/U ratios and U-Pb systematics). Similar to NC17-6, individual zircon analyses plot along concordia spanning 120 m.y. An upper intercept date is 1175 ± 30 Ma (Fig. 9a; MSWD 2.0; n=76) and the weighted mean $^{207}Pb/^{206}Pb$ date is 1112 ± 5 (Fig. 9b MSWD 23.4; n=74). A lower intercept was determined to be 1041 ± 30 Ma.

Twelve total edges were analyzed for NC17-3, five of which are characterized as simple edges and seven characterized as textural rims. Two potential date populations were identified based on this characterization (Fig. 9c); edges have a concordia date of 1101 ± 6.0 Ma (MSWD 0.8; n=5) and textural rims have a concordia date of 996 ± 3.6 Ma (MSWD 29; n=7). Weighted mean $^{207}Pb/^{206}Pb$ dates of 1106 ± 16 (MSWD 5.0) and 1015 ± 11 Ma (MSWD 6.6) are determined for edge and textural rims, respectively (Fig. 9d).

6.1.4.2 Interpretation

The best estimate of the crystallization age is interpreted to be the upper intercept date of 1175 ± 30 Ma. The best estimate for the age of the textural rim domain

is 1015 ± 11 Ma, which is similar (within error) to the lower intercept date of 1041 ± 29

Ma. We interpret these as metamorphic ages and they corroborate the robustness of

the model-1 discordia age for this sample. Altogether, this is interpreted to be evidence

of an Ottawan metamorphic event, causing the complex U-Pb behavior of the core

domain in this sample. Based on their interpreted age of 1101 ± 6.0 Ma, edges are

most likely correlative to the core domain.

6.1.5 NC17-10 (Ytg- Toxaway Gneiss)

6.1.5.1 Results

Zircon grains from NC17-10 are euhedral, elongate to blocky, have moderate l/w,

and are typically in the 100-200 μm size range. Backscattered electron images reveal

these grains are variable in the amount of fractures among grains and are inclusion-rich.

Alkali-feldspar, plagioclase, apatite, and quartz inclusions are abundant and can be 20-

50 μm in diameter. Care was taken not to place the analytical spot near these

inclusions. Cathodoluminescence textures are complex (Fig. 5). ~20% of grains have

simple oscillatory zoning, whereas most show an oscillatory zoned core that is either

truncated by new growth zones or by a bright mottled CL texture. Healed cracks are

visible in CL, evidenced by bright CL intensity. No unique age domains were identified

despite categorizing analyzed grains based on their respective CL intensity.

Additionally, this sample has similar U-Pb characteristics as previous samples above,

i.e., a large spread in individual U-Pb analyses along concordia. An upper intercept

date of 1159 ± 28 Ma (Fig. 10a; MSWD 2.1; n=78) and a weighted mean $^{207}Pb/^{206}Pb$

date of 1121 $\pm$ 1.9 (Fig. 10b; MSWD 30; n=78) were determined. A lower intercept date

of 1063 $\pm$ 34 Ma was also determined.

Twenty-three crystal edge analyses were performed for NC17-10, nineteen of

which were characterized as simple edges and four as true textural rims. On the

concordia diagram (Fig. 10c), the four textural rims plotted as the youngest of the edge

and textural rim domains; however, they are not concordant (within the same criterion

used for the core domains) and when plotted together with the nineteen edge analyses,

they define a model-1 discordia date nearly identical to the model-1 discordia date

determined for the core domains (1165 $\pm$ 11 Ma vs 1159 $\pm$ 28 Ma, respectively).

6.1.5.2 Interpretation

The crystallization age for NC17-10 is best estimated by an upper intercept date

of 1159 $\pm$ 28 Ma. An upper intercept date for the rim domains of 1165 $\pm$ 11 Ma is

statistically indistinguishable from the upper intercept age of the core domains. Hence,

we interpret both the edge and textural rim analyses to be of the same zircon growth

generation as the core domains. The lower intercept date of 1063 $\pm$ 34 Ma may indicate

an Ottawan metamorphic event.

6.1.6 NC17-1 (pCga- Great Smoky Mountains augen gneiss)

6.1.6.1 Results

Zircon grains from NC17-1 are subhedral and elongate, length to width ratios of

3:1, and are typically in the 100-225 μm size range in their longest dimension.

Backscattered electron maging reveals grains typically contain small fractures and

contain relatively few inclusions. Of Inclusions that were identified, apatite and

plagioclase were evident. Cathodoluminescence textures are typified by very dark to light cores (Fig. 5). Oscillatory zoning is common in these cores. Grains that contained lighter cores are often mantled by very dark zones and no zoning is evident in these regions. All grains show evidence of a very bright CL intensity rim; they are typically very thin and were not analyzed due to their size. Single analyses are less variable in their age than previous samples described above. A concordia date of 1142 ± 1.0 Ma (Fig. 11a; MSWD 0.5; n=106) and a ^{207}Pb/^{206}Pb age weighted mean date of 1147 ± 5.3 Ma (Fig. 11b; MSWD 7.0; n=100) was calculated for this sample.

Six edges were analyzed for NC17-1, five of which are characterized as simple edges and one as a true textural rim. Edges yield a concordia date of 1123 ± 4.7 Ma (Fig. 11c; MSWD 10; n=5) and a ^{207}Pb/^{206}Pb weighted mean date of 1130 ± 11 Ma (Fig. 11d; MSWD 3.3).

6.1.6.2 Interpretation

The crystallization age of NC17-1 is best estimated by the concordia date of 1142 ± 1.0 Ma. The best estimate for the age of the core domain is a ^{207}Pb/^{206}Pb date of 1130 ± 11 Ma. The ^{207}Pb/^{206}Pb weighted mean age of the edge domain is nearly identical (within error) to the determined age of the core domains. Therefore, the edges are interpreted to be part of the same zircon growth generation as the core domains. The single true textural rim shares a similar date as two of the youngest analyses from the core domains and may represent a second, minor Ottawan zircon growth event at ca. 1030 Ma.

6.1.7 NC17-2 (Ymg- mafic granulite of Fines Creek gneiss)

6.1.7.1 Results

Zircon grains from NC17-2 are blocky to slightly elongate, slightly rounded, and are in the 150-300 μm size range. Backscattered electron images show very few grains contain fractures and inclusions; however, inclusions of apatite and plagioclase were identified. Cathodoluminescence textures reveal that most grains contain dark cores, with oscillatory zonation grading into lighter edges of the core region (Fig. 5). Several grains were identified that do not contain dark core regions and instead are bright throughout. In some cases these grains also show oscillatory zoning. All grains that contain dark cores have thin, bright rims and in some cases these bright zones truncate the dark core regions. Less common to these grains are very bright mottled CL textures; these regions were avoided for analysis. Single grain concordant U-Pb analyses are complex and are spread over a 250 m.y. period from ~975 Ma to 1225 Ma. An upper intercept date of 1139 $\pm$ 25 Ma (Fig. 12a; MSWD 2.4; n=102) and a ^{207}Pb/^{206}Pb age of 1100 $\pm$ 5.3 (Fig. 12b; MSWD 36; n=101) were calculated. A lower intercept age of 1051 $\pm$ 25 Ma was also calculated.

Twelve grain edges were analyzed for NC17-2, all of which are characterized as true textural rims. concordia and ^{207}Pb/^{206}Pb dates of 1026 $\pm$ 3.6 Ma (MSWD 2.9; n=9) and 1036 $\pm$ 9.0 Ma (MSWD 10.7; n=11) were determined for this textural domain, respectively (Figs. 12c, d). Although the ^{207}Pb/^{206}Pb dates are identical with the concordia date the latter is more precise and yields a considerably lower MSWD.

6.1.7.2 Interpretation

The best estimate for the crystallization age of NC17-2 is interpreted to be the upper intercept date of 1139 $\pm$25 Ma. A concordia date of 1026 $\pm$ 3.6 Ma is interpreted

to be the crystallization age of the textural rim domain. The lower intercept date of 1051 $\pm$ 25 Ma for the core domain in addition to the concordia age of the textural rim domain is interpreted to represent an Ottawan metamorphic event lasting ca. 25 m.y.

6.1.8 NC17-5 (Ym- Max Patch granite)

6.1.8.1 Results

Zircon grains from NC17-5 are pale pink to very light brown, blocky, have length to width ratios approaching 1:1, and are typically in the 70-250 μm size range. Backscattered electron images are the simplest of any sample for this study, showing very few fractures with a moderate amount of inclusions. Of the inclusions present, both single-mineral and multi-mineral inclusions of quartz, biotite, K-feldspar, and apatite were the most common. Cathodoluminescence images reveal two main types of textures, either simple oscillatory zoning or weakly developed oscillatory zoning with a distinct mottled texture (Fig. 5). Oscillatory zones have a bright CL intensity while the mottled zones are lighter in CL intensity. In terms of U-Pb characteristics, NC17-5 is the least complex of any sample in this study. A $^{207}Pb/^{206}Pb$ weighted mean date of 1034 $\pm$ 2.0 (Fig. 13b; MSWD 3.8; n=107) and a concordia date of 1034 $\pm$ 0.9 Ma (Fig. 13a; MSWD 0.3; n=107) were determined. Of important note is the analysis of one obvious xenocryst with a $^{207}Pb/^{206}Pb$ date of 1297 Ma. The importance of this will be explored further in the discussion section.

Twenty-one grain edge analyses were conducted on NC17-5, four are characterized as simple edges while seventeen are characterized as true textural rims. Similar to the relatively simple U-Pb systematics displayed by the core domains, no age

difference is evident between the two "rim" domains. concordia and $^{207}Pb/^{206}Pb$

weighted mean dates of 1034 $\pm$ 2.0 Ma (MSWD 0.3; n=21) and 1036 $\pm$ 3.8 Ma (MSWD

4.1) were determined, respectively (Figs. 13c, d).

6.1.8.2 Interpretation

The crystallization age of NC17-5 is best estimated by the concordia date of

1034 $\pm$ 0.9 Ma due to its lower MSWD (0.3) than the weighted mean $^{207}Pb/^{206}Pb$ date

(MSWD 3.8). Also based on MSWD, the best estimate of the crystallization age of the

core domain is provided by the concordia date of 1034 $\pm$ 2.0 Ma. However, since there

is no statistical difference between the core and rim domains, they are taken to

represent the same zircon forming event.

6.2 Major Element Chemistry

6.2.1 Results

Mesoproterozoic basement rocks from the Asheville area display normative

mineral assemblages indicative of igneous origin, including quartz diorite, quartz

monzodiorite, granodiorite, and monzogranite (data in Table 3; Fig. 14). One pyroxene

gneiss from the Earlies Gap granitoid gneiss map unit Yegpg (NC19-9) is a notable

exception, characterized by a normative composition transitional between gabbro and

quartz gabbro (Fig. 14).

Chemical variation diagrams were used to assess any potential petrogenetic

relationships between sampled plutons. Plutons from the study area are variable in

their SiO_2 contents, ranging from 54.2 – 73.6 wt%. All plutons are subalkaline and

moderately- to weakly metaluminous to weakly peraluminous (Fig. 15a). All plutons are

magnesian except the Max Patch granite (map unit Ym; NC17-5) and Toxaway gneiss (map unit Ytg; NC17-10), which display ferroan characteristics. The two oldest Grenville plutons sampled, a protomylonitic charnockite of the Dogget Gap (Ydgc; NC19-7) and the Toxaway gneiss (Ytg; NC17-10), are also the most chemically evolved (Figs. 15b, c).

6.2.2 Interpretation

The normative mineral assemblages from these units strongly suggest an igneous origin, and therefore allow for the interpretation of major and trace element characteristics as an indicator of igneous processes. All plutons also show calc-alkaline affinities, suggesting their origins may be related to magmatism associated with a subduction zone environment. Major element characteristics from the Shawinigan- and Ottawan-aged plutons show no systematic trend with age, suggesting the plutons are not the product of fractionation from a common parental magma.

6.3 Trace Elements and Tectonic Affinity

Minor and trace elements were measured to decipher both petrologic evolution and tectonic setting. Our study is the first to measure the chemistry of Mesoproterozoic basement rocks in the Asheville area. From this we aim to better understand how Mesoproterozoic rocks from the Asheville area correspond to previous workers' interpretation of the tectonic setting for the southern Appalachians.

Chondrite normalized major and trace elements reveal that all units sampled for this study show moderate positive anomalies for the elements K, La, and Nd but show moderate depletions in the elements P, Ti, and Nb (Fig. 16). Normalized patterns are

mildly negatively sloped, with an average Ba_N/Yb_N of 19 (Fig. 16). Large ion lithophile elements (LILE) are enriched relative to the HFSE, yet Hf and Zr show a marked enrichment relative to both chondrite and upper crustal normalized values (Thompson, 1982; Taylor and McLennan, 1985, respectively). The Max Patch Granite is enriched in Zr (573 ppm) three times that of the upper crustal value of 190 ppm (Taylor and McLennan, 1985). This enrichment in Zr of Grenville plutons has been documented in other areas within the Appalachians (Moecher et al., 2014; Samson et al., 2018). Rare earth element (REE) diagrams normalized to chondrites following McDonough and Sun (1995) show consistently negative HREE slopes and flat to weakly negative slopes through the MREE and LREE (Fig. 17).   The Dogget Gap protomylonitic granitoid gneiss is the most evolved lithology with respect to SiO_2 content and shows a markedly stronger negative HREE slope, and relative to every other unit sampled is depleted in MREE and HREE.

The tectonic setting in which Mesoproterozoic magmas from the Asheville area were produced was evaluated using chemical variation diagrams. Figure 18a shows the differentiation between I, S, and A type granites (Whalen et al., 1987). The older 1250 to 1283 Ma Earlies Gap granitoid gneiss, 1187 Ma Dogget Gap protomylonitic gneiss, and 1160 Ma Toxaway gneiss lie in the I- and S-type section of figure 18a. Transitional between the I- and S-type and A-type fields is the 1142 Ma Great Smokey Mountains augen gneiss. The younger Fines Creek gneiss lies in the transitional space between I- and S-type and A-type granites whereas the Max Patch granite lies wholly within the A-type field. In Ta-Yb space (Fig. 18b), all units sampled lie within the volcanic arc granite field, with the Max Patch granite and Dogget Gap protomylonitic

gneiss being exceptions, occupying the within plate granite and ocean ridge granite regions, respectively. It is not believed the Dogget Gap protomylonitic gneiss was generated in this tectonic setting due to its calc-alkaline and peraluminous major element characteristics. On a diagram of Rb vs (Y+Nb) (Fig. 18c) all units sampled lie within the volcanic arc granite region except the Max Patch granite, which similar to the plot of Ta vs Yb, shows within plate granite characteristics.

6.4 Interpretation

Based on the combination of major, minor, and trace elements three potential sources may have melted to produce the Mesoproterozoic rocks in the Asheville area. First, the older Earlies Gap granitoid gneiss (map unit Yegpg; sample NC19-9) shows a relatively flat REE pattern with values near chondrite (red lines and circles on Fig. 17). In contrast, map unit Yegp of the Earlies Gap granitoid gneiss shows enrichment relative to its more mafic counterpart Yegpg, suggesting either fractionation of a common parental magma or assimilation of previous continental material. The depleted nature of LILE elements (Ba, Rb, K) and similar chondrite normalized REE patterns for the Fines Creek gneiss and Toxaway gneiss (map units Ymg, and Ytg; samples NC17-2 & 3, NC17-10, all respectively) reveal they may be the products of melting from a similar source region. Based on similar enrichments in both LILE and HFSE, in addition to similarly shaped and sloped REE patterns, The Great Smokey Mountains augen gneiss and Max Patch granite (map units pCga and Ym, samples NC17-1 and NC17-5, all respectively) were derived from a different source than both the Earlies Gap gneiss and the Fines Creek and Toxaway gneisses. Lastly, the Dogget Gap gneiss (map unit Ydgc, sample NC19-7) has the highest enrichment in Th and greatest depletions in Zr,

Ti, Y, P, and Yb as well as the lowest chondrite normalized values for the middle and heavy REE. The depletions in Ti, P, and K may be the result of fractionation of Fe-Ti oxides and K-felspar, respectively. Due to its low Zr content and low yield when separating zircon for geochronology, the depleted chondrite normalized REE signature may be best explained by the lack of zircon in this sample, where zircon is a major source of HREE in crustal rocks (Nagasawa, 1970; Watson, 1980; Bea, 1996). All other major element characteristics such as high SiO_2 and K_2O values and low MgO and CaO values for this unit suggest that it is most likely the product of fractionation and not from the derivation of an additional local source. Additionally, very weak Eu* (Eu* = $Eu_N/[(Sm_N + Gd_N)^0.5]$ values averaging 0.85 (except map unit Ydgc; sample NC19-7, with Eu* value of 1.4) suggest minimal plagioclase fractionation. Trace element characteristics suggest these rocks were emplaced in an evolving tectonic environment transitional between arc-type and within-plate settings.

7. Discussion

The geochemistry and geochronology of Mesoproterozoic basement rocks from the Asheville area provide new insights into the nature and timing of Mesoproterozoic magmatism in the French Broad Massif. With respect to major zircon forming events, Mesoproterozoic rocks from the Asheville area share similar chronologies to those of other Grenville terranes (e.g., Adirondacks, VA Blue Ridge). The area of exposed Grenville crystalline basement in this area is widespread and arguably the best mapped in all of the Grenville Appalachian Inliers; thus their correlation to other terranes provides for a more robust understanding of the tectonomagmatic evolution of the SE

Laurentian margin, and by extension our understanding of the Grenville orogenic cycle as a whole. Additionally, older pre-Elzevirian events are recorded by the Earlies Gap granitoid gneiss and to a lesser extent by xenocrysts from the Max Patch Granite, suggesting 1.26 to 1.3 Ga crust was incorporated into 1.16 to 1.04 Ga magmas.

7.1 Geochemical comparisons to other Grenville-aged Laurentian terranes

Geochemical characteristics of rocks sampled in the study area are remarkably similar to those from the northern French Broad massif and Shenandoah massif (Figs. 15-18). For example, rocks from the southern French Broad massif are consistent with the chemistry of Early Magmatic Suite of the Shenandoah massif (Tollo et al., 2017) in that they exhibit characteristics atypical of A-type granitoids (high Sr and Eu, etc), which can be explained by an absence of plagioclase fractionation, which is inferred from low to non-existent negative Eu* anomalies. Rocks in the Shenandoah and northern French Broad massifs are petrologically continuous and bimodal, respectively. Southern French Broad samples share similarities in this regard to rocks of the Shenandoah massif, but are generally more mafic in composition. The presence of orthopyroxene in map units Ymg (Fines Creek gneiss), Yepg and Yegpg (Earlies Gap gneiss), along with their low SiO_2 and elevated K_2O contents are similar to charnockitic rocks of the Shenandoah (Tollo et al., 2006), the New Jersey Highlands (Drake and Volkert., 1991), and the AMCG suite in the Adirondacks (McLelland et al., 1996). Therefore charnockites are a common, albeit discontinuous element of the main Grenville province south to the French Broad Massif. Charnockites in Precambrian orogens are often associated with anorthosite, but the latter is rare in the central and southern

Appalachian Inliers (Montpelier and Roseland anorthosites are examples; Owens and Dymek, 2016). Enrichment in HFSE's is apparent in rocks from many Laurentian Grenville terranes as well, stretching from at least as far north as the Adirondacks (e.g., Valley et al., 2011; Lyon Mt. granite, their sample AH-06-1a, [Zr] = 1403 ppm) southward to the southern French Broad massif (this study). This enrichment is typified by very high Zr concentrations, ranging from 2000 ppm to 300 ppm, a corresponding enrichment relative to upper crustal values (Taylor and McLennon, 1985; [Zr] = 190 ppm) of ~10x to 1.5x, respectively (Moecher et al., 2014; Burk, 2017; this study). Interestingly, this enrichment is typically found in Ottawan aged, intermediate A-type granitoids of charnockitic affinity. The melting of pre-existing, fertile continental crustal sources could explain this enrichment of A-type granitoids in the region.

7.2. Deciphering U-Pb discordance and disturbance in high-grade meta-igneous granitoids

Nearly all units sampled for this study display varying degrees of discordance in measured zircon U-Pb ratios. This observation is not surprising as all units underwent either syn- or post-emplacement high-grade metamorphism, with several units reaching granulite facies and migmatization being widespread (Moecher et al., 2020). Discordance in these samples is most often revealed by either random groups of normally-discordant analyses or by nearly linear arrays that project to an upper intercept (see rims from NC17-10, Toxaway gneiss). Typical protocols for determining igneous crystallization ages usually involves measuring 20-30 isotope ratios (via LA-ICPMS techniques). In younger (i.e., Phanerozoic) plutons, the rocks are less likely to have

been disturbed by subsequent thermal events. Hence, the zircon U-Pb systematics are typically simple and do not require more than 30 measurements to determine a statistically robust and meaningful geologic age interpretation. High-grade Grenville meta-igneous rocks often yield ion probe or laser ablation U-Pb dates that span nearly 300 m.y. (e.g., Halpin et al., 2012; Moecher et al., 2020). This phenomenon was also observed in the rocks sampled for this study. Meaningful geologic age interpretations from these data sets are not straightforward. Halpin et al. (2012) evaluated several strategies for age interpretation and concluded that using the oldest, most concordant group of analyses may provide the minimum crystallization age. In this study, we have chosen not to use this method because, unlike Halpin et al. (2012), we did not simultaneously measure trace elements and therefore cannot group zircon crystals into separate geochemical groups. Additionally, it seems likely that choosing an arbitrary cutoff to define this group may also lead to an age bias. Instead, by measuring upwards of 100-200 spots per unit sampled, it was the aim to fully characterize the potential spread of ages along concordia while simultaneously allowing for the disposal of a significant number of discordant analyses without degrading the robustness of the age interpretation. In cases where a significant spread in ages along concordia was observed, the method of applying a linear regression typically reserved for discordant analyses was used. This is because taking a weighted mean of the ^{207}Pb/^{206}Pb dates or using the concordia date won't necessarily produce a meaningful geologic age. When using the linear regression method (i.e., model-1 discordia), the calculated lower- and upper-intercept ages correlated well to the interpreted relative age of the rocks based on field relationships (Merschat and Cattanach, 2008). Additionally, of all methods that

could be used to make a geologic age interpretation in the complex samples (i.e., concordia age, weighted mean, model-1 discordia age, etc.), the model-1 discordia linear regression produced the lowest MSWD, albeit in some cases also increasing the uncertainty.   However, in complex rocks such as the ones sampled for this study it is better to sacrifice some degree of precision if accuracy is significantly improved.

7.3 Tectonic evolution of southern French Broad massif from zircon U-Pb ages

Mesoproterozoic rocks of the southern Appalachian Grenville inliers record three significant tectonic events with respect to zircon formation. These events effectively span the range of Grenville-aged events also recorded in Grenville-terranes to the north (i.e., western Blue Ridge, Dysart Mt. Holly, and the Adirondacks). Two units sampled from the Earlies Gap granitoid gneiss and a single xenocryst from the Max Patch granite record magmatic events prior to the occurrence of Shawinigan and Ottawan orogenies. A recent study by Moecher et al. (2020) provides a robust framework in which to interpret the significance of these older pre-Grenville ages.

Evidence for pre-Grenville magmatism in the study area comes from interpreted crystallization ages of the Earlies Gap granitoid gneiss and from xenocrysts contained in Earlies Gap granitoid gneiss map unit Yepg (NC17-6), Fines Creek mafic granulite (NC17-3), Great Smoky Mountains augen gneiss (NC17-1), and the Max Patch granite (NC17-5), which have $^{207}Pb/^{206}Pb$ ages of 1353 Ma, 1226 Ma, 1339 Ma, and 1297 Ma, respectively. Although volumetrically minor, rocks of this age are present in areas to the north (i.e., northern Appalachians and Adirondacks) and southward in the southernmost French Broad massif (Moecher et al., 2020 and references therein). Despite their

limited exposure, their occurrence in all parts of the paleo-Laurentian margin suggests they are remnants of a significant magmatic event prior to the onset of Grenville orogenesis. The age of the Earlies Gap granitoid gneiss and limited xenocrysts from this study are unique to rocks along the southeast margin of Laurentia in that they are too young to be included in the extensive Granite-Rhyolite Province yet too old to be associated with Elzevirian magmatism. Moecher et al. (2020) also recognized this in their study and using zircon U-Pb and whole-rock Pb-isotopes concluded these rocks are not native to Laurentia but instead are interpreted as remnants of Amazonian crust sutured to the paleo-Laurentian margin prior to 1.2 Ga. It is likely the Earlies Gap granitoid gneiss is part of the so-called "greater Mars Hill terrane", into which the younger units sampled in this study were intruded, and in the process incorporating chemical and U-Pb fingerprints of this older material (e.g., Ownby et al., 2004; Moecher et al., 2020).

A period of magmatic quiescence that lasted for nearly 60 m.y. followed the pre-Elzevirian emplacement of the Earlies Gap granitoid gneiss. Magmatism resumed at 1187 Ma, evidenced by generation of the Dogget Gap gneiss and continued for at least 48 m.y. The final stage of Shawinigan age magmatism ended with the emplacement of the Fines Creek gneiss at 1139 Ma. These dates correlate almost exactly with the Early Magmatic suite of Tollo et al. (2017) and are indistinguishable considering analytical error. Shawinigan age magmatism is also prevalent to the south of the study area. Moecher et al. (2020) identified a series of Shawinigan orthogneisses in the Dellwood quadrangle (which is the same quadrangle from which our sample NC17-1 was taken). Altogether, these ages are similar to those identified in the northern Appalachians and

Adirondacks. Based on whole-rock Pb-isotopes and zircon U-Pb geochronology, Moecher et al. (2020) concluded that Amazonian pre-Elzeverian material was sutured to the Laurentian margin prior to 1.2 Ga. Within this context, and since our study area closes the geographic gap between the study area in Moecher et al. (2020) and of previous work stretching from the northern French Broad massif north to the Adirondacks (i.e., the southernmost extent of the main Canadian Grenville province), evidence provided in this study suggests that magmatism was geographically continuous from at least the southern Appalachians north to the northern Shenandoah massif.

Ottawan events in the study area include emplacement of the Max Patch granite, new magmatic zircon growth in the Earlies Gap gneiss (unit NC19-9), and widespread by thermal disturbances in zircon U-Pb systematics of previously emplaced plutons. Lower intercept ages from NC17-2, NC17-3 (both members of the Fines Creek gneiss), and NC17-10 (Toxaway gneiss) range from 1063 to 1041 Ma. Textural rim analyses from samples NC17-1, NC17-2, and NC17-3 are similar to lower intercept ages from samples listed above but are generally younger, ranging from 1050 to 1015 Ma. The age of the rim analyses supports the use of the model-1 discordia method for determining primary crystallization ages, especially when taking analytical error into account. The youngest Ottawan event apparent in the study area is recorded by analyses of two textural rims from the Earlies Gap gneiss (NC17-6), with a concordia age of ~1008 Ma. These two grains record metamorphic growth of zircon at the waning stages of the Ottawan orogeny (Rivers, 2008; McLelland et al., 2013). The Ottawan orogeny has long been recognized as a major thermal event produced from collision

leading to the final assembly of Rodinia (Rivers, 2008; 2012; McLelland et al., 2013). Evidence of Ottawan high-grade metamorphism includes field relationships, new zircon growth, and disturbance of zircon and titanite U-Pb systematics throughout all Grenville terranes, including the Canadian Grenville Province, Adirondacks, and the Grenville Appalachian Inliers. As described above, rocks from the southernmost French Broad massif also exhibit evidence for Ottawan deformation and metamorphism.

8. Conclusions

The large-n analytical approach of this study, which combines multiple analytical methods applied to dating zircons with a protracted, complex magmatic and metamorphic history within the southernmost Appalachian Grenville inliers leads to the following:

1. Whole-rock geochemistry reveals all lithologies have an igneous protolith with compositions ranging from quartz gabbro to monzogranite.

2. Trace-element geochemistry infers that the plutonic protoliths are not the result of fractional crystallization of a shared parental magma source, but instead are more likely the result of melting of unique sources.

3. Trace-element-based tectonic affinities are consistent with plutons being produced in a regime transitional from a subduction-related environment to a post-orogenic environment.

4. Pre-Elzevirian magmatism is supported by the 1283-1250 Ma Earlies Gap granitoid gneiss (map units Yepg and Yegpg).

5. Zircon xenocrysts within Earlies Gap granitoid gneiss (Yepg), Fines Creek gneiss (Ymg), and Max Patch granite (Ym) provide additional evidence that pre-Elzevirian crust was involved in the generation of the magmas from which they crystallized.

6. Shawinigan magmatism is pervasive in the study area, with all units being produced between 1190 and 1130 Ma. This is identical to the "Late Magmatic Suite" of Tollo et al. (2017) and suggests that Shawinigan magmatism is continuous between the northern and southern portions of the French Broad Massif.

7. A magmatic hiatus lasting ~60 m.y. separates Shawinigan and Ottawan events in the study area. Again, the duration of this lull in magmatism is identical to the duration seen in the northern French Broad Massif (see Tollo et al., 2017).

8. Ottawan magmatism is represented by new zircon growth in the Dogget Gap gneiss and by the emplacement of the Max Patch granite at both at 1034 Ma.

9. Ottawan metamorphism is characterized by new zircon growth (seen as bright rims in CL surrounding magmatic cores) in the Great Smoky Mountains augen gneiss, Earlies Gap orthogneiss unit Yepg (sample NC17-6), and both subunits of the Fines Creek gneiss. Lower intercept ages from both subunits of the Fines Creek gneiss, Earlies Gap gneiss (map unit Yepg), and the Toxaway gneiss yield Ottawan ages ranging from 1063-1008 Ma.

10. Ages determined from textural rims support the use of a model-1 discordia regression, albeit through concordant points, as a robust way to make age interpretations in rocks having experienced protracted thermal histories.

11. Textural characterization via CL imaging in conjunction with producing large-n U-Pb data sets may be required to adequately characterize measured U-Pb ratios and subsequent dates determined in rocks having experienced protracted thermal histories. When ages spread nearly 300 m.y. along concordia, the traditional method of analyzing ~30 grains may not adequately characterize this spread, thus leading to meaningless age interpretations and erroneous tectonic reconstructions.

Table 1. Sample descriptions, locations, and analytical methods used for zircon U-Pb, and references from which map unit symbols are derived.

Sample	Unit Name	Map Unit	WGS84 Lat.	WGS84 Long.	Description	References	Analytical Method(s)
NC17-1	Great Smokey Mtns augen gneiss	pCga	35.56942	-83.06814	Biotite augen gneiss	Hadley and Goldsmith (1963)	SC-LA-ICPMS; LA-SS-ICPMS; SHRIMP-RG
NC17-2	Fines Creek gneiss	Ymg	35.67841	-82.98088	Mafic granulite-	Merschat and Cattanach (2008)	SC-LA-ICPMS; LA-SS-ICPMS
NC17-3	Fines Creek gneiss	Ymg	35.68028	-82.98291	Granulitic charnockite	Merschat and Cattanach (2008)	SC-LA-ICPMS; LA-SS-ICPMS; SHRIMP-RG
NC17-5	Max Patch granite	Ym	35.80241	-82.91576	Plag-kspar-qtz-hbl(?)	Merschat and Cattanach (2008)	SC-LA-ICPMS; LA-SS-ICPMS; SHRIMP-RG
NC17-6	Earlies Gap granitoid gneiss	Yepg	35.76521	-82.6138	Granitic granulite	Merschat and Cattanach (2008)	SC-LA-ICPMS; LA-SS-ICPMS
NC17-10	Toxaway gneiss	Ytg	35.12734	-82.92554	Plag-kspar-qtz-biot	Robinson et al. (1979)	SC-LA-ICPMS; LA-SS-ICPMS; SHRIMP-RG
NC19-7	Dogget Gap charnockite	Ydgc	35.71236	-82.82867	Protomylonitic kspar-qtz-biot	Merschat and Cattanach (2008)	LA-ICAP; LA-SS-ICPMS
NC19-9	Earlies Gap granitoid gneiss	Yegpg	35.7282	-82.6402	Pyroxene granulitic charnockite	Merschat and Cattanach (2008)	LA-ICAP; LA-SS-ICPMS

Table 2. Summary of zircon U-Pb ages. All errors are 2 s.d. Refer to table 1 for

analytical methods used for each sample.

SAMPLE	LITHOLOGY	BEST AGE	MSWD	INTERPRETATION
NC17-1	Alkali feldspar augen gneiss	1142 ± 1.0	0.5	Protolith concordia crystallization age
		1130 ± 11	3.3	Metamorphic rim weighted mean $^{207}Pb/^{206}Pb$ age
NC17-2	Mafic granulite	1139 ± 25	2.4	Upper intercept protolith crystallization age
		1026 ± 3.6	2.9	Metamorphic rim concordia age
NC17-3	Mafic granulite	1175 ± 29	2.0	Upper intercept protolith crystallization age
		1015 ± 11	6.6	Metamorphic weighted mean $^{207}Pb/^{206}Pb$ age
NC17-5	Granite	1034 ± 0.9	0.3	Concordia crystallization age
NC17-6	Pyroxene granulite	1283 ± 9.4	3.1	Upper intercept protolith crystallization age
		1008 ± 14	3.7	Metamorphic concordia rim age
NC17-10	Alkali feldspar granitic gneiss	1159 ± 28	2.1	Upper intercept protolith crystallization age
NC19-7	Pyroxene granulite	1191 ± 8.1	1.8	Weighted mean $^{207}Pb/^{206}Pb$ crystallization age
	Pyoxene granulite	1031 ± 13	1.3	Weighted mean $^{207}Pb/^{206}Pb$ metamorphic age
NC19-9	Charnockite	1250 ± 54	2.1	Upper intercept protolith crystallization age- dark cores
		1126 ± 23	1.0	Weighted mean $^{207}Pb/^{206}Pb$ protolith crystallization age- light cores
		1112 ± 12	6.6	Metamorphic rim weighted mean $^{207}Pb/^{206}Pb$ age

Table 3. Whole-rock major and trace element geochemistry.

Sample	NC17-1	NC17-2	NC17-3	NC17-5	NC17-6	NC17-10	NC19-7	NC19-9
SiO2	63.43	60.01	56.48	63.15	56.83	70.38	73.62	54.18
TiO2	0.795	1.074	1.302	1.283	0.985	0.410	0.354	0.563
Al2O3	16.46	17.20	18.13	14.50	17.06	14.39	13.43	17.65
FeO*	5.07	6.19	7.84	6.22	8.13	2.91	1.73	9.23
MnO	0.112	0.108	0.128	0.137	0.139	0.056	0.019	0.189
MgO	1.68	2.43	3.10	1.37	4.58	0.60	0.41	4.73
CaO	3.94	5.86	6.46	3.74	5.87	2.43	1.63	8.34
Na2O	3.53	3.56	3.92	3.32	4.07	3.20	3.19	3.79
K2O	3.59	2.10	1.84	4.20	1.74	4.66	4.64	0.33
P2O5	0.262	0.321	0.379	0.593	0.492	0.114	0.079	0.102
LOI (%)	0.37	0.70	-0.04	0.80	-0.12	0.36		
Maj+LOI	99.24	99.54	99.55	99.31	99.76	99.52	99.10	99.10
sum All	99.49	99.95	99.95	99.69	100.03	99.75	99.58	99.54
Cl >=	0.00	0.04	0.02	0.00	0.01	0.00	0.01	0.01
SO3 >=	0.00	0.07	0.07	0.01	0.02	0.01	0.01	0.05
Br >=	0	0	0	0	0	0	0	1
As >=	1	2	1	3	1	1	1	0
Ni	9	16	19	7	32	2	2	16
Cr	17	30	34	13	39	6	6	38
V	72	105	139	52	166	24	28	223
Sc	12.3	14.2	20.0	15.6	29.6	6.9	1.8	32.2
Zn	94	82	109	168	101	55	16	111
Ga	21	22	25	22	22	19	12	15
Ba	996	1316	1268	1617	928	1099	1262	178
Rb	131	33	24	132	21	163	120	4
Cs	4	0	3	0	0	0	0	0
Sr	505	733	764	500	605	225	386	441
Y	28	24	32	67	26	41	8	15
Zr	337	309	346	573	147	273	179	19
Hf	8.4	6.4	7.9	14.7	3.0	7.9	2.6	0.0
Nb	15.4	12.0	14.6	32.9	10.3	10.0	13.2	2.4
Ta	0	0	0	3	0	0	0	0
La	63	39	48	94	23	54	70	4
Ce	135	85	103	208	58	114	109	12
Nd	48	40	56	104	34	48	28	9
Sm	8.2	6.9	9.5	17.8	5.7	8.7	3.0	2.5
Dy	4.9	4.3	5.8	11.6	5.1	6.6	1.0	2.3
Yb	0	4	2	5	4	6	0	1
Th	15	0	0	10	0	8	36	0
U	1	0	0	3	0	0	2	0
Pb	15	9	6	26	6	24	16	2
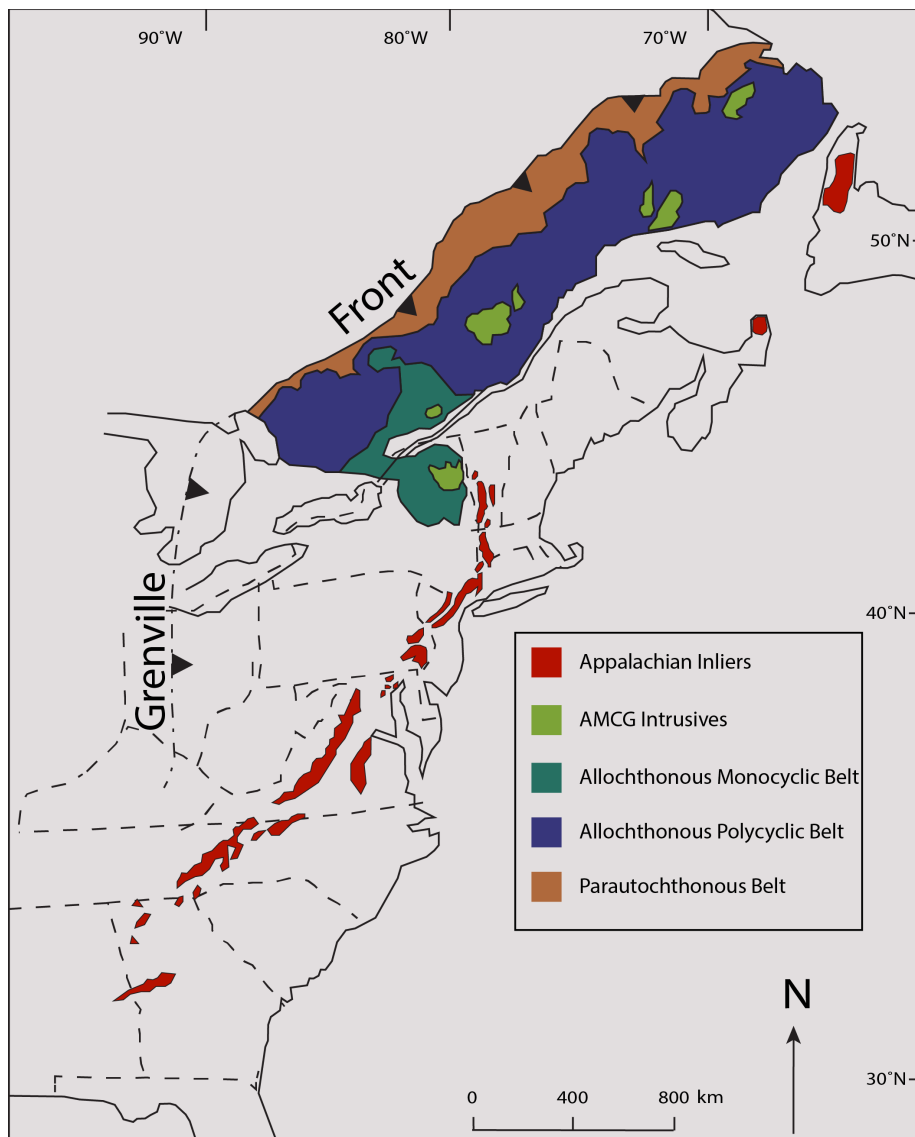
Fig. 1. Orogen-scale map of exposed Grenville-aged terranes in eastern North America. The main Grenville Province is located in eastern Canada, connected to the United States by the Adirondack terrane (dark green). The area in orange represents reworked Laurentian material. The area in dark purple represents material that was accreted to the Laurentian margin during Grenville Orogenesis. Light green areas delineate the emplacement of AMCG suites. Areas shown in red delineate Grenville-aged crystalline basement massifs exposed in the Appalachian Mountains. Modified from McLelland et al. (2013).
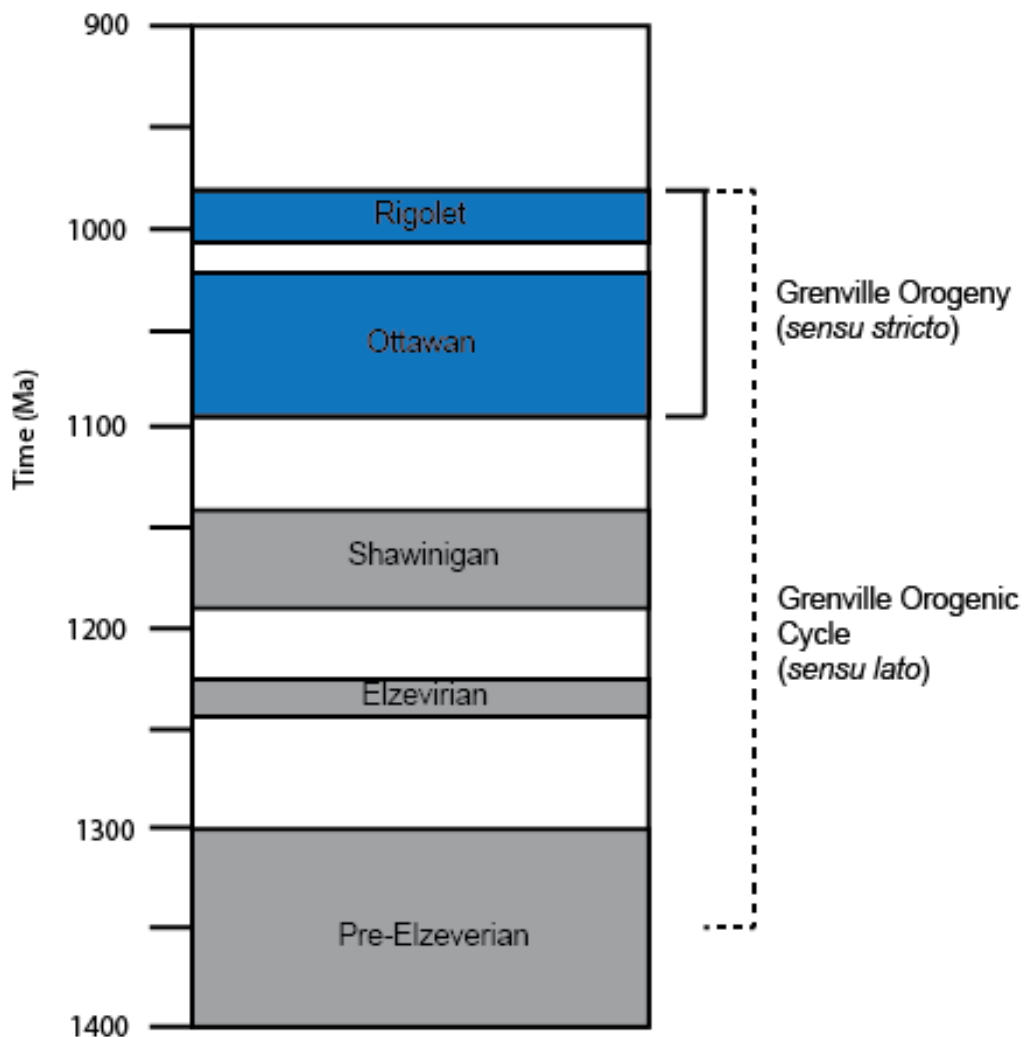
Fig. 2. Simplified chronology of major tectonomagmatic events affecting the eastern paleo-Laurentian margin. In this study we use the framework established by McLelland et al. (2013) to compare the timing of events in the southern Appalachians to the timing of events in the Adirondacks and main Grenville Province. Modified from Rivers (2008).
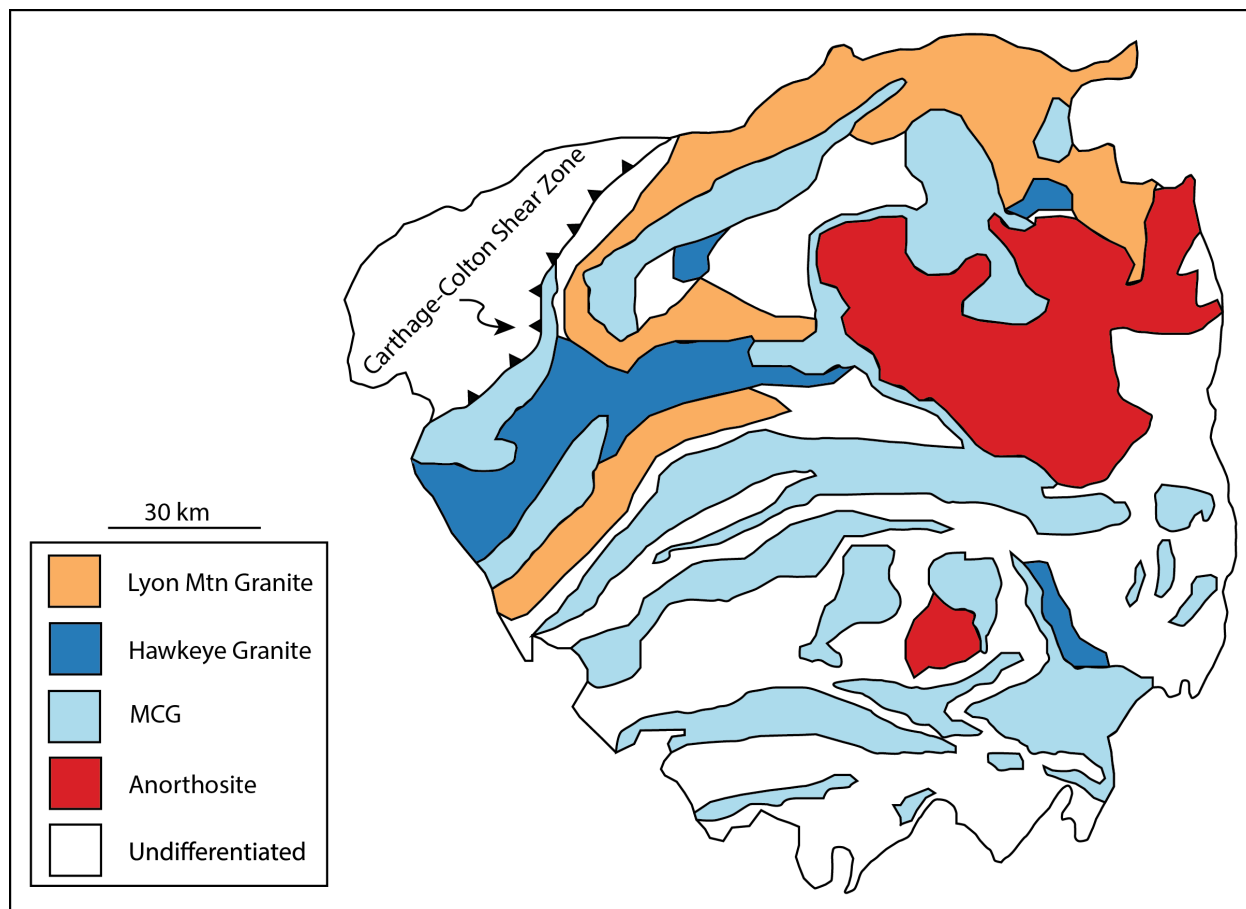
Fig. 3. Simplified geologic map of the Adirondack terrane, NY, USA. The Carthage-Colton shear zone separates the Adirondack Highlands terrane (AHT) on the east from the Adirondacks Lowlands terrane (ALT) on the west. The Mt. Marcy massif is a major Anorthosite body and is associated with contemporaneous emplacement of mangerite, charnockite, and granite plutons. The timing of events in the Adirondacks is correlative to the main Grenville province. The timing of these events will be compared to the results from this study to aid in the understanding of Grenville orogenesis in the southern Appalachians. Figure modified from McLelland et al. (2013).
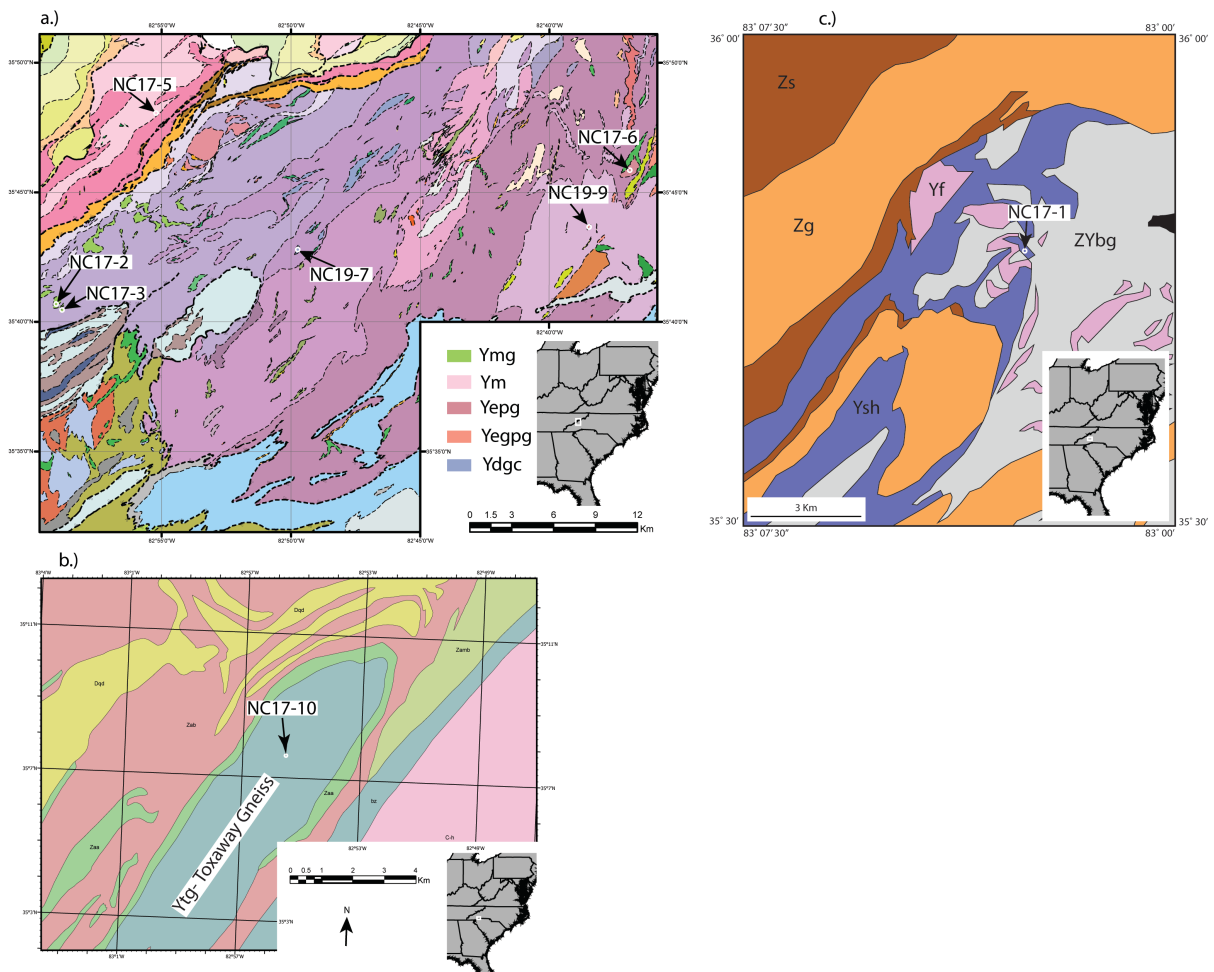
Fig. 4. Geologic maps showing sample locations- a) Geologic map of Merschat and Cattanach (2008) with locations for samples NC17-2;3 (Fines Creek gneiss), NC17-5 (Max Patch granite), NC17-6 (Earlies Gap granitoid geniss, Yepg), NC19-7 (Dogget Gap granitoid gneiss, and NC19-9 (Earlies Gap granitoid gneiss, Yegpg); b) geologic map from Robinson et al. (1979) with location for sample NC17-10 (Toxaway gneiss); c) Simplified geologic map from Moecher et al. (2020) showing the location for sample NC17-1 (Great Smokey Mountains augen gneiss).

Sample	Bright	Light	Dark	Sample	Bright	Light	Dark
NC17-1				NC17-2			
NC17-3				NC17-5			
NC17-6				NC17-10			
NC19-7				NC19-9	Not Obs.		

Fig. 5. Representative zircon CL textures from units sampled in this study. Most CL images were taken using an automated routine on the Cameca SX5 at Syracuse University, where the CL detector settings remained constant during the automated routine. Single spot analyses were categorized by their CL intensities to aid in the identification and interpretation of potential age domains. Because CL intensity is associated with chemical zoning within each grain, it therefore represents chemical evolution of the magma from which it crystallized, which is assumed to be time-transgressive under normal fractional crystallization processes. Circles are scaled to the appropriate analytical spot size for each image, which ranged from 10-30 microns.
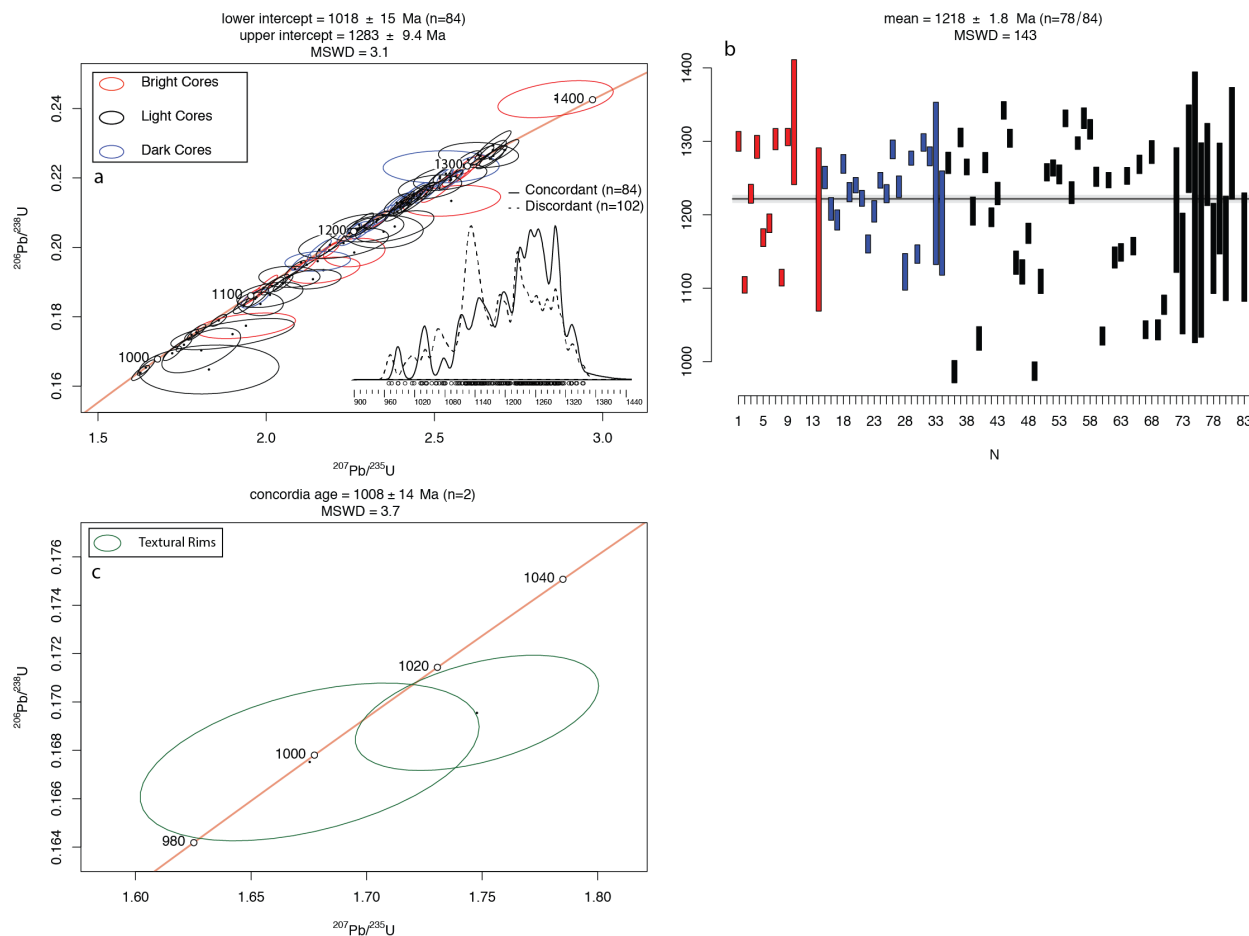
Fig. 6. Plot of concordant-only zircon U-Pb analyses from NC17-6 (Earlies Gap pyroxene granulite). a) Concordia diagram- ellipses outlined in red are from analytical spots ablating bright CL zones, black outlined ellipses from light CL zones, and blue outlined ellipses from dark CL zones. Inset PDP shows the distribution of all [207]Pb-[206]Pb analyses, both concordant (solid line) and not concordant (dashed line). Discordant grains show similar date peaks as the concordant grains, with a notable exception at 1140 Ma. b) Weighted mean [207]Pb/[206]Pb plot, colors on bars follow the outlined color of the ellipses on the concordia diagram. c) Concordia diagram for the two rim analyses from this sample. All subsequent concordia diagrams and weighted mean plots for both core, rim and edge domains will follow this coloring convention.
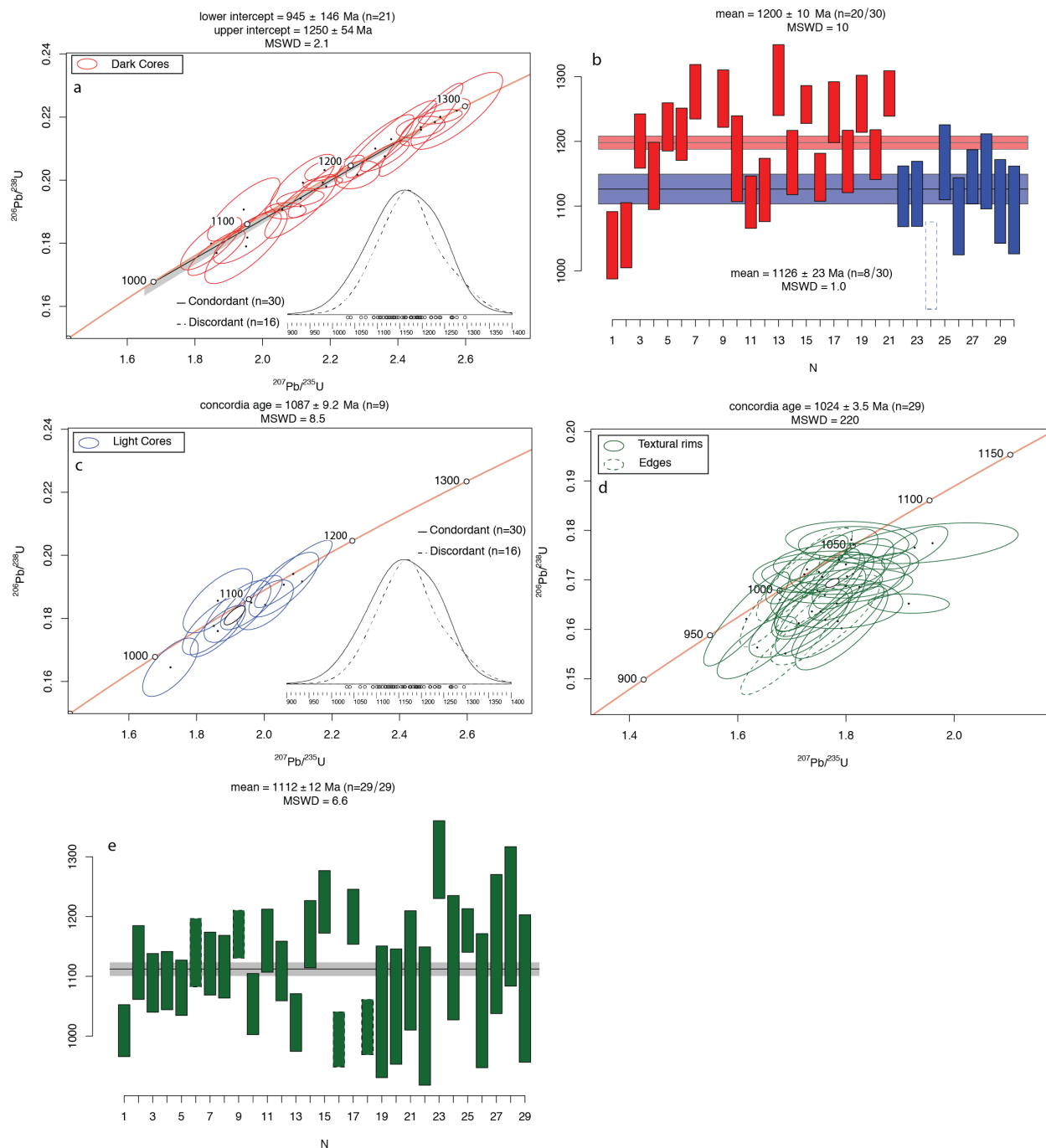
Fig. 7. Plots of concordant-only zircon U-Pb analyses for NC19-9 (Earlies Gap pyroxene granulite). Two age populations were evident based on their CL intensities. a) Concordia diagram showing model-1 discordia age for the dark core domain. b) Weighted mean plot of $^{207}Pb/^{206}Pb$ dates for both dark and light core domains. c)

Concordia diagram showing age of the light core domain. d) Concordia diagram of textural rim and edge analyses. e) Weighted mean plot of $^{207}Pb/^{206}Pb$ dates from the rim and edge domains. For concordia diagrams showing textural rim and edge analyses, ellipses will be dashed for edges and solid for textural rims. For weighted mean plots showing textural rim and edge analyses, boxes outlined in dashed lines correspond to edges and boxes with solid outlines represent textural rim analyses. If an analyses was not included in the age determination, it will be explicitly stated and represented on weighted mean plots as an unfilled, dashed outlined box.
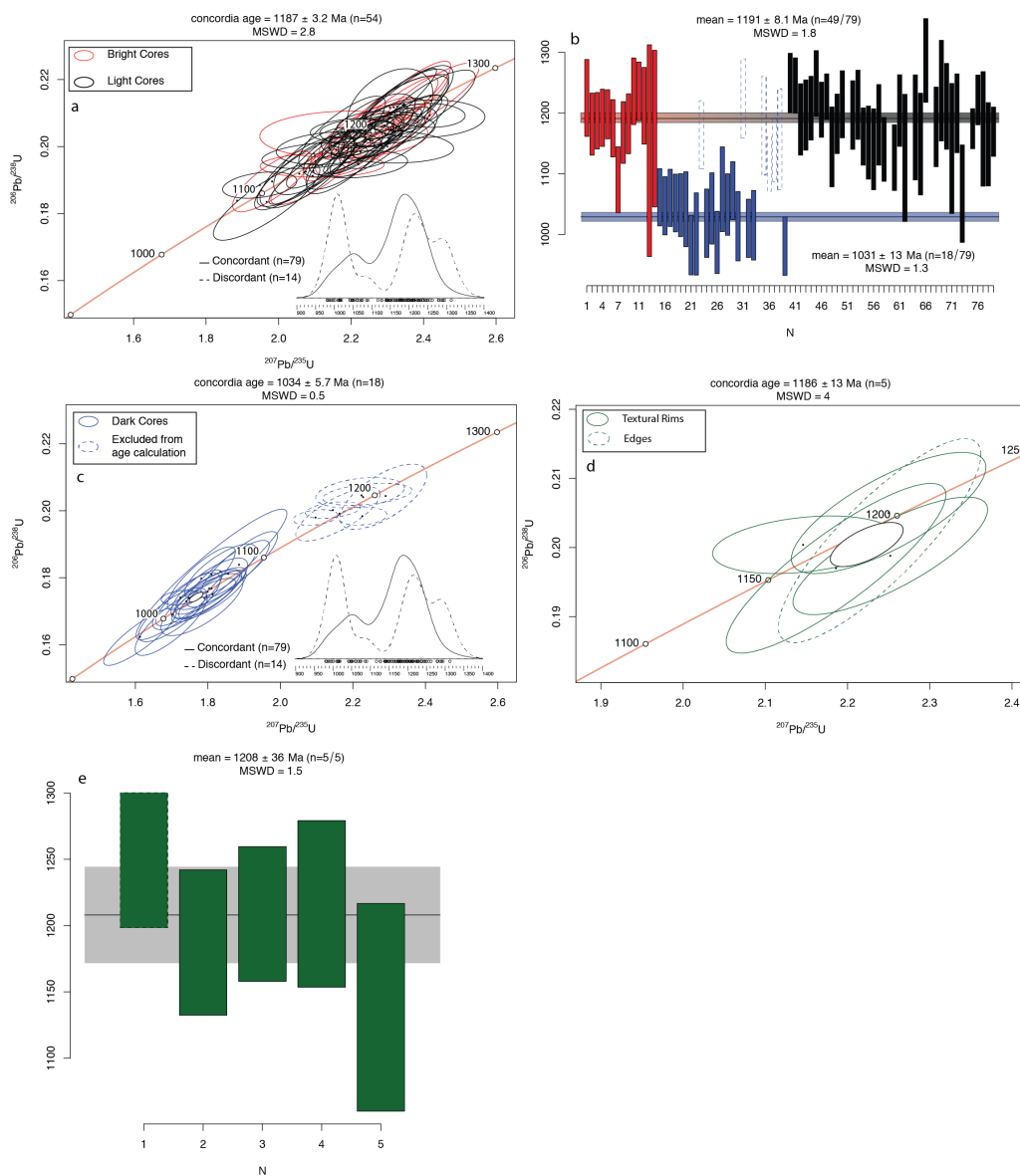
Fig. 8. Plot of concordant-only zircon U-Pb analyses for NC19-7 (Dogget Gap protomylonitic gneiss). Two age populations are evident based on their CL intensities. a) Concordia diagram showing concordia date for bright and light core domains. b) Weighted mean ^{207}Pb/^{206}Pb plot for both bright/light and dark core domains. c) Concordia plot of dark core domains. Dashed ellipses are excluded from the dark core age determination. d) Concordia plot of both textural rim and edge domains. e) Weighted mean ^{207}Pb/^{206}Pb plot for both textural rim and edge domains.
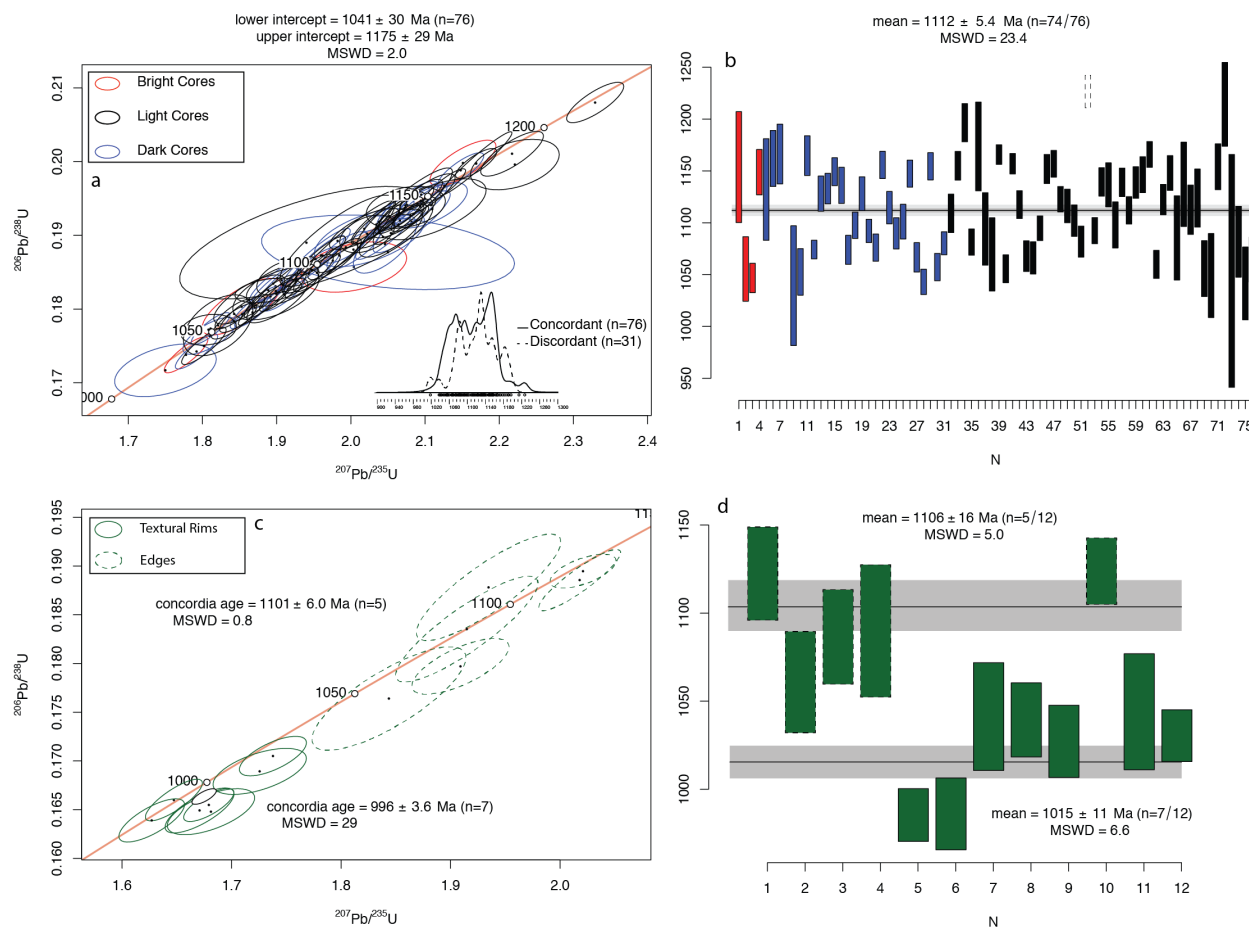
Fig. 9. Plot of concordant-only zircon U-Pb analyses for NC17-3 (Fines Creek mafic granulite). a) Concordia diagram showing concordia date for all core domains. b) Weighted mean ^{207}Pb/^{206}Pb plot for all core domains. c) Concordia plot of both textural rim and edge domains. d) Weighted mean ^{207}Pb/^{206}Pb plot for both textural rim and edge domains.
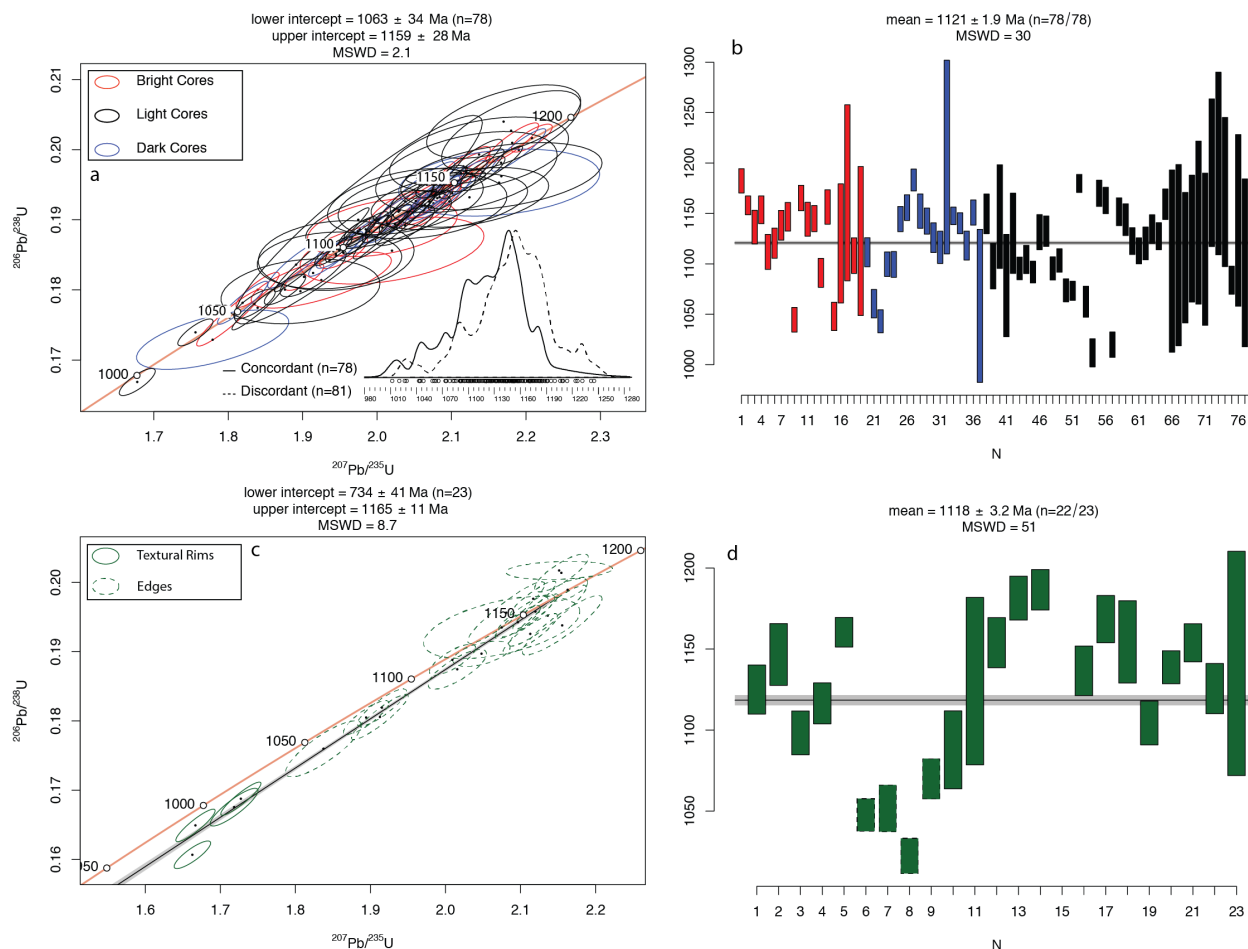
Fig. 10. Plot of concordant-only zircon U-Pb analyses for NC17-10 (Toxaway gneiss).
a) Concordia diagram showing concordia date for all core domains. b) Weighted mean
$^{207}Pb/^{206}Pb$ plot for all core domains. c) Concordia plot of both textural rim and edge
domains. d) Weighted mean $^{207}Pb/^{206}Pb$ plot for both textural rim and edge domains.
The youngest 4 analyses are true textural rims, the rest are interpreted to be the same
zircon growth generation as the cores.
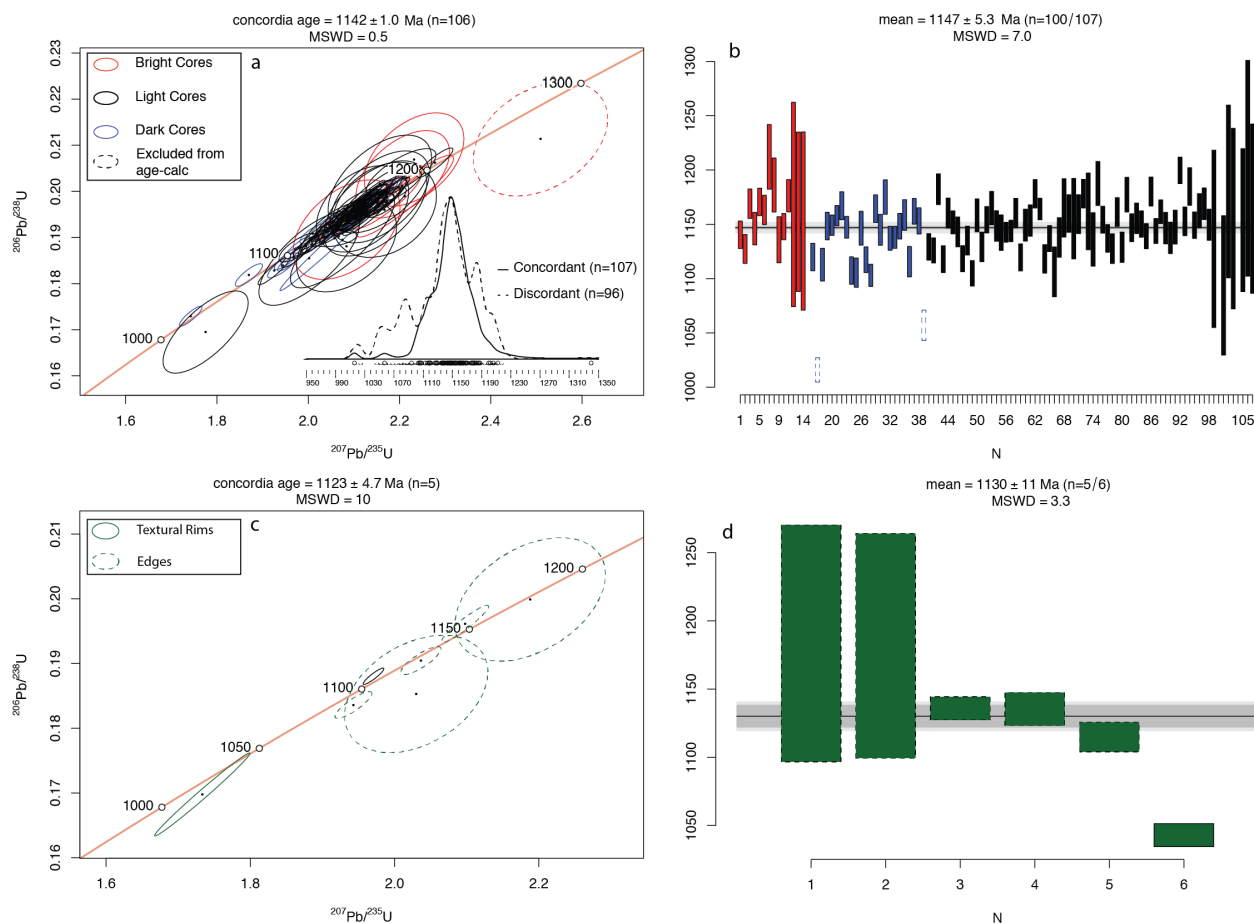
Fig. 11. Plot of concordant-only zircon U-Pb analyses for NC17-1 (Great Smokey Mountains augen gneiss). a) Concordia diagram showing concordia date for all core domains. b) Weighted mean ^{207}Pb/^{206}Pb plot for all core domains. c) Concordia plot of both textural rim and edge domains. d) Weighted mean ^{207}Pb/^{206}Pb plot for both textural rim and edge domains. The youngest analyzed "rim" was indeed characterized as a true textural rim, whereas all others were characterized as edges and are similar in age to the core domains.
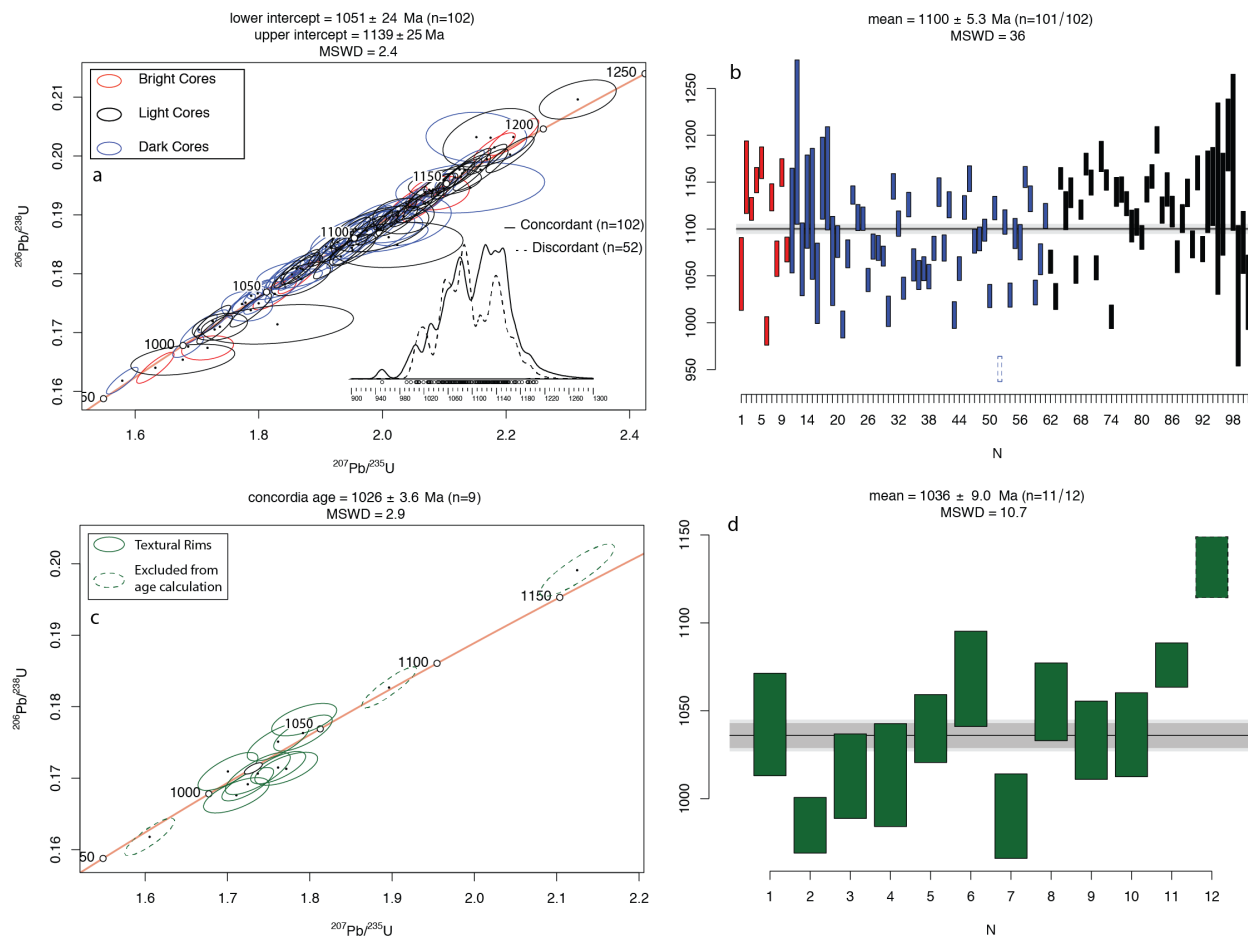
Fig. 12. Plot of concordant-only zircon U-Pb analyses for NC17-2 (Fines Creek gneiss). a) Concordia diagram showing concordia date for all core domains. b) Weighted mean ^{207}Pb/^{206}Pb plot for all core domains. c) Concordia plot textural rim domain. d) Weighted mean ^{207}Pb/^{206}Pb plot for textural rim domain. All "rims" were characterized as textural rims. The oldest of which is similar in date to the core domain. The concordia date for the textural rims is similar to the lower intercept date determined for the core domains.
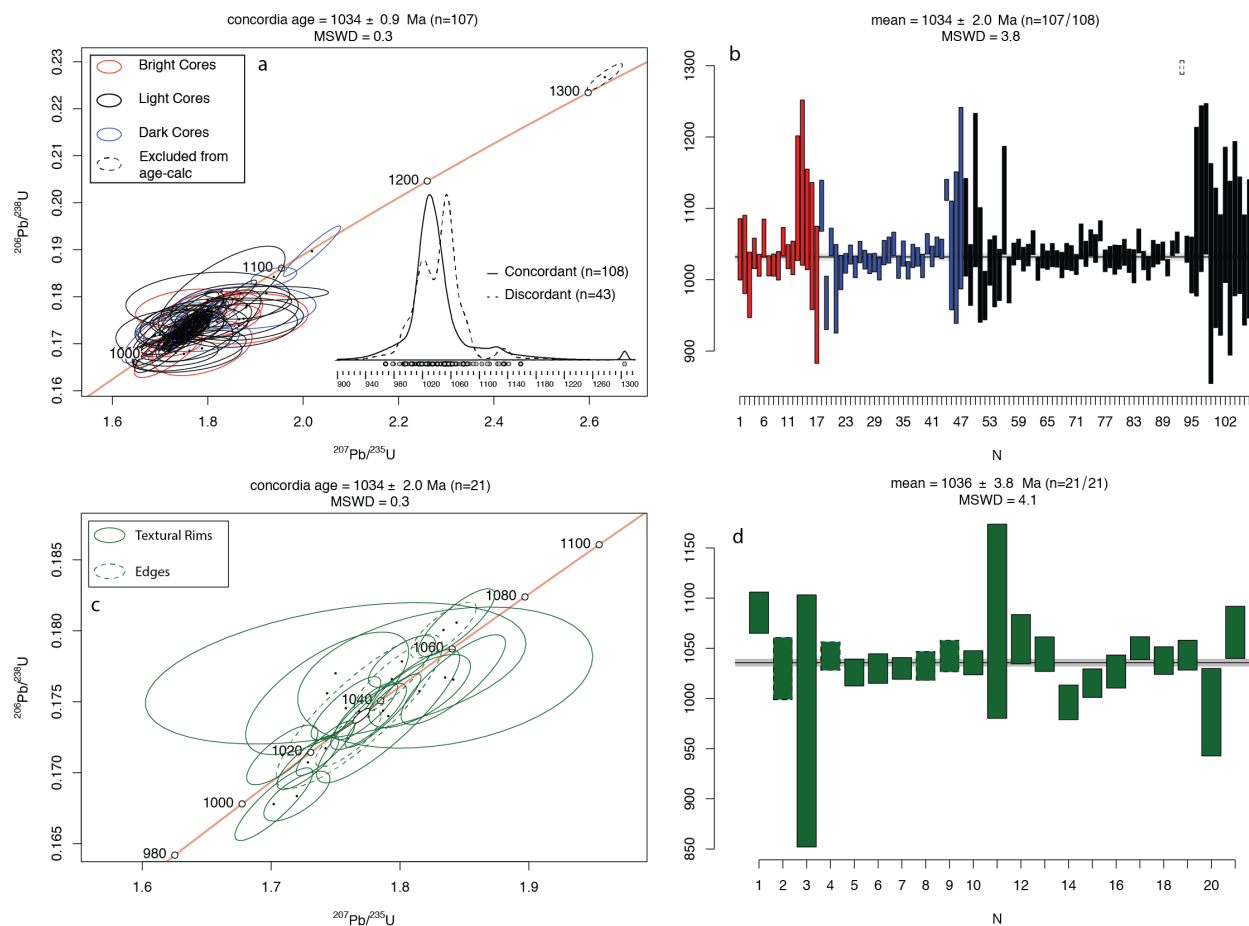
Fig. 13. Plot of concordant-only zircon U-Pb analyses for NC17-5 (Max Patch granite).

a) Concordia diagram showing concordia date for all core domains. b) Weighted mean $^{207}Pb/^{206}Pb$ plot for all core domains. c) Concordia plot of both textural rim and edge domains. d) Weighted mean $^{207}Pb/^{206}Pb$ plot for both textural rim and edge domains.
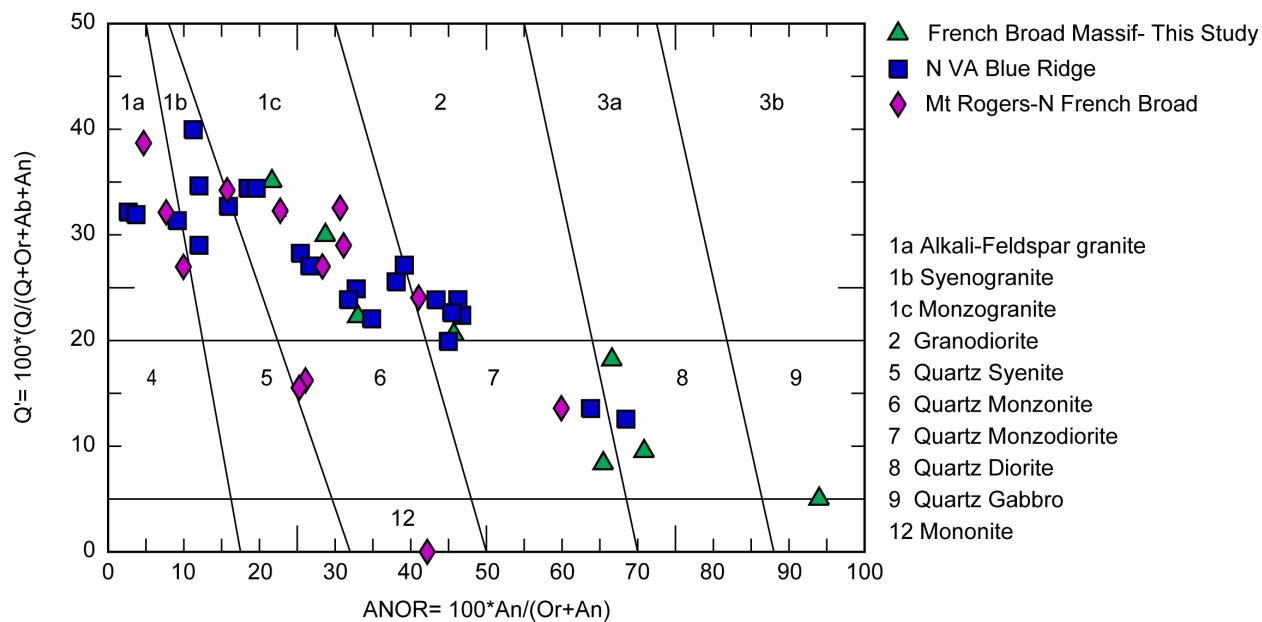
Fig. 14. Plot of Q'-ANOR; ANOR (100 x normative anorthite/(orthoclase + anorthite) vs Q' (normative quartz/(quartz + orthoclase + albite + anorthite) for rocks in the study area and for rocks from Tollo et al. (2006; 2017). Normative compositions were calculated with Fe^{2+}/Fe_{total} following Irvine and Baragar (1971). Figure after Streckeisen and Le Maitre (1979).
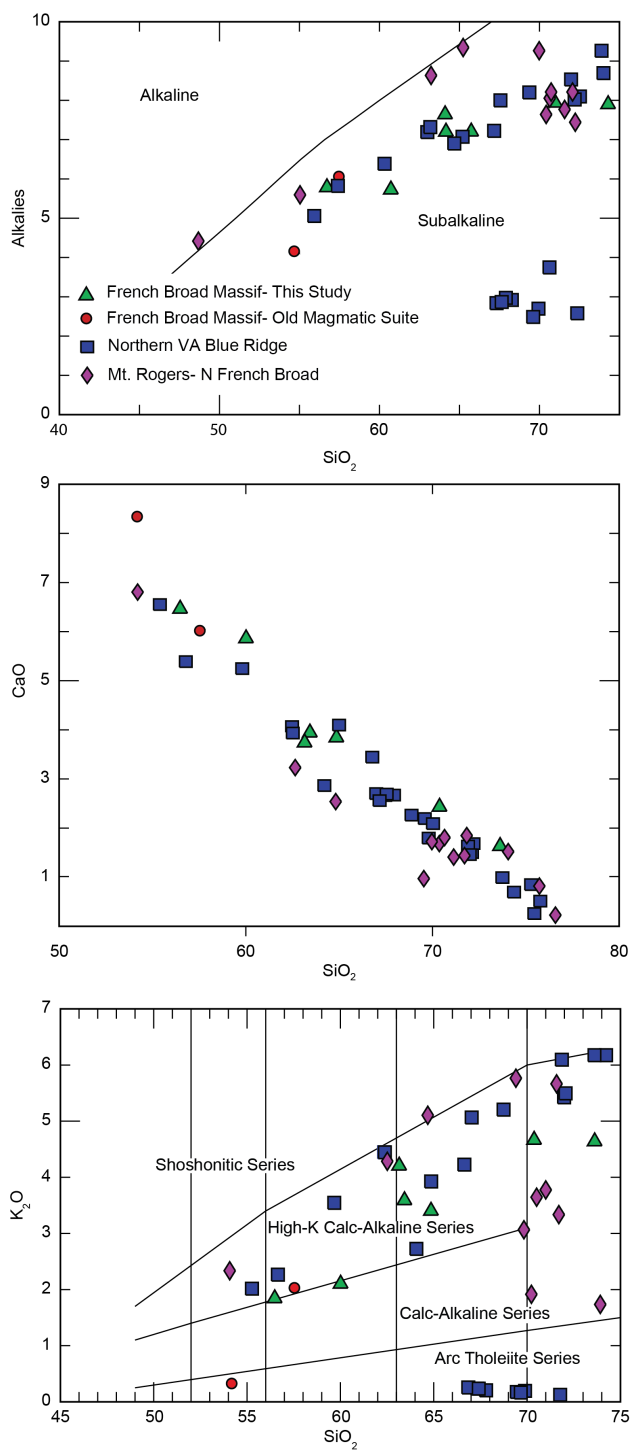
Fig. 15. Select major element diagrams for meta-igneous rocks from the study area and from rocks from Tollo et al. (2006; 2017). a) Alkalies (Na$_2$O + K$_2$O) vs SiO$_2$; b) CaO vs SiO$_2$; c) K$_2$O vs SiO$_2$.
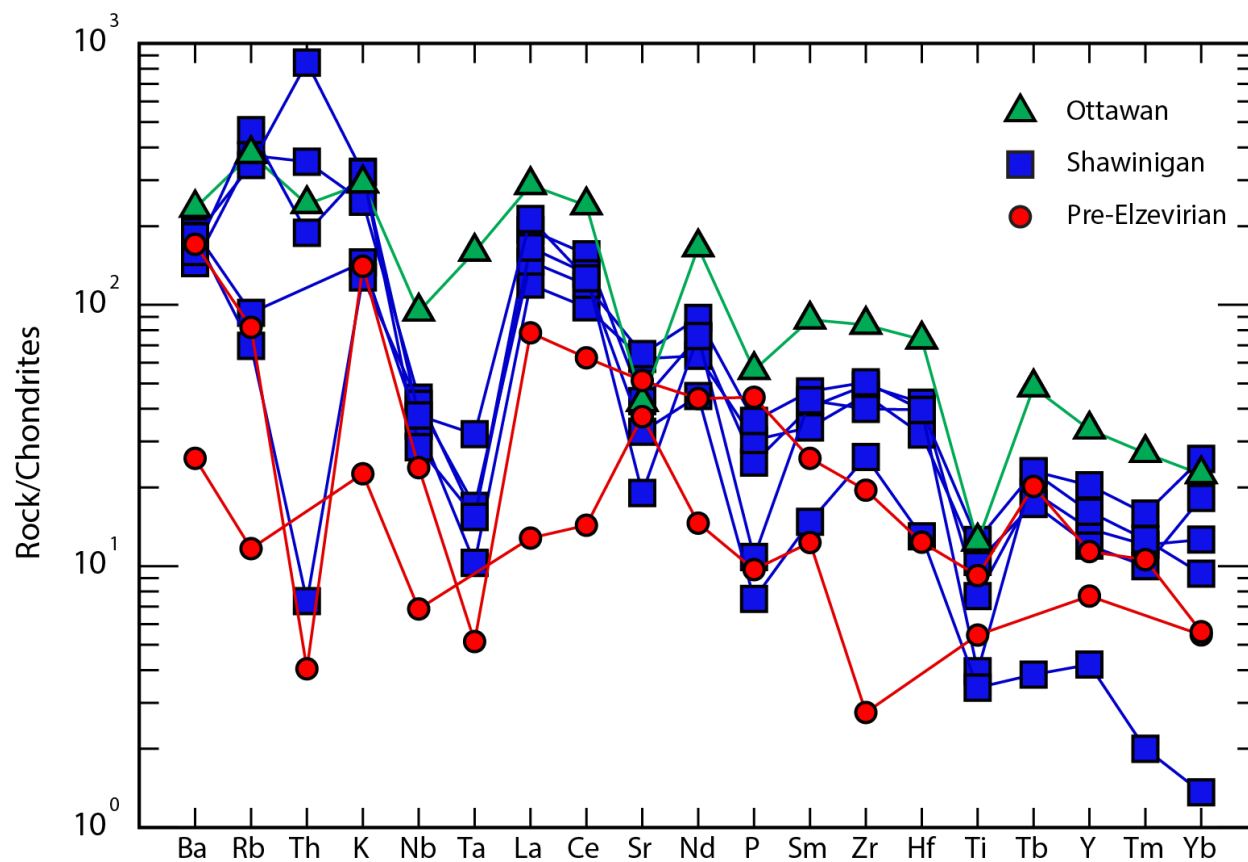
Fig. 16. Chondrite-normalized trace element values (after Thompson, 1982) for all units sampled in the study area. Analyses in red correspond to those units determined to be pre-Elzevirian in age (Earlies Gap gneiss); analyses in blue correspond to units determined to be Shawinigan age (Great Smokey Mountains augen gneiss, Fines Creek gneiss, Toxaway gneiss, Dogget Gap gneiss); and the single unit determined to be Ottawan in age is shown in green (Max Patch granite).
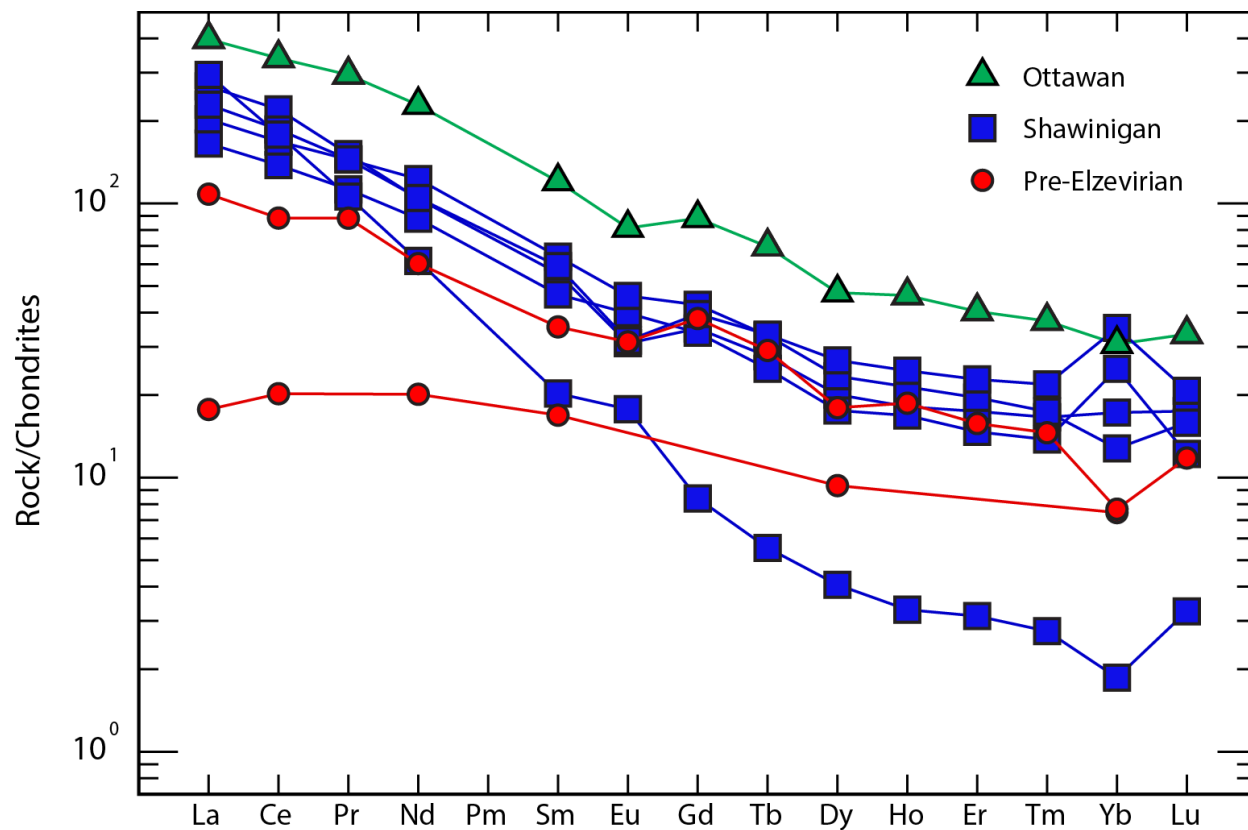
Fig. 17. Chondrite-normalized rare earth elements (REE) for all units sampled in the study area. Color scheme follows that of figure 16. Chondrite values after McDonough and Sun (1995).
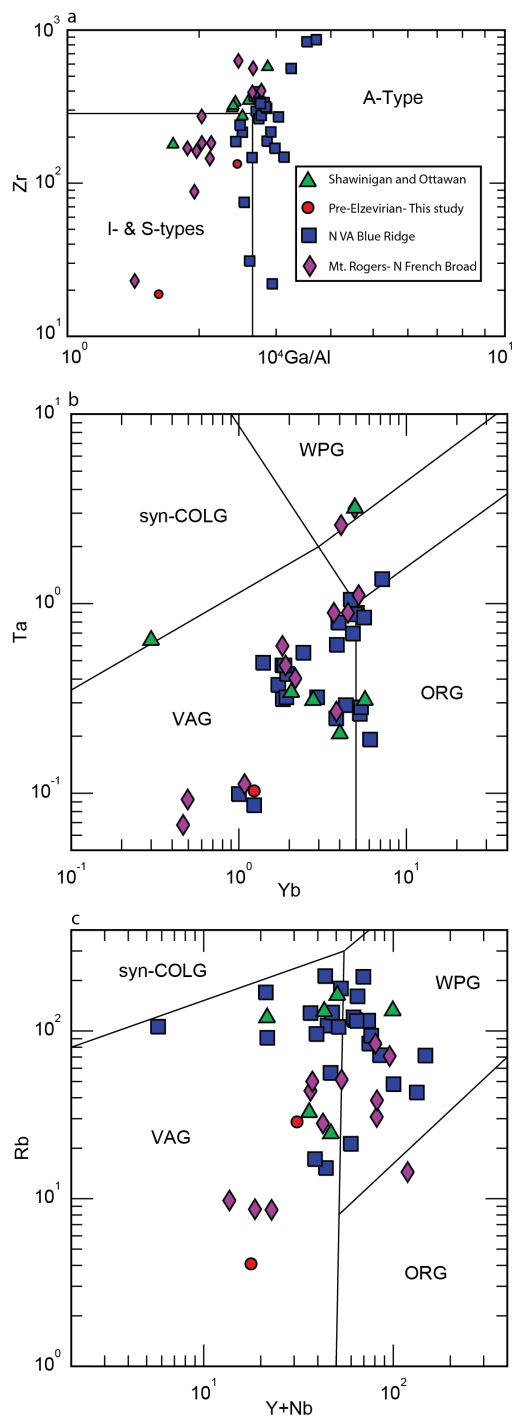
Fig. 18. Trace-element tectonic discrimination diagrams for all units sampled in this study and from the northern Blue Ridge, VA and Mt. Rogers area, northern French Broad massif, NC (Tollo et al., 2006; 2017). Figures modified after Pierce et al. (1984).

Chapter 2: Evaluation of the Eastern Laurentia – Western Amazonia

Mesoproterozoic Terrane Transfer Hypothesis: Isotopic Characterization of 1.4 –

1.0 Ga Granitoids in Southeastern USA and Southern Colombia

In preparation for submission to:

Journal of Geology

Abstract

New in-situ zircon U-Pb, Hf, and O isotopic data are presented from Mesoproterozoic basement from the Hudson-Highlands, Reading Prong, Honey Brook Uplands, Baltimore Gneiss, Virginia Blue Ridge, southern French Broad massif, and from the Garzón massif in Colombia. These data combined with existing whole-rock Pb and Nd data from other Mesoproterozoic terranes corroborate a growing consensus in the literature that basement in these regions is not of Laurentian affinity.

Zircon U-Pb ages from basement in the Reading Prong and Honey Brook Uplands in Pennsylvania are some of the oldest exposed in the Appalachians and record island-arc magmatism at c.a. 1390 Ma. Hafnium isotopic compositions from these rocks are the most juvenile of those studied, containing initial εHf values near that of the depleted mantle at 1390 Ma. Based on these results, it is suggested the geographic position of the suture between Laurentia and Amazonia be moved to a location north of the Reading Prong.

Initial εHf values between -1 and +3 and δ^{18}O values between 6.9 and 8.0‰ from zircon from the Baltimore gneiss, Shenandoah and French Broad massifs indicate significant incorporation of evolved supracrustal material. Hf-model ages between 1.5 and 2.0 Ga are significantly older than any known material to have been present at the southeastern Laurentian margin during the Grenville orogeny. Mesoproterozoic basement in the Garzón massif (southern Colombia) display similar zircon isotope systematics as those from the paleo-Laurentian margin studied here and are used as an analogue for comparison of recycled crust of known Amazonian origin.

1. Introduction

Mesoproterozoic rocks from the southern and central Appalachians have been interpreted as exotic to Laurentia based on whole-rock Nd mantle model ages and Pb isotope compositions, and potentially of Amazonian origin (Sinha et al., 1996; Tohver et al., 2004; Ownby et al., 2004; Moecher et al., 2020). Amazonia is interpreted to have collided with Laurentia by ca. 1.2 Ga, although the extent of this suture north of the central Appalachians remains to be tested. However, based on Pb-isotope data the boundary between Laurentia and Amazonia may exist north of the Honey Brook Uplands (SE Pennsylvania, USA) along a line running east-west in southeastern Pennsylvania (Sinha et al., 1996; Rivers et al., 2012; Fig. 1a).

To assess the purported Amazonian origin of southern and central Appalachian Mesoproterozoic rocks, we use U-Pb, Hf, and O isotopes in igneous zircon from several Appalachian massifs as well as the Garzón massif exposed in the northern Andes in Colombia. These data place constraints on potential magma sources and help decipher the relative roles of juvenile magmatism vs crustal reworking. Few combined zircon Hf and O data sets exist for Mesoproterozoic igneous rocks in the Appalachian Inliers. Our new results are thus important to place further constraints on the source(s) of these rocks and to further test the possibility of an Amazonian affinity of this crustal region.

2. Regional Setting

2.1 Southern Laurentia

Laurentia expanded southward by a series of Paleoproterozoic continental accretion and collision events. Growth of Laurentia began by the amalgamation of

Archean cratons by the c.a. 2.0-1.8 Ga Trans-Hudson Orogen (Whitmeyer and

Karlstrom, 2007). Subsequent southward growth of Laurentia is evidenced by the c.a.

1.88 Ga Penokean, c.a. 1.71-1.68 Ga Yavapai, and 1.65-1.60 Ga Mazaztal orogenies

(Schulz and Cannon, 2007; Whitmeyer and Karlstrom, 2007). The final pre-Grenvillian

continental growth event is recorded by the Granite-Rhyolite province of the central and

east-central US (as currently configured). This terrane consists of a volumetrically

significant and geographically extensive region composed of both A-type and calc-

alkaline granitic plutons and associated volcanic rocks (Fig. 2; Bickford et al., 2015).

Bickford et al. (2015) interpreted the boundary between these two igneous rock types to

be evident by differences in εNd and $^{Nd}T_{DM}$ model ages, where rocks in the western

zone represent intracontinental magmatism involving older crust compared to rocks in

the eastern zone that were interpreted as juvenile arcs accreted to the Laurentian

margin. This accretion evidently started in what is now the northeastern U.S. and

progressed southwestward (Bickford et al., 2015). The eastern boundary of this region

is thought to extend east of the Grenville Front (Fig. 2; Fisher et al., 2010; McLelland et

al., 2013). Hence, it can be envisaged that any continental-arc magmatism within the

Grenville orogen could incorporate this crust via assimilation/contamination.

The oldest unambiguous igneous rock exposed in the northern Appalachians of

New England is a ca. 1390 Ma hornblende diorite orthogneiss in the Green Mountains

massif (Aleinikoff et al., 2013). Metaplutonic and associated metavolcanic rocks dated

in nearby in Vermont are interpreted to be related to continental arc magmatism

(Ratcliffe et al., 1991). Though the details are beyond the scope of this paper, it is

important to note these occurrences because if younger Grenville-aged (1280-1000)

magmas intruded and incorporated this material, then their signature will be present in the Hf isotope characteristics and resulting model ages.

Igneous and metaigneous rocks within the Adirondack massif and in select Appalachian inliers share ages similar to those in the Green Mountains of Vermont. Orthogneisses exposed in the Adirondacks are dated at 1350 Ma (McLelland et al., 1996; 2013) and have $^{Nd}T_{DM}$ model ages slightly older than their interpreted crystallization ages, consistent with being juvenile additions to Laurentia (Daly and McLelland, 1991). Currently, the southernmost known continuous extent of the Pre-Elzeverian tectonomagmatic event is in the New Jersey Highlands, which include two subunits of the Wanaque tonalitic gneiss at 1363 ± 17 and 1366 ± 9 Ma. 1350-1310 Ma orthogneisses are also present within the southern Appalachians (Tollo et al., 2017; Moecher et al., 2020), which correlates with rocks further north in the New Jersey Highlands, Green Mountains, and the Adirondacks. Although volumetrically minor these rocks represent a continuous magmatic episode along eastern Laurentia preceding Eastern Granite-Rhyolite magmatism.

Mid- to late-Mesoproterozoic (1.3-1.0 Ga) growth of eastern Laurentia is dominated by events related to the Grenville Orogeny (Rivers et al., 2012; McLelland et al., 2013). The most well-studied province within the U.S. is the Adirondacks of New York state (Daly and McLelland, 1991; Peck and Valley, 2000; Bickford et al., 2010; McLelland et al., 2013). Grenville-aged Appalachian basement inliers stretch quasi-continuously from Vermont southwest to Alabama. Grenville-aged crystalline rocks are also exposed in the Llano Uplift and Van Horn area, in Texas; Pikes Peak in Colorado, and in northwestern Mexico. All regions generally share a similar tectonic evolution,

showing evidence for distinct phases of magmatism and metamorphism at 1280-1250

Ma (Elzevirian), 1190-1130 Ma (Shawinigan) and 1090-1020 Ma (Ottawan) (Roback,

1996; Bickford et al., 2000; Mosher et al., 2004; Farmer et al., 2005; Howard et al.,

2015).

2.2 Western Amazonia

Evolution of Amazonia begins with the amalgamation of microcontinents in the

Archean; Proterozoic growth is punctuated by a series NW-SE oriented (present

configuration) accreted oceanic island arcs and crustal additions from collisional events

(Fig. 1b; Cordani and Teixeira, 2007; Ibanez-Meija et al., 2011). The Ventauri-Tapajos

and Rio Negro-Juruena belts are a part of these Paleoproterozoic crustal additions that

formed from 1.95-1.8 Ga and 1.8-1.55 Ga, respectively (Ibanez-Meija et al., 2011).

Paleogeographic reconstructions place the southwestern margin of Amazonia (current

position) juxtaposed to the southeast margin of Laurentia during Rodinian assembly,

with an orogenic belt trending NE-SW (Tohver et al., 2004). In this paleogeographic

context, it has been proposed that the Paleoproterozoic terranes of southwestern

Amazonia were juxtaposed against the southeastern Laurentian margin during Grenville

orogenesis (Tohver et al., 2004; Cordani et al., 2009). Evidence for these older

terranes may be manifest in the Hf isotope signatures of igneous zircon produced at the

developing proto Laurentian-Amazonian margin.

The Garzón massif in the Eastern Cordillera of the northern Andes in southern

Colombia (Figs. 1b and 2b). It is the largest exposure of Mesoproterozoic crust in the

northern Andes and contains a series of orthogneisses and paragneisses emplaced

contemporaneously with rocks of the Sunsás belt (Teixeira et al., 2010; Ibanez-Meija et al., 2011; 2015; Pepper et al., 2016). Previous zircon geochronological studies by Ibanez-Meija et al. (2011; 2015) indicate the evolution of the Garzón massif is punctuated by 2 crustal growth events between 1.45-1.15 Ga and 1.15-0.99 Ga. Although assumed to be autochthonous to Amazonia, the position of the Garzón massif relative to Amazonia during the latter stage of its crustal growth history is uncertain. It was either part of (1) a previously connected but now segmented belt of Mesoproterozoic basement rocks, described in the modern northern and central Andes, which were later translated to their current location from more southerly latitudes (Cardona et al., 2010; Chew et al., 2011); or (2) the northwest flank of the paleo-Amazonian margin in a volcanic arc associated with the Oaxaquia terrane (Ibanez-Meija et al., 2011). Despite these complexities, Ibanez-Meija et al. (2011; 2015) interpreted the Garzón massif as autochthonous to Amazonia on the basis of zircon U-Pb, Hf, and O characteristics. These data, in addition to similar data sets from deep boreholes in the Putumayo foreland basin, helped identify what they call the Putumayo Orogeny. Importantly, they argue the late Mesoproterozoic paleogeographic position of northwest Amazonia implies interaction with Baltica (Ibanez-Meija et al., 2015). They identified extensive crustal recycling in Mesoproterozoic rocks of this area, evidenced by elevated $\delta 18O$ values and mildly positive initial eps Hf values (Ibanez-Meija et al., 2015). This is the only known study that has produced coupled zircon U-Pb, Hf, and O isotopic data demonstrating that a significant amount of older, Amazonian material was incorporated into Mesoproterozoic (i.e., "Grenvillian" age) magmas. Hence, the Garzón massif is the best suited analogue for comparisons between it and the Appalachian inliers because of

its known Amazonian affinity, voluminous Grenvillian-age magmatism, and the

incorporation of older, evolved Amazonian crustal material.

3. Samples

Granitoids from the southern-central Appalachians were sampled to characterize

any potential differences in source terranes during the Grenville Orogeny. Figures 1

and 2 show the massifs and sample locations, respectively, and exact coordinates of

sample locations are provided in Table 1. The southernmost units sampled are located

within the southern French Broad massif in western North Carolina. The general

character, age, and geochemistry have previously been described by Chapter 1. Most

of the units were sampled within the west half of the Asheville 1:100,000 scale

quadrangle (Merschat and Cattach, 2008). Units outside of this quadrangle that were

also sampled and re-analylzed for zircon U-Pb, Hf, and O isotopes include charnockites

of the State Road Suite from the Lovingston massif (VA12-1; VA15-1) in Virginia

(Hughes et al., 2004; Tollo et al., 2006; Moecher et al., 2014; Burk 2017), a charnockite

from the Pedlar massif (VA15-2) in Virginia (Tollo et al., 2004; Moecher et al., 2014;

Burk 2017), a low-silica charnockite from the Shenandoah massif in Virginia (VA15-2;

Tollo et al., 2004), and a granite from the New Jersey Highlands (NJ15-1) in southern

New York State (Gorring et al., 2004; Burk, 2017). The State Farm gneiss of the

Goochland terrane (SF98-1) described by Owens and Tucker (2003) and Owens and

Samson (2004) was analyzed for O isotopes only.

Three previously undated units from central Appalachian Grenville massifs were

also analyzed for whole-rock geochemistry and zircon U-Pb and Hf isotopes. These

include a biotite K-feldspar augen gneiss (MD18-5) of the Baltimore Gneiss complex sampled in the Towson quadrangle (map unit =ba of Crowley and Cleaves, 1974), a quartz monzonite (PA18-2) from the Wagontown quadrangle within the Honey Brook Uplands (map unit Yqm of Marquez, 2005; Fig. 1), and a granitic gneiss (Qtz + Plag + Afs ± Hbl) from the Reading Prong (PA18-3; map unit gh of MacLachlan et al., 1975) were all analyzed.

Four orthogneisses were sampled along a SE-NW transect from the eastern half of the Garzón massif in southern Colombia (Fig. 2b; map unit PRmfl and PRngm of Rodríguez et al., 2003). Sample FLOR18-1050 is medium gray, consists of Plag + Qtz + Hbl and is part of the Guapotón-Mancagua gneiss (Rodríguez et al., 2003). Samples FLOR18-1515, FLOR18-1925, and FLOR18-2275 are subunits of the Garzón Complex (Florencia migmatites; Rodríguez et al., 2003). Sample FLOR18-1515 is medium to light gray and contains Qtz + Plag + Hbl. Samples FLOR18-1925 is a white to pinkish white metagranite containing abundant Qtz + K-fs + Plag + minor Hbl. Sample FLOR18-2275 is a white to light pink, moderately to strongly foliated gneiss containing Qtz + K-fs + minor Hbl. These orthogneisses were analyzed for their major and trace-element geochemistry and zircon U-Pb and Hf isotopes.

4. Methods

4.1 Whole-rock geochemistry

Whole rock powders were created from small unweathered chips approximately 25 mm in diameter using a ceramic-crucible shatterbox at Syracuse University. A 10.5 g mixture consisting of 3.5 g of rock powder and 7 g of Lithium Tetraborate flux was

used to create glass beads for XRF analyses. Further details are provided in Chapter 1.

All samples were analyzed in the Hamilton Analytical Laboratory at Hamilton College

(NY, USA) using a Thermo ARL Perform'X XRF spectrometer.

4.2 Zircon preparation and characterization

Zircon for most samples was concentrated following standard mineral separation

techniques. Methods for zircon concentration for the Shenandoah massif charnockites,

Mount Eve Granite, and the State Farm gneiss are presented in Burk (2017) and Owens

and Samson (2004), respectively. Zircon grains were hand-picked under a microscope

with both reflected light and transmitted light capabilities. Reflected light was used to

identify grains with obvious cracks, which were not picked for mounting. Transmitted

light was used to identify optically clear grains (i.e., non-metamict) as well as to identify

grains containing inclusions. Suitable grains were mounted onto double-sided tape,

cast in epoxy, and cured for 36 hours. Further analytical methods are described in the

supplementary material.

4.3 Hf isotope analysis

Zircon U-Pb and Hf isotopes for new samples were measured by laser-ablation

split-stream inductively coupled plasma mass spectrometry (LASS-ICPMS) using a Nu

Plasma II at Curtin University in Perth, Australia. Analytical conditions and procedures

follow Spencer et al. (2019). The zircon standards FC1, GJ1, Plesovice, Amigo, R33,

Mud Tank, and 91500 were analyzed during the same analytical session. To determine

U-Pb concordancy, concordia diagrams were employed using IsoPlotR (Vermeesch,

2019). Similar to Chapter 1, if the error ellipse did not intersect concordia, then the analysis was rejected and not used for age determination. Additionally, the Hf results for discordant grains were not used. After concordance was determined, several Hf data filters were applied following that of Spencer et al. (2019). First, $^{178}Hf/^{177}Hf$ and $^{180}Hf/^{177}Hf$ ratios were evaluated to ensure they fell within previously determined ranges (Spencer et al., 2019). If they did not, they were rejected. Secondly, reproducibility of the analyses was evaluated by multiplying the quotient of standard deviation (s.d.) divided by the mean of analyzed $^{178}Hf/^{177}Hf$ and $^{180}Hf/^{177}Hf$ ratios. If the calculated reproducibility is less than 200 ppm then the analyses are accepted (Spencer et al., 2019). To ensure an appropriate ^{176}Yb correction was applied to all samples, two items were addressed: (1) the measured $^{176}Yb/^{177}Hf$ ratios for the unknowns lie within range of $^{176}Yb/^{177}Hf$ ratios in the standards; and (2) there is no linear correlation between $^{176}Hf/^{177}Hf$ and $^{176}Yb/^{177}Hf$ ratios within the unknowns (Spencer et al., 2019). In summary, if the U-Pb result of an analysis was concordant, its measured $^{178}Hf/^{177}Hf$ and $^{180}Hf/^{177}Hf$ were within acceptable ranges, its reproducibility was confirmed, the range in $^{176}Yb/^{177}Hf$ ratios measured in the analysis was within the $^{176}Yb/^{177}Hf$ ratios of the standards, and no linear correlation existed (via Pearson's R coefficient) between $^{176}Hf/^{17}7Hf$ ratios and $^{176}Yb/^{177}Hf$ ratios of the analysis, then it was accepted and used to determine the εHf(i) value and model age. Initial εHf values were determined using a present day $^{176}Hf/^{177}Hf$ value of 0.282785, $^{176}Lu/^{177}Hf$ value of 0.0336, and a decay constant of $1.867x10^{-11}$ (Bouvier et al., 2008, Soderlund et al., 2004, respectively). Two-stage model ages were calculated using the equation of Payne et al. (2016) and R package detzrcr of Kristoffersen and Elburg (2018) with present day Depleted Mantle

^{176}Hf/^{177}Hf and ^{176}Lu/^{177}Hf values of 0.28325 and 0.0384, respectively (Belousova et al., 2006). All Hf data from the literature used for comparison in this study was recalculated using the parameters above.

4.4 Oxygen isotope analysis

Oxygen isotope values were determined using the CAMECA IMS-1280 secondary ion mass spectrometer (SIMS) in the WiscSIMS laboratory at the University of Wisconsin, Madison. Analytical conditions and procedures are provided by Kita et al. (2009) and Valley and Kita (2009). During the analytical session, instrumental mass fractionation biases were offset by bracketing a block of 15 unknown analyses within 8 measurements on the standards (4 on each side of the unknown block). Sizeable pieces of the KIM-5 zircon oxygen standard (δ^{18}O 5.09‰ VSMOW; Valley, 2003) and UWQ-1 quartz oxygen standard (δ^{18}O 12.33‰ VSMOW; Kelly et al., 2007) were located at the center of the mount and used for the preceding procedure. Individual spot uncertainties are equal to the 2 s.d. of the bracketing standard uncertainties. The values in this study are reported in δ-notation relative to Vienna Standard Mean Ocean Water (VSMOW). Post-analysis Secondary Electron (SE) images were collected to verify the analytical spot was wholly contained within one CL zone and that it did not hit any cracks or unintended inclusions (see supplementary data files). All data reported here satisfied these conditions.

5. Results

5.1 Zircon U-Pb Geochronology

To better assess the crustal evolution of the Grenville margin and its potential affinity to Amazonia during the Mesoproterozoic we build upon the data of previous workers (e.g., Bickford et al., 2010; Valley et al., 2010; Howard et al., 2015; Ibanez-Meija et al., 2015; Peterssen et al., 2015; Burk, 2017; Moecher et al., 2020). Six metaigneous units, ranging in location from central Virginia to southern New York, and four orthogneisses from the Garzón massif, Colombia, were sampled for zircon U-Pb analysis. The geochronological results are ordered from oldest to youngest on the basis of their region. Graphical results of concordia diagrams and weighted mean plots are provided in figure 3. Depending on the analytical data, preferred dates were determined from either upper intercept dates, weighted mean $^{206}Pb/^{238}U$ or $^{207}Pb/^{206}Pb$ dates, or concordia dates. The preferred method used to make an age interpretation was generally guided by which date produced a minimum of mean square weighted deviates (MSWD). Table 2 provides a summary of all analyses performed for each sample.

Standards were measured simultaneously with unknowns. The primary age standard during the session was FC1, for which 41 analyses yielded a weighted mean $^{207}Pb/^{206}Pb$ age within 2 s.d. of the accepted age of 1099 ± 1 Ma (Paces and Miller, 1993; Schmitz et al., 2003). Table 2 summarizes the results from analysis of all standards for U-Pb, Hf, and O.

5.1.1 North Central Appalachians

PA18-2 (quartz monzonite, Honey Brook Uplands)

Zircon from PA18-2 are optically clear, have a slight pinkish color, are blocky to subhedral, and are generally 100 μm in length. Backscattered electron images reveal mostly inclusion free grains, but nearly every grain contained cracks. Cathodoluminescence textures reveal most grains are cored with structureless dark zones transitioning into mostly oscillatory outer cores. Most core domains are truncated by rims with a mottled texture and light CL intensity. Analytical spots were placed in zones categorized as inner core (white ellipses on concordia diagram), outer core (dark grey ellipses), and rims (blue); all subsequent samples follow this color scheme. No obvious separation in dates was apparent between the inner and outer core domains and spread nearly 400 m.y. along concordia. This phenomenon has been observed in other rocks that have experienced a protracted thermal history (e.g., Mezger and Krogstad, 1997; Halpin et al., 2011; Chapter 1). In Chapter 1, I determined that in such rocks using a regression (i.e., model-1 discordia) through these points provides one robust way to interpret complex U-Pb behavior in zircon. Using this approach here, the inner core and outer core domains produce an upper intercept date of 1395 ± 71 Ma (2σ; MSWD 1.1; n = 25) that is interpreted to be the crystallization age of the protolith. Significant precision may be lost using this method, but accuracy is retained (see Chapter 1). Two rims were analyzed and overlap within uncertainty of one inner core domain analysis. Therefore, these two analyses were included to produce the upper intercept date above.

PA18-3 (granitic gneiss, Reading Prong)

Zircon from PA18-3 are euhedral, moderately elongate, and are generally 150-250 μm in length. Backscattered electron images reveal relatively inclusion free grains

with abundant cracks. Textures shown by CL images are relatively simple with most grains having oscillatory zoned cores characterized by light CL intensity. All core domains are truncated by bright CL intensity and structureless rim domains. Similar to PA18-2, this sample shows an appreciable spread of individual analyses along concordia, spanning 300 m.y. in the inner and outer core domains. An upper intercept date of 1372 ± 49 Ma (MSWD 1.2; n = 25) was determined and is interpreted as the current best estimate of the crystallization age of the protolith. One rim analysis produced a $^{207}Pb/^{206}Pb$ date of ~1066 Ma and is interpreted to represent the high-temperature event which caused the complex U-Pb systematics observed in this sample. This age corresponds well to the timing of Ottawan orogenesis in Grenville terranes both north and south of the sample location (e.g., McLelland et al., 2013; Tollo et al., 2006; Moecher et al., 2020; Chapter 1).

MD18-5 (K-feldspar augen gneiss, Baltimore gneiss complex)

Zircon grains from MD18-5 are optically clear with a slight light brown tint, subhedral, display high length/width ratios, and are generally 75-300 μm in length. Backscattered electron images show abundant small inclusions with minor amounts of thin elongate inclusions, the latter being dominantly apatite. Textures revealed by CL imaging are variable, with most cores displaying a mottled texture and varying degrees of CL intensity. The inner core domains typically transition to an oscillatory zoned outer core region. Core domains are truncated by new growth of thin bright to dark CL intensity rims. For analysis, 3 domains were used to characterize the crystallization history of this sample, inner core, outer core, and rim domains. Similar to PA18-2 and PA18-3, MD18-5 shows no systematic difference between the domains and has a ~200

m.y. spread in individual dates along concordia. Thus, an upper intercept date of 1270 $\pm$ 60 Ma (MSWD 1.2; n = 21) was determined and is interpreted to be the age of crystallization of the igneous protolith.

VA12-1 (Stage Road Suite orthogneiss)

Zircon grains from VA12-1 are mostly subhedral and elongate and are generally 75-250 μm in length. Grains are both inclusion and crack free as seen in BSE images. CL textures in the cores display mostly bright CL intensity oscillatory zoning. No obvious rim domain was observed and therefore only two domains were used for categorizing the analytical spots, inner and our cores. A weighted mean $^{206}Pb/^{238}U$ date of 1009 $\pm$ 7.7 Ma (MSWD 1.5; n=28) was calculated and is interpreted to represent the crystallization age of this unit.

VA15-1 (Stage Road Suite biotite granite; Shenandoah massif)

Zircon from VA15-1 are blocky to subhedral, have varying l/w ratios, and are generally 150-250 μm in length. The grains are relatively crack free and contain few exposed inclusions as revealed by BSE imaging. Textures in CL are relatively simple and consist mostly of bright oscillatory zoned cores with some grains displaying a swirled texture. No obvious rim domains were observed, hence for analysis the grains were categorized by two domains, inner cores, and outer cores. Plotting the measured ratios on a concordia diagram reveals simple U-Pb systematics for this sample and a concordia date of 1012 $\pm$ 7.8 Ma (MSWD 1.1; n=25) was determined. This date is interpreted to represent the crystallization age of this unit.

VA15-2 (leuco-charnockite, Pedlar River massif)

Zircon grains from VA15-2 are optically transparent with a slight light pink color, blocky, and typically 100-250 μm in length. Backscattered electron imaging shows very few cracks and minor exposed inclusions. Textures revealed by CL for this sample are complex. Two common textures prevail within the core domains; the most common is a structureless zone of dark CL intensity, the other, less commonly seen texture, is weak oscillatory zoning. The core domain is truncated by a structureless rim domain with irregular zone boundaries. Analytical spots were placed in 3 zones: inner core, outer core, and rims. However, upon inspection of the resulting measurements, no obvious difference in age exists between them. A concordia date of 1034 ± 2.9 Ma (MSWD 3.9; n = 23) was determined and is interpreted as the best estimate of the igneous crystallization age.

5.1.2. Garzón massif

FLOR18-2275 (orthogneiss; Garzón Complex)

Zircon grains from FLOR18-2275 are optically clear, with a mixture of light pink to light brown colors, euhedral, and are generally 75-300 μm in length. The grains are generally inclusion rich and some have a considerable number of cracks. Textures revealed by CL are variable but relatively simple. Several grains contain bright cores with little to no structure, however the most grains display simple oscillatory zoning in the inner and outer core domains. No obvious rims were identified. The U-Pb systematics of this sample are complex. Despite the attempt to use CL zones and intensity as a guide for potential growth episodes and therefore age domains, there was no systematic correlation between the two. However, two predominant age domains

were identified when plotting the measured ratios on a concordia diagram. A group of analyses from both the inner and outer core domains produced a weighted mean concordia date of 1329 ± 4.6 Ma (MSWD 1.5; n=12). Another subset of grains from both the inner and outer core domains produced a weighted mean $^{207}Pb/^{206}Pb$ date of 1254 ± 18 Ma (MSWD 2.5; n=11). Finally, a single analysis in one outer core domain produced a $^{206}Pb/^{238}U$ date of ~1027 Ma. Since neither the older nor the younger subset of grains are systematically correlated to CL texture or location within the grain (i.e., bright vs dark CL intensity, or inner vs outer core), it is interpreted that the two populations are the result of two zircon growth events and each with a long enough history to preserve their ages in both the inner and outer core domains. We interpret the older domain to represent the crystallization age of the unit rather than a xenocrystic component. The younger domain is interpreted to represent a secondary zircon growth event. The single analysis of ~1027 Ma is interpreted to represent a high temperature event that caused partial recrystallization, equivalent to Ottawan age orogenesis as in many of the Laurentian samples. Further analyses are required to determine a more robust interpretation.

FLOR18-1050 (orthogneiss, Guopotón-Mancagua gneiss)

Zircon grains from FLOR18-1050 are blocky, elongate, subhedral to euhedral, and are generally 75-250 μm in length. Backscattered electron imaging reveals abundant exposed inclusions primarily of apatite with minor alkali feldspar. Cathodoluminescence textures are dominated by simple oscillatory zoned inner and outer cores, however some inner cores are structureless, commonly with dark CL

intensities. All grains show a very thin and bright CL intensity rim.
Cathodoluminescence zones were characterized into 3 domains for analysis, inner core,
outer core, and rims. No systematic difference was observed between the domains and
thus a weighted mean ^{207}Pb/^{206}Pb date of 1159 $\pm$ 22 Ma (MSWD 0.7; n=26) was
determined and is interpreted to represent the crystallization age of this unit.

FLOR18-1515 (orthogneiss, Garzón Complex)

Zircon grains from FLOR18-1515 are elongate with high l/w ratios, euhedral to
subhedral, and are generally 200 μm in length. Abundant single and multiphase
inclusions are exposed in these grains consisting mostly of apatite, quartz, and feldspar.
Relatively few cracks were observed in BSE images. Cathodoluminescence textures
consist mostly of dark CL intensity oscillatory zoned inner cores grading to lighter
oscillatory zoned outer cores. No obvious rims were observed. A ^{207}Pb/^{206}Pb weighted
mean date of 1048 $\pm$ 20 Ma (MSWD 1.8; n=27) was calculated and is interpreted to
represent the crystallization age of this unit.

FLOR18-1925 (orthogneiss Garzón Complex)

Zircon from FLOR18-1925 are subhedral, have low l/w ratios, and are generally
100-200 μm in length. Backscattered electron imaging shows that most grains contain
few inclusions and are relatively crack free. Cathodoluminescence textures are
dominated by dark to light CL intensity oscillatory zoned inner and outer cores, although
some inner core domains are structureless. For analysis, two CL domains were used to
characterize the resulting measured ratios, inner and outer cores. No systematic

difference in dates were observed for these domains and therefore a weighted mean ^{207}Pb/^{206}Pb date of 1008 $\pm$ 19 Ma (MSWD 1.4; n=15) was determined. This date is interpreted to be the current best estimate of the crystallization age of this unit.

5.2 Whole Rock Geochemistry

5.2.1 North-Central Appalachians

Three samples from the north-central Appalachians were analyzed for their whole-rock geochemistry to better understand their petrogenesis. Normative mineralogy for these samples ranges from gabbro (PA18-2), quartz monzodiorite (PA18-3), and monzogranite (MD18-5). Samples PA18-2 and PA18-3 are metaluminous whereas samples MD18-5 is peraluminous, and all are subalkaline. Trace element concentrations suggest these units are I-type granites based on a Zr vs Ga/Al diagram (Fig. 4). These samples plot in the volcanic arc granite field in Rb vs (Y+Nb) space (Fig. 4; Pearce et al., 1984).

Results from major and trace-element analysis are consistent with derivation within a volcanic arc. The intermediate SiO_2 values, metaluminous character, and the presence of hydrous minerals (i.e., biotite and amphibole) attest to their production at a subduction zone. Their trace element characteristics also show a strong affinity to a subduction zone environment. Rocks of the same age and type as samples PA18-2 and PA18-3 are present farther north in the Green Mountains of Vermont (e.g., Rattcliffe et al., 1991) and thus the rocks sampled here may constitute a southern extension of the volcanic arc at this time.

5.2.2 Garzón Massif

Normative mineralogy for these samples ranges from quartz monzonite

(FLOR18-1515), monzogranite (FLOR18-1050 and FLOR18-1925), and syenogranite

(FLOR18-2275). Samples FLOR18-1050 and FLOR18-1515 are metaluminous

whereas samples FLOR18-1925 and FLOR18-2275 are weakly peraluminous; however,

all are subalkaline. On a Zr vs Ga/Al diagram, sample FLOR18-1925 plots in the I-type

granite field whereas samples FLOR18-1050, FLOR18-1515, and FLOR18-2275 all plot

in the A-type granite field (Fig. 4). Similarly, sample FLOR18-1925 plots in the volcanic

arc field and the remaining three lie in the within plate granite field in Rb vs (Y+Nb)

space (Fig. 4).

Major and trace element analysis leads to the interpretation that rocks from the

Garzón massif represent magmatism within an evolving tectonic setting beginning with

magmas produced in anorogenic settings to those produced in arc settings. The three

oldest samples (FLOR18-2275- 1329 Ma; FLOR18-1050- 1159 Ma; FLOR18-1515-

1048 Ma) crystallized from A-type magmas in an anorogenic setting whereas FLOR18-

1925 (1008 Ma) crystallized from an I-type magma in a volcanic arc setting. This history

is in contrast to the magmatic history observed elsewhere in the U.S. Appalachian

inliers, where Pre-Elzevirian to Shawinigan age (~1350-1140 Ma) magmas are

generally believed to be the results of subduction followed by accretion and the

production of A-type magmas during the Ottawan phase (1090-1040 Ma). The

significance of these differences will be highlighted in the discussion section.

5.3 Zircon oxygen isotope analysis

Zircon O-isotopes were measured to better assess the potential source(s) of the magmas producing the granitoids examined in this study. Stable O isotopic values of igneous zircon can be used to delineate potential magmatic sources and processes (Valley et al., 1994). Zircon extracted from rocks considered to be mantle derivatives have δ^{18}O values near 5.3 ±0.3‰ (Valley et al., 1998; Valley, 2003), whereas melts incorporating supracrustal material are enriched in ^{18}O and range from +7‰ to +12‰ (Valley et al., 2005). The enriched nature of crustal melts indicate they incorporated material that had been involved in hydrothermal fluid-rock interactions in near-surface to midcrustal settings (Valley, 2003; Trail et al., 2007).

Similar to the U-Pb methodology presented above, each analysis was characterized on the basis of its CL texture. Three categories were used for each sample, inner cores, outer cores, and rims. This was done to resolve potential differences in O-isotope domains related to changing magmatic conditions. The mean and 1 s.d. for each domain was explored. However, because of the homogenous δ^{18}O values between domains obtained within any given sample, it became evident each domain was statistically indistinguishable. Therefore, only the mean values and 1 s.d. for all analyses for each sample are presented in table 2 and shown in Figure 5.

The zircon oxygen isotope standard KIM5 and quartz standard UWQ-1 were measured repeatedly throughout the analytical sessions. A total of 216 measurements of KIM5 yield a mean δ^{18}O value of 5.09 $\pm$ 0.2‰ (accepted value = 5.09‰: Valley, 2003). A relative mass bias between UWG-1 and KIM5 was determined to be 5.81‰. In total, 13 measurements of UWQ-1 yielded a mean of 11.97 $\pm$ 0.3‰, which is within 2σ of the accepted value of 12.33 $\pm$ 0.07‰ (Kelly et al., 2007).

5.4 Zircon Hf-isotopes

Hf isotopes were measured for 14 units within Appalchian basement massifs from the New Jersey Highlands to the southern French Broad massif, and 4 units from the Garzón massif. Approximately 750 measurements were made in total but as was outlined in the methods section, the data were scrutinized by very conservative U-Pb and Hf filters, ensuring the reported results are as robust as possible. Average εHf(i) values are reported in this section; additional information for each sample can be found in Table 2. The most northerly sample in the data set is from the Reading Prong in southern Pennsylvania (PA18-3), which has an average εHf(i) value of 4.5. One sample from the Honey Brook uplands (PA18-2) has an average εHf(i) value of 10.0 and is one of the most juvenile samples within the data set. An augen gneiss from the Baltimore gneiss complex (MD18-5) has an average εHf(i) value of 3.5. Moving south to the Shenandoah and Pedlar River massifs, VA12-1, VA15-1, and VA15-2 have average εHf(i) values of -0.4, 0.1, and 0.9, respectively. In the southern French Broad massif, the Great Smoky Mountains augen gneiss, Fines Creek (NC17-2;3), Max Patch granite, Earlies Gap (NC17-6; NC19-7 cores/rims; NC19-9 (bright and dark cores)), and Toxaway gneiss have average εHf(i) values of 0.3, 0.6, 1.4, 3.3, 6.5, -0.2, -3.5, 0.4, -0.8, and 3.7, respectively. Three orthogneiss units from the Garzón Complex, FLOR18-1515, FLOR18-1925, and FLOR18-2275 (old cores, young cores) have average εHf(i) values of -0.1, -2.6, 2.5, and 1.3, respectively. One orthogneiss unit from the Guapotón-Mancagua gneiss, FLOR18-1050 has an average εHf(i) value of -0.2.

6. Discussion

The zircon O and Hf isotopes, zircon U-Pb geochronology, and whole-rock geochemistry of Mesoproterozoic rocks exposed from the New Jersey Highlands south to the French Broad massif provide additional insights into the tectonic evolution of the southeastern Laurentian margin during the Grenville orogenic cycle. Previous work on whole-rock and feldspar Pb isotopes and whole-rock Nd isotopes have illustrated the possibility that crust exposed in the southern Appalachians is of exotic origin and sourced from the southwestern Amazonia craton (Sinha et al., 1996; Loewy et al., 2003; Ownby et al., 2004; Tohver et al., 2004; Fisher et al., 2010; Moecher et al., 2020). The data presented in this contribution offer additional insights to previous hypothesized tectonic models.

6.1 Origin of Central and Southern Appalachian crust

6.1.1 Pb isotopes

Several studies of whole-rock and feldspar derived Pb-isotope compositions concluded that crust exposed in the southern Appalachians is not of Laurentian affinity (Sinha et al., 1996; Sinha and McLelland, 1999; Loewy et al., 2003; Tohver et al., 2004; Fisher et al., 2010; Moecher et al., 2020). The discussion here relies on a recent compilation of Pb-isotope results for the Great Smoky Mountains basement complex (French Broad massif) and other Grenville terranes presented by Moecher et al. (2020). The reader is referred to that study for more details. Work spanning several decades produced an extensive data base of Pb isotope values for rocks associated with the Grenville orogenic cycle. Rocks with a so-called "Laurentian" signature are defined by

lower values of $^{207}Pb/^{204}Pb$ for a given $^{206}Pb/^{204}Pb$ value than their Amazonian counterparts (Moecher et al., 2020, their figure 13a and b). The distinction requires a difference in initial $^{238}U/^{204}Pb$ established early on in the evolution of each craton. The Pb isotope composition of rocks from the French Broad massif are therefore difficult to account for (i.e., 207Pb/204Pb values between 15.50 and 16.0), other than an Amazonian origin following initial collision between Laurentia and Amazonia and subsequent terrane transfer (Loewy et al., 2004; Tohver et al., 2004; Fisher et al., 2010).

Lead isotope compositions may be used to delineate the location of the suture between Amazonia and Laurentia (Sinha et al., 1996; Tosdal, 1996; Loewy et al., 2003). This was an important breakthrough for the understanding of the Grenville margin as a whole (Rivers et al., 2012). Namely, it confirmed that the Grenville Orogen (*sensu stricto*) involved continent-continent collision, and the most likely candidate for the conjugate continent was Amazonia. Sinha et al. (1996) originally defined the boundary between Laurentian and Amazonian crust from the analysis of several lithologies exposed in several Appalachian inliers, including the region of our samples from Virginia and Maryland. They determined the boundary most likely occurs along a line running west from the eastern U.S. coast north of the Honey Brook Uplands, where it then turns SW and extends to at least western North Carolina (Fig.1), but possibly as far SW as western Mississippi (Fig. 1 in Rivers, 2015).

6.1.2 Nd isotopes

Similar to Pb, Nd isotope compositions have been employed to decipher the origin of Grenville tectonic terranes (Dickin and McNutt, 2003; Tohver et al., 2004;

Ownby et al., 2004; Fisher et al., 2010). Fisher et al. (2010) evaluated the feasibility of three tectonic models based on a compilation of new and previous Nd studies. Their preferred model states that rocks in the northern French Broad massif (Roan Mountain-Stage Road layered gneiss) and the southern and central Appalachians were derived from an exotic source, although some reworking of Granite-Rhyolite rocks may be possible (Fisher et al., 2010). Evidence cited leading to these conclusions are $\varepsilon Nd(t)$ values that necessitate an evolved source and anomalous (with respect to Laurentia) Nd depleted-mantle model ages as old as 2.3 Ga (McLelland et al., 2010). In the northern U.S. Appalachians, $\varepsilon Nd(t)$ values are generally more positive and thus indicative of a more juvenile source. Additionally, maximum Nd model ages of ~1.46 Ga preclude their derivation from such a non-radiogenic source as in the southern Appalachians (McLelland et al., 2010). The changes in the maximum Nd model ages can geographically be placed somewhere near the Reading Prong-Honey Brook Uplands in southern Pennsylvania. This location is near the boundary between Laurentia and Amazonia identified by Pb isotopes described above.

6.1.3 New in situ igneous zircon Hf-O isotopes

This section focuses on the Appalachian samples of this study as well as those previously described in Chapter 1. Three main points can be taken from the Hf and O results of this study: (1) all samples except one (PA18-2) show significant incorporation of an evolved, nonradiogenic source (Fig. 6); (2) Hf model ages for all samples from the French Broad massif to the Reading Prong (PA18-3) have maximum and average model ages significantly older than any Laurentian crust known to be at the Laurentian margin during the mid- to late-Mesoproterozoic (Fig. 7); (3) Oxygen isotope values (only

measured for rocks considered to be Grenville sensu lato) are only slight variable, with average $\delta^{18}O$ values ranging from 6.5 to 8.0‰ (Table 2, Fig. 5). These values are indicative of the incorporation of supracrustal material and fit well with the interpretation that the Hf isotopes are produced by the same mechanism as the O-isotopes (i.e., mildly positive to mildly negative εHf(t) values).

Samples MD18-5 (Baltimore Gneiss), PA18-2 (Honey Brook Uplands), and PA18-3 (Reading Prong) are discussed further as they inform the tectonic setting prior to the Grenville orogenic cycle (*sensu stricto*; 1080-980 Ma; Gower and Krogh, 2002) and the possible location of the Laurentian-Amazonian suture. Sample PA18-2 (Honey Brook Uplands; 1395 ± 71 Ma), with an average εHf(t) value of +9.9, approximately 0-2 εHf units below that of the depleted mantle at the time it crystallized, is the most juvenile of any measured in this study. The relatively juvenile nature of this sample and its geochemistry suggest that it was derived from the partial melting of depleted mantle in a subduction zone environment where it incorporated a minor amount of older, more evolved continental crust. Conversely, it could also have gained its Hf isotope characteristics by melting of an evolved juvenile source such as the Granite-Rhyolite province. Similar in age (1372 ± 49 Ma) but measurably different in its Hf isotope composition is sample PA18-3 (Reading Prong). Based on its Hf isotope values, it incorporated a higher proportion of evolved material, with an average εHf(t) value of +5.7. The crystallization age of these units is similar to rocks within the Green Mountains of Vermont, suggesting they may be part of the fragmented arc system accreted to the Laurentian margin during the pre-Elzevirian Orogeny. However, maximum model ages for these samples are 1.67 (PA18-2) and 1.87 Ga (PA18-3)

leading to the interpretation they incorporated crust significantly older than any believed to be present at the Laurentian margin at the time they crystallized. Previous isotopic studies (Daly and McLelland, 1991; McLelland et al., 2010) have shown Nd model ages from the New Jersey-Hudson Highlands range from 1.4-1.46 Ga. Thus, the suture between Amazonia and Laurentia should be revised to a be along a region north of the Reading Prong (red dashed line on Fig. 1a). The Baltimore Gneiss sample MD18-5 (1270 ± 60 Ma), with an average $\varepsilon Hf(t)$ value of +3.4, shows evidence of incorporation of more evolved crustal material. Based on its Hf model ages, the age of this material may be as old as 1.97 Ga, providing further evidence that the most northerly samples from this study incorporated material of non-Laurentian affinity.

The zircon O data, similar to the Hf data, support the interpretation that pre-existing supracrustal material was incorporated into the magmas that produced the rocks studied here. Also, the O isotope values vary systematically in both space and time. For example, Figure 5 shows histograms of the measured ratios and mean values with 2 s.d. Although the Elzevirian-aged samples in this study are limited to the southern French Broad massif, they show only minor ^{18}O enrichment, indicative of I-type granitoids produced at a volcanic arc, consistent with their interpreted tectonic setting at the time of emplacement based on whole-rock geochemistry (Valley et al., 2005; Chapter 1). Similarly, the Shawinigan age samples are restricted in geographic extent to the French Broad massif but show a clear ^{18}O enrichment from south to north from 6.1 to 7.4‰ (Fig. 5) and are also in the range of I-type granitoids (Valley et al., 2005), consistent with the interpreted tectonic environment as state in Chapter 1 based on whole-rock geochemistry. This is an interesting observation as it allows for speculation

as to the tectonic process responsible for this trend. Note however, it may simply be a product of the sampling methodology. This notwithstanding, three possible scenarios are envisioned, all which require the incorporation of evolved material into juvenile melts. The source of the juvenile melts could be (1) juvenile magmas produced at a subduction zone, for which the ratio of evolved material/juvenile magma increases northward: (2) delamination of a subducted oceanic slab followed by subsequent uprising of hot asthenospheric mantle material that led to anatexis of the lower crust: or (3) the subduction of an ocean ridge spreading center that opened a slab window allowing for rejuvenated melting of the overlying asthenospheric mantle and anatexis of the lower crust. Using the major and trace elements measured in these rocks as a guide, the most likely scenario is the first. Oxygen isotope compositions from Ottawan age units are not restricted to the French Broad Massif, extending from there north through the Blue Ridge and Goochland terrane of VA, north to the Mt. Eve granite in the New Jersey Highlands. The average $\delta^{18}O$ values for these units are generally higher, indicating the incorporation of more ^{18}O enriched material than in those of Shawinigan or Elzevirian age (Fig. 5). Although being more enriched, the range in values is relatively restricted, with only a 0.8‰ range along an ~800 km transect of the paleo-Laurentian margin. The enriched values are overlap values observed in S-type granites (Valley et al., 2005); however, based on their whole rock geochemistry, all have Alumina Saturation Indices (ASI) less than 1.1, commonly used as the lower limit for S-type granites (e.g., Chapter 1). Thus, considering this along with the Hf and O results, it is more likely they are the result of the melting of evolved (per Hf isotopes) mid-crustal

material (per O-isotopes) with minor amounts of juvenile magma in a tectonic

environment transitional between those that produce I-type and A-type granites.

6.2 Garzón massif as a case-study for reworked Amazonian crust

The Garzón massif has recently been studied in detail and provides a potential

analogue for the French Broad massif (Ibanez-Meija et al., 2011; 2015; Ibanez-Meija,

2020). It is important to note that no direct linkage between the French Broad massif

(and by extension the "greater Mars Hill terrane" of Moecher et al., 2020) and the

Garzón massif is here implied; however, both the Garzón massif and the southeastern

Laurentian margin would have been juxtaposed against the same Paleoproterozoic

terrane on the western margin of Amazonia (Rio Negro-Juruena terrane; Fig. 1b). This

conceptual model relies on the paleogeographic reconstruction of Tohver et al. (2004),

in which southwestern Amazonia and southeastern Laurentia were adjacent to one

another at 1.2 Ga, eventually evolving into a transpressional, sinistral-sense margin until

the final assembly of Rodinia at ~1.0 Ga. Ibanez-Meija et al. (2015) interpret the

Garzón massif to be autochthonous to Amazonia based on zircon U-Pb, Hf, and O data

sets. An important implication of this interpretation is that the older Hf model ages

(compared to zircon-derived igneous crystallization ages) are most likely the result of

incorporation of evolved crust, of which the Rio-Negro Juruena terrane is an obvious

candidate (Ibanez-Meija et al., 2015). Thus, if it is autochthonous to Amazonia and the

paleogeographic reconstruction of Tohver et al. (2004) was the correct configuration at

that time, then it is permissive to use the Hf and O results of Ibanez-Meija et al. (2015)

and this study as an analogue for what the Hf and O isotope signatures look like in the French Broad massif.

The Geon 13 to Geon 10 magmatic history between the Garzón massif and the French Broad massif are broadly similar. The Geon notation is used here to avoid explicitly implying any tectonic or genetic relations between the two regions. Both regions contain orthogneisses with protolith ages from Geon 13 (e.g., 1325 Ma: Ibanez-Meija et al., 2011; 1350-1310 Ma: Moecher et al., 2020). Geon 12 magmatism is revealed by our sample FLOR18-2275, where a subset of inner magmatic zircon cores are dated at ca. 1254 Ma and two subunits of the Earlies Gap granitoid gneiss in the southern French Broad were dated at ca. 1283 and 1250 Ma (see Chapter 1). Geon 11 magmatism is pervasive in the French Broad massif but slightly more subdued (at least for the limited number of available samples) in the Garzón massif. However, two units from the Guopotón-Mancagua gneiss, one dated by Ibanez-Meija et al. (2015) at 1154 Ma and our sample FLOR18-1050, dated at ca. 1159 Ma, provide evidence that magmatism in Geon 11 is evident in both locations. Finally, Geon 10 magmatism is more prevalent in the Garzón massif than in the French Broad massif. An orthogneiss was dated at ca. 1022 Ma by Ibanez-Meija et al. (2015) and two orthogneisses were dated here at ca. 1041 and 1008 Ma compared to the single Geon 10 granite in the French Broad massif (the Max Patch granite: 1034 Ma; see Chapter 1). Conversely, metamorphism in the southern French Broad massif, associated with the Ottawan phase of the Grenville Orogeny, is pervasive and was identified by disturbances in U-Pb systematics in zircon (e.g., Chapter 1; Moecher et al., 2020). The northern French Broad does contain evidence of late Geon 10 early Geon 9 metamorphism (Aleinikoff et

al., 2013), which is attributed to metamorphism during the Rigolet phase of the Grenville Orogeny, whereas metamorphism of the same age in the Garzón massif is attributed to interactions with Baltica (Ibanez-Meija et al., 2015).

The εHf(t) values and model ages determined from the units described above in both the Garzón and French Broad massifs are strikingly similar. Figures 6b and 7b present the results from the Garzón massif (this study and Ibanez-Meija et al., 2015) and from the French Broad massif. The similarity between the two subsets of data is illustrated in Figure 6b. For both regions, initial εHf values range from -2 to +4 epsilon units, implying that magmas generated through the interval 1.35-1.0 Ga incorporated evolved crust (see section 6.1). Model ages (Fig. 7), between the French Broad and Garzón massifs are also similar, with averages ranging from 1.68 to 2.08 Ga. Therefore, the material incorporated into the melts that produced these rocks contains similar Hf-isotope characteristics and is of similar age. These facts allow for a potential correlation between the two terranes, especially given that the French Broad massif is presumably no longer in its original location. As more igneous zircon Hf data for the Mesoproterozoic portion of southwest Amazonia become available, a more appropriate candidate for comparison may arise.

6.3 Contrasting Hf-isotope domains

Few studies have been published that present igneous zircon Hf-isotope measurements for the Mesoproterozoic in southeastern Laurentia. Figure 7b compiles available data along with the results from this study. Values of εHf(t) and model ages

were recalculated using the parameters for this study from the reported $^{176}Hf/^{177}Hf$ and $^{176}Lu/^{177}Hf$ ratios.

Nearly all Garzón massif and southern and central Appalachian samples plot in the same $\varepsilon Hf(t)$ space. Also, units from the Pikes Peak igneous complex in Colorado, USA plot in a similar region, but this is interpreted to reflect the incorporation of Yavapi-Mazatzal age material, given its geographic location (Figs. 2a and 7a). Samples from terranes previously interpreted to be either juvenile (i.e., Adirondacks; Bickford et al., 2010; Valley et al., 2010) or having incorporated crust of known Laurentian affinity (Ohio Drillcore; Peterssen et al., 2015; Llano region/NW Mexico- Howard et al., 2015) plot above a crustal evolution curve representing a hypothetical mantle extract at 1.7 Ga, meaning any calculated Hf model age will be younger than this (assuming a crustal reservoir $^{176}Lu/^{177}Hf$ ratio of 0.015). This observation is in line with the age, and type of material that may have been at the locations from which these samples were taken at the time of their crystallization. A few exceptions to this are evident as well. Namely, sample NC17-6 (French Broad massif, Earlies Gap granitoid gneiss, Chapter 1), which displays a large range in calculated $\varepsilon Hf(t)$ values, mostly skewing to more positive $\varepsilon Hf(t)$ values, suggests a greater contribution of less evolved material into the melt. Similarly, the Blowing Rock gneiss from the French Broad massif also may have incorporated less evolved material, possibly of Laurentian origin. This was also observed by Fisher et al. (2010) with Nd isotopes in samples ~100 km west of this location. Given the projected location of the Grenville front in the subsurface, it is easy to envision that samples close to this boundary are more likely to have incorporated material of Laurentian origin (Fisher et al., 2010).

Homogeneity of Hf isotopic characteristics in pre-Ottawan age samples appears to be stronger than in Ottawan age samples (Fig. 6b). This likely reflects the tectonic environment in which the magmas formed and zircon crystallization occurred. For example, if a magma is intruded into crust that is homogenous in its $^{176}Hf/^{177}Hf$ composition, the resulting melt will reflect this homogeneity and should therefore be easily distinguished from domains with different, yet equally homogenous $^{176}Hf/^{177}Hf$ values. Late Ottawan age units for which igneous zircon Hf data are available do not reflect a simple homogenous reservoir. If continent-continent collision is reflected by pervasive metamorphism throughout the Grenville province and Appalachian inliers (Rivers et al., 2012; McLelland et al., 2013), then the likelihood of multiple Hf-reservoirs being in close proximity to one another should increase. Subsequent magma genesis in this newly amalgamated setting will in turn increase the likelihood of the incorporation of Hf-isotope signatures that reflect this heterogeneity. This is interpreted to be an explanation for the complexity of Ottawan-age igneous zircon Hf-isotope systematics seen in figure 6b. Lastly, a series of crustal evolution curves representing hypothetical mantle extracts from 2.0 to 1.4 Ga in 100 m.y. increments are provided to assist in the visualization of potential age domains from which the sampled zircon were derived. All sampled units from the Garzón and southern and central Appalachians, except for NC17-6 (described above) and the highly variable sample PA18-2 from the Honey Brook Uplands, lie below the crustal evolution curve at 1.7 Ga. In comparison, most samples from the Adirondacks, Ohio basement, and Llano Uplift lie above this same line. Although Hf-model ages should be interpreted with caution (e.g., effects of discordance, choice of DM parameters, choice of $^{176}Lu/^{177}Hf$ ratio of crustal reservoir,

etc.) the evidence provided in figure 6b and the above discussion allow for the identification of discrete crustal reservoirs and resulting Hf-isotope domains.

6.4 Tectonic Reconstruction of southeast Laurentia (~1.35-1.0 Ga)

A compilation of zircon U-Pb and Hf data presented here and from the literature allow for the development of a plate tectonic reconstruction for southeast Laurentia during the mid- to late-Mesoproterozoic. To best reconstruct the paleo-Laurentian margin during the Mesoproterozoic, the tectonic history of both the Laurentian and Amazonian margins will be considered.

The existence of Amazonian crust in southeast Laurentia can be explained by a long-lived active continental margin leading to the formation of Rodinia followed by its breakup in the late Neoproterozoic. For the purposes of this reconstruction, and based on Nd, Pb, and new Hf and O isotopes, the French Broad massif is taken to be a part of the greater Mars Hill terrane (MHT), an interpretation consistent with recent detailed zircon U-Pb, whole-rock Nd and Pb isotopes presented in Moecher et al. (2020). In this scenario, ca 1.35 to 1.30 Ga magmatism occurred on both the southeast Laurentian and southwest Amazonian margin, represented by Pre-Elzevirian continental magmatism and the San Ignacio Orogeny, respectively (Fig. 8). Beginning around 1.30 Ga, sinistral transpressional convergence between Laurentia and Amazonia commenced. Slab-rollback underneath the Laurentian margin caused back-arc rifting and continental-arc magmatism of the Elzevirian Orogeny from ~1290-1250 Ma. Magmatism of similar age, evidenced by protolith emplacement of the Earlies Gap granitoid gneiss in the MHT (ca. 1280 to 1250 Ma; Chapter 1) occurred in southwestern

Amazonia by continued closing of an ocean basin and resulting subduction. Initial

collision of Amazonia and Laurentia occurred at 1.2 Ga in the Llano region (e.g., Tohver

et al., 2004), essentially closing the ocean basin in a northeasterly direction (modern

direction) and suturing the two continents. The Shawinigan Orogeny produced

geographically extensive magmatism along the entirety of the southeast Laurentian

margin from 1190-1140 Ma (Bickford, et al., 2000; McLelland et al., 2013; Tollo et al.,

2006; Tollo et al., 2017; Moecher et al., 2020; Chapter 1; this study). The geochemistry

of Shawinigan age rocks in the MHT are transitional between I- and A-type granitoids

(Tollo et al., 2017; Chapter 1), making it difficult to determine if subduction-related

magmatism was responsible for producing the magmas (represented by the 1.14 Ga

time slice on Fig. 8). Continued collision is characterized by high temperature

metamorphism and minor magmatism in the MHT during the Ottawan phase of the

Grenville Orogeny (Tollo et al., 2017; Moecher et al., 2020; Chapter 1). Subsequent

rifting of Rodinia took place at ca. 0.7 Ga and left the Mars Hill terrane stranded from its

parental Amazonian source.

7. Conclusions

Pb, Nd, and Hf isotope systematics have been used to propose Mesoproterozoic

rocks associated with the Grenville Orogenic cycle from the central and southern

Appalachians are not native to Laurentia. This study adds a geographically extensive

igneous zircon Hf data base for rocks produced during the Grenville Orogenic cycle.

Zircon O-isotopes provide additional information into the nature of the magmas that

were produced during the interval ~1390 to 1030 Ma. Additionally, a geochemical

analogue is provided for direct comparison of the Hf-isotope characteristics in Laurentia to a terrane in Amazonia suggested to be autochthonous to the Amazonian craton during the Mesoproterozoic. With these considerations in mind, the following conclusions can be drawn:

1: New zircon U-Pb and Hf measurements refine the northern suture between Laurentia and Amazonia to be in a location north of the Reading Prong, i.e., further north than previously suggested by other workers.

2: Zircon U-Pb and Hf isotopes from orthogneisses in the Garzón massif support the interpretation of Ibanez-Meija et al. (2015) that Mesoproterozoic rocks from that area represent reworked older evolved crust of the Amazonian craton, likely the Rio-Negro Juruena terrane. This provides a useful analogue for the Hf isotopes signatures one might see in rocks that have incorporated this crust. Based on this comparison, it is likely that Mesoproterozoic magmas within the Mars Hill terrane incorporated crust with similar Hf-isotope characteristics

3: Zircon oxygen isotopes support Hf data in that the rocks studied here are the products of crustal reworking and incorporated supracrustal material. Additionally, within the southern French Broad massif, a systematic decrease in ^{18}O enrichment is seen from north to south, suggesting a progressive change in the degree of melting of supracrustal material

4: The combined results of this study, paired with the interpretations made from previous Pb and Nd isotope studies, support the hypothesis that central and southern Appalachian Mesoproterozoic rocks are not native to Laurentia and instead likely are annexed Amazonian crust.

Table 1. Sample names, locations, and analyses. References- 1 Chapter 1; 2 Merschat

and Cattanach (2008); 3 Burk (2017); 4 Moecher et al. (2014); 5 Owens and Tucker

(2003); 6 Tollo et al. (2004); 7 Hughes et al. (2004); 8 Gorring et al. (2004); 9 Tollo et al.

(2006); 10 Crowley and Cleaves (1974); 11 Marquez (2005); 12 MacLachlan et al.

(1975); 13 Rodríguez et al. (2003).

Sample Name	Geologic Unit	Massif	Lat WGS84	Long WGS84	Reference	Analysis
NC17-1	Great Smoky Mtns Augen Gneiss	French Broad	35.56942	-83.06814	1,2	Zircon U-Pb, Hf, O
NC17-2	Fines Creek Gneiss	French Broad	35.67841	-82.98088	1,2	Zircon U-Pb, Hf, O
NC17-3	Fines Creek Gneiss	French Broad	35.68028	-82.98291	1,2	Zircon U-Pb, Hf, O
NC17-5	Max Patch Granite	French Broad	35.80241	-82.91576	1,2	Zircon U-Pb, Hf, O
NC17-6	Earlies Gap Granitoid Gneiss	French Broad	35.76521	-82.6138	1,2	Zircon U-Pb, Hf, O
NC17-10	Toxaway Gneiss	French Broad	35.12734	-82.92554	1,2	Zircon U-Pb, Hf, O
NC19-7	Doggett Gap Granitoid Gneiss	French Broad	35.71236	-82.82867	1,2	Zircon U-Pb, Hf, O
NC19-9	Earlies Gap Granitoid Gneiss	French Broad	35.7282	-82.6402	1,2	Zircon U-Pb, Hf, O
NJ15-1	Mount Eve Granite	Hudson Highlands	41.30608	-74.422164	3	Zircon O
SF	State Farm Gneiss	Goochland Terrane	37.629816	-77.813385	4,5	Zircon O
VA12-2	Low Silica Charnockite	Shenandoah	38.438333	-78.4008333	4,6	Zircon O
VA12-1	Stage Road Suite Orthogneiss	Shenandoah	37.823489	-78.803367	4,7	Zircon U-Pb, Hf, O
VA15-1	Stage Road Biotite Granite	Shenandoah	38.458054	-78.29916	3,6,7,8,9	Zircon U-Pb, Hf, O

Sample Name	Geologic Unit	Massif	Lat WGS84	Long WGS84	Reference	Analysis
VA15-2	Pedlar River Leuco-charnockite	Pedlar River	38.457775	-78.350826	3,6,7,8,9	Zircon U-Pb, Hf, O
MD18-5	Towson Quad Augen Gneiss	Baltimore Gneiss	39.4295	-76.51498	10	Zircon U-Pb, Hf, WR XRF
PA18-2	Wagontown Quad Qtz Monzonite	Honey Brook	40.11862	-75.83447	11	Zircon U-Pb, Hf, WR XRF
PA18-3	Sinking Creek Quad Granitic Gneiss	Reading Prong	40.32195	-76.11997	12	Zircon U-Pb, Hf, WR XRF
FLOR18-1050	Guapotón-Mancagua Orthogneiss	Garzón	1.7101	-75.6922	13	Zircon U-Pb, Hf, WR XRF
FLOR18-1515	Garzón Complex Orthogneiss	Garzón	1.7163	-75.7202	13	Zircon U-Pb, Hf, WR XRF
FLOR18-1925	Garzón Complex Orthogneiss	Garzón	1.7427	-75.7367	13	Zircon U-Pb, Hf, WR XRF
FLOR18-2275	Garzón Complex Orthogneiss	Garzón	1.7597	-75.7791	13	Zircon U-Pb, Hf, WR XRF

Table 2. Summary of zircon U-Pb, Hf, and O results.

Sample Name	Age (Ma ± 2σ) ^This study; *Published	Average εHf(i)	Range Tdm Hf (Ga)	I.C. δ18O (‰)	O.C. δ18O (‰)	Avg δ18O (‰)
NC17-1	*1142 ± 1.0	0.3	1.79-2.03			8.0 ± 0.2
NC17-2	*1139 ± 11	0.5	1.62-2.07			7.5 ± 0.2
NC17-3	*1175 ± 29	1.5	1.72-2.05			7.5 ± 0.3
NC17-5	*1034 ± 0.9	3.1	1.50-1.83			7.8 ± 0.3
NC17-6	*1283 ± 9.4	6.7	1.39-1.84			6.9 ± 0.2
NC17-10	*1159 ± 28	3.6	1.58-1.81			6.5 ± 0.2
NC19-7	*1191 ± 8.1; 1034 ± 5.7	Cores: -0.3, Rims: -3.5	1.76-2.32	7.4 ± 0.3	7.2 ± 0.4	
NC19-9	*1250 ± 54; *1126 ± 23	Brt Cores: 0.4, Drk Cores: -0.8	1.78-2.11	6.0 ± 0.2	6.1± 0.2	
NJ15-1	*1017 ± 5	n.d.	n.d.			8.0 ± 0.6
SF	*1046 ± 7	n.d.	n.d.			8.0 ± 0.2
VA12-2	*1050 ± 8	n.d.	n.d.			7.7 ± 0.4
VA12-1	^1009 ± 7.7	-0.4	1.74-1.97			7.4 ± 0.1
VA15-1	^1012 ± 7.8	0.1	1.70-1.95			7.6 ± 0.1
VA15-2	^1034 ± 2.9	0.9	1.73-1.92			8.0 ± 0.2
MD18-5	^1270 ± 60	3.4	1.65-1.92			n.d.
PA18-2	^1395 ± 71	9.9	1.33-1.67			n.d.
PA18-3	^1372 ± 49	5.7	1.47-1.87			n.d
FLOR18-1050	^1159 ± 22	-0.2	1.84-2.07			n.d
FLOR18-1515	^1048 ± 20	-0.1	1.76-1.93			n.d
FLOR18-1925	^1008 ± 19	-2.6	1.83-2.10			n.d
FLOR18-2275	^1329 ± 4.6; 1254 ± 18; 1027 ± 5 (1σ)	Old Cores: 2.5, Young Cores- 1.3	1.74-2.17			n.d

Table 3. Summary of zircon standards.

Standard (U-Pb and/or Hf)	U-Pb age (Ma)	Ref. age (Ma)	$^{176}Hf/^{177}Hf_{(o)}$ ± 2 S.D.	Ref. $^{176}Hf/^{177}Hf_{(o)}$	^{176}Yb interf.-standard (%)
FC1	1087 ± 10 (n=39; MSWD=1.5)	1099 ± 1	0.282333 ± 51	0.282183 ± 12	7-64
GJ1	605 ± 0.9 (n=93; MSWD=2.6)	608.5 ± 0.4	0.282026 ± 10	0.282000 ± 5	3-4
Plešovice	341 ± 0.6 (n=71; MSWD=2.8)	337.13 ± 0.37	0.282478 ± 6	0.282482 ± 13	1-4
R33	418 ± 1.1 (n=85; MSWD=2.0)	419.26 ± 0.38	0.282632 ± 40	0.282764 ± 14	7-54
Mud Tank	714 ± 5.6 (n=75; MSWD= 1.0)	731.0 ± 0.2	0.282507 ± 4	0.282523 ± 10	0.14-0.47
91500	1064 ± 17 (n=90; MSWD=0.8	1066.4 ± 0.3	0.282312 ± 10	0.282313 ± 12	2-4
OG-1	3434 ± 4.0 (n=33; MSWD=9.2)	3465.4 ± 0.6	0.280649 ± 15	N.A.	5-42
MACQ	2984 ± 5.9 (n=23; MSWD=6.6)	N.A.	0.280867 ± 8	N.A.	8-9
MUN	N.A.	N.A.	0.282134 ± 8	0.282135 ± 25	0-58
Zircon Standard $\delta^{18}O$	Measured mean $\delta^{18}O$ (‰) ± 2 S.D	Ref. $\delta^{18}O$ (‰) ± 2 S.D			
KIM5	5.09 ± 0.2	5.09 ± 0.12			
Quartz Standard $\delta^{18}O$	Measured mean $\delta^{18}O$ (‰) ± 2 S.D	Ref. $\delta^{18}O$ (‰) ± 2 S.D			
UWQ-1	11.97 ± 0.3	12.33 ± 0.07			
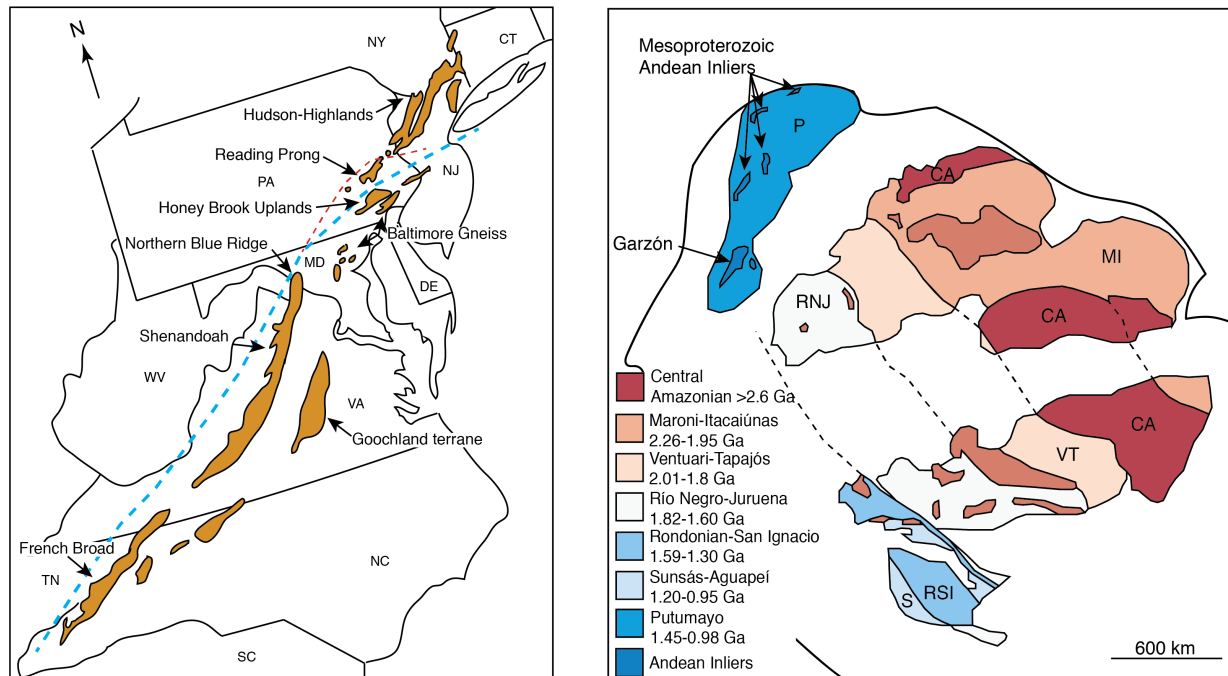
Fig. 1. Map of Grenville Appalachian Inliers. Mesoproterozoic rocks sampled for this study come from the French Broad, Shenandoah/Pedlar River, and Hudson Highlands massifs, Goochland terrane, Baltimore gneiss complex, Honey Brook Uplands, and the Reading Prong b) Tectonic map of the Amazonian craton showing major Archean-Paleoproterozoic terranes; modified from Ibanez-Meija et al. (2015).
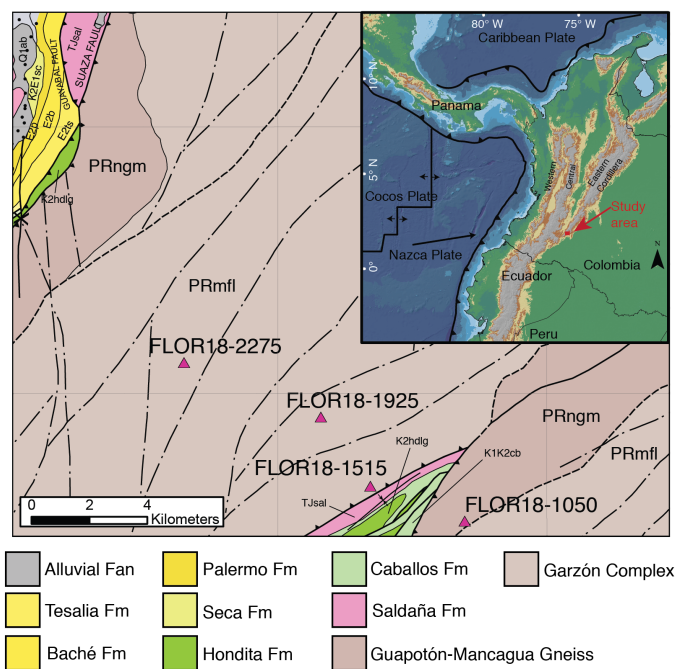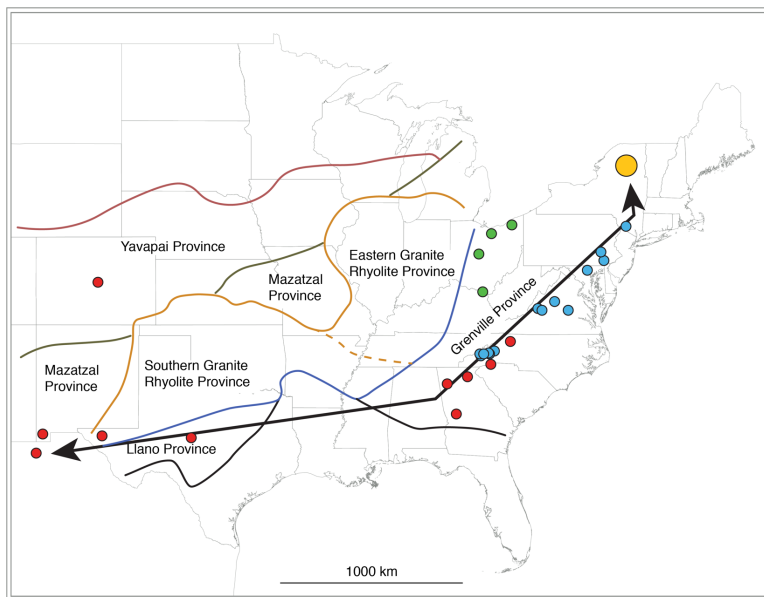
Fig. 2. a) Map of U.S. showing distribution of sample locations with major Paleo- and Mesoproterozoic tectonic provinces discussed in text. Black line with arrows is line of transect in figure 7b, figure modified from Howard et al. (2015) and Bickford et al. (2015) b) Sample location map for Garzon massif, modified from Rodriguez et al. (2003).
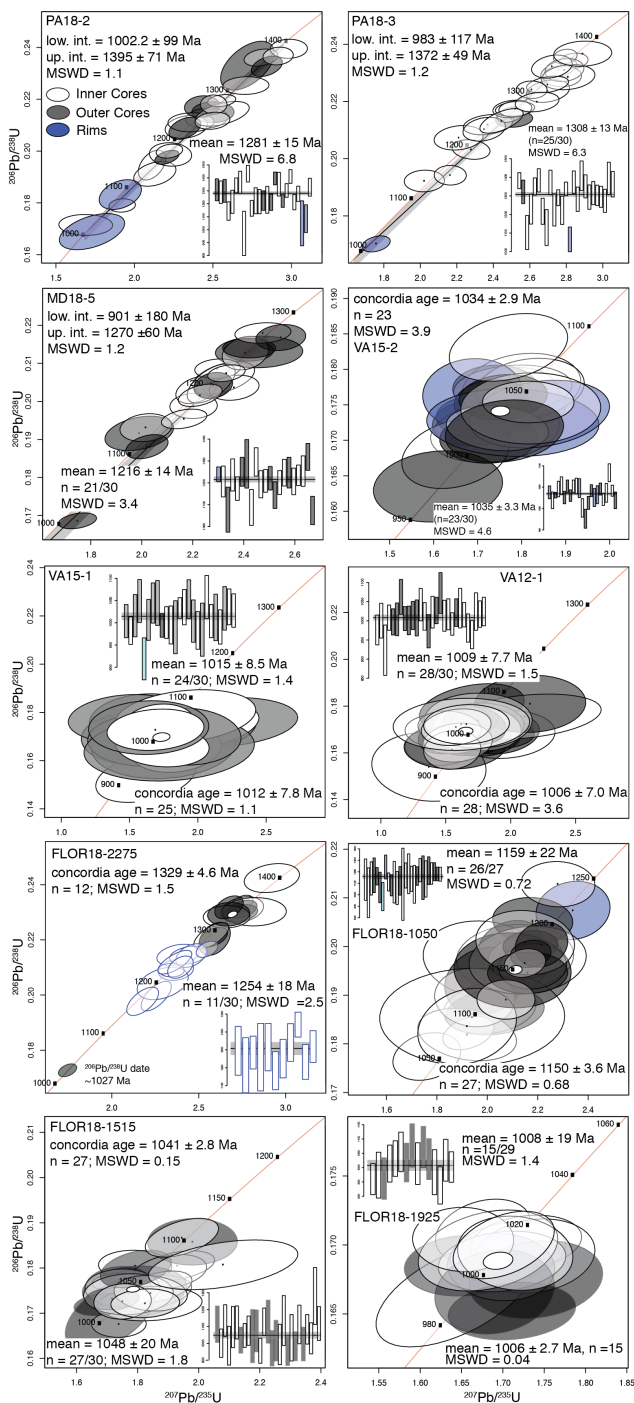
Fig. 3. Concordia and weighted mean plots for new samples presented in this study. White ellipses are from inner core CL zones, black ellipses are from outer core CL zones, and blue ellipses are from rim analyses. Inset weighted mean plots are all $^{207}Pb/^{206}Pb$ except for samples VA15-1 and VA12-1, which are $^{206}Pb/^{238}U$ dates.
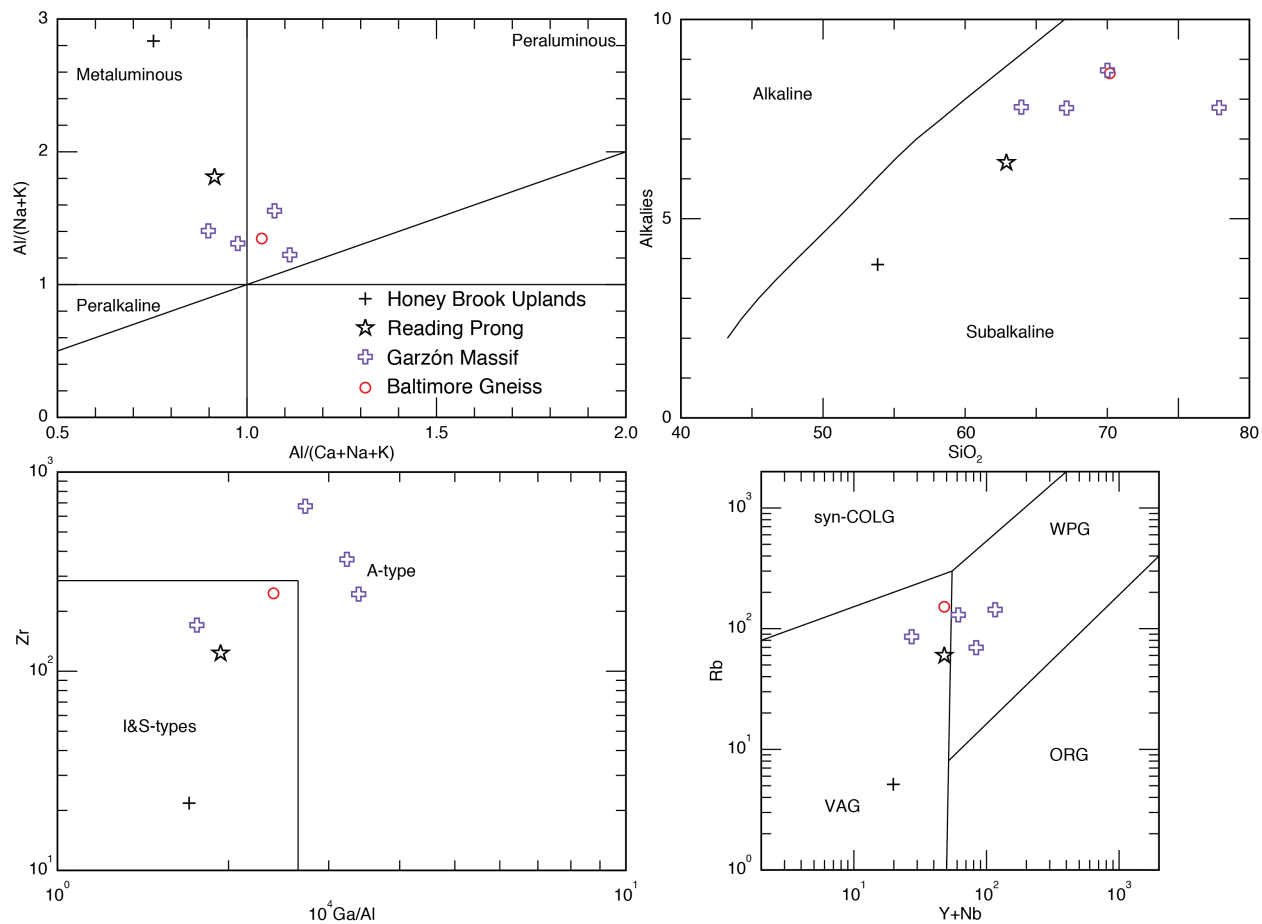
Fig. 4. Geochemical plots used to aid in the interpretation of tectonic setting following Pearce et al. (1984).
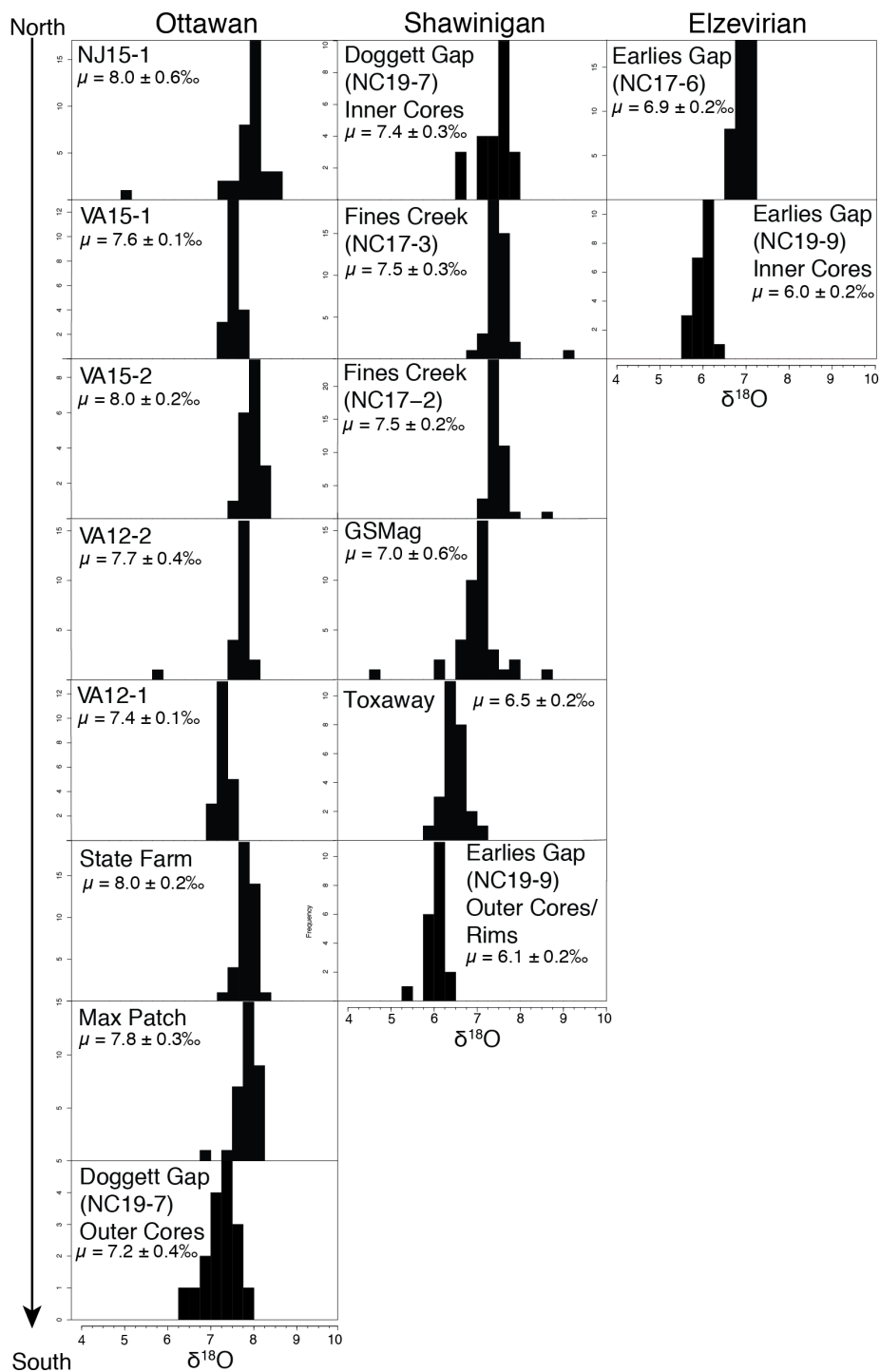
Fig. 5. Graphical summary of zircon O-isotope results. Individual plots are arranged north to south based on their U-Pb age and placed into Grenville Phase categories (i.e., Elzevirian, Shawinigan, and Ottawan). See section 6.1.3 for further discussion.
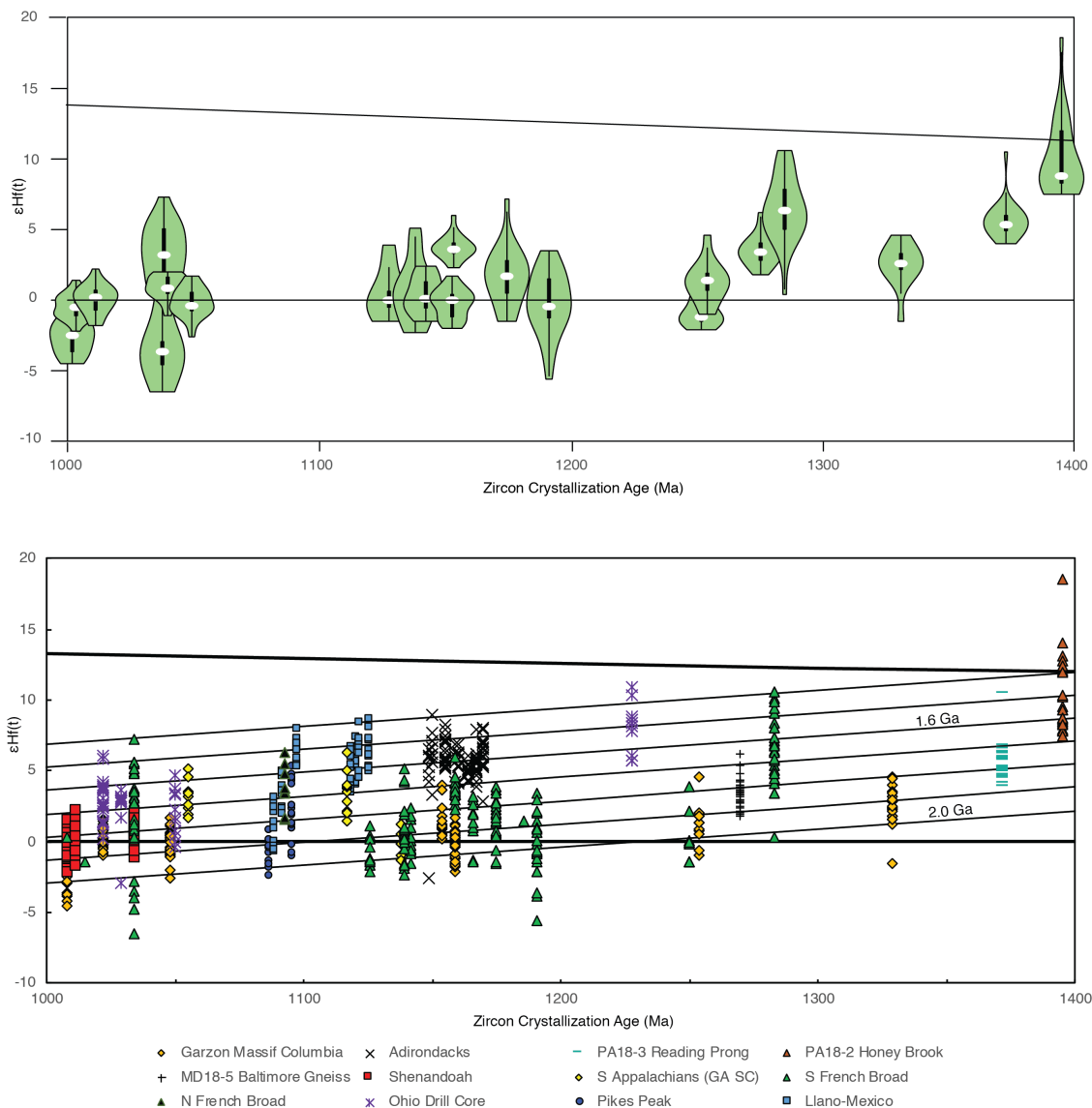
Fig. 6. Upper panel shows violin plots, where one side of the violin plot is a Probability Density Function (PDF), the other side is the same PDF mirrored about a vertical axis. Bottom panel shows data from this study plus data from the literature, colored by region. Note great agreement between Garzón massif and southern French Broad samples, as well the Pikes Peak complex (Howard et al., 2015). Modeled crustal evolution curves from 2.0 to 1.4 Ga represented by thin black lines using a crustal reservoir Lu/Hf of 0.015 (Payne et al., 2016).
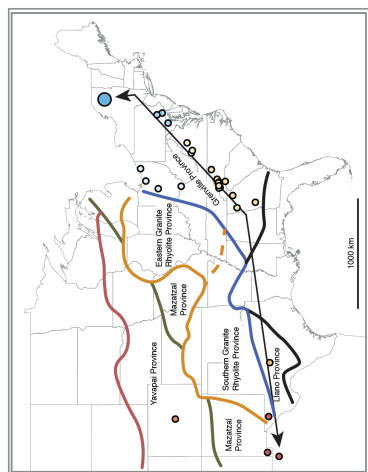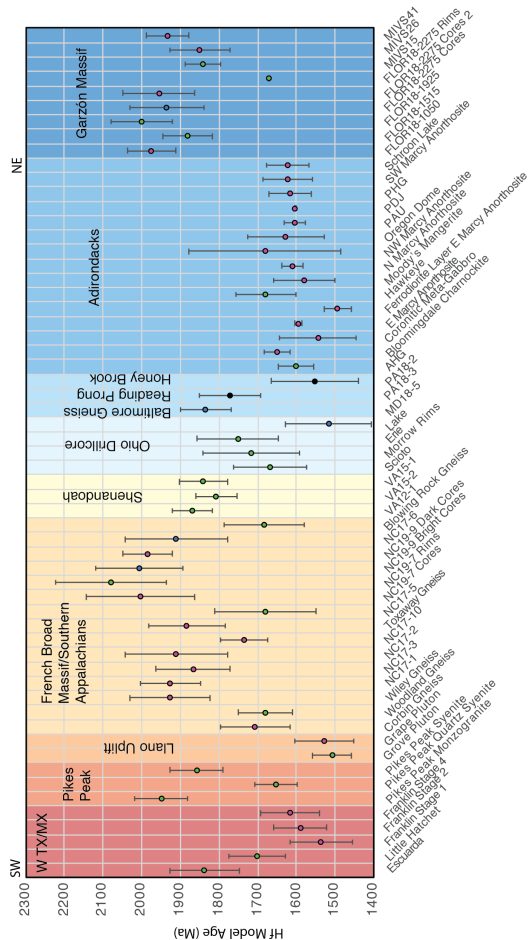
Fig. 7. Figure on left panel shows location of transect. Figure on right panel shows the average model age with 2sd. Dot colors on left figure correspond to shaded color regions on right panel. Colors of dots on right panel correspond to their age- Ottawan-green, Shawinigan- magenta, Elzevirian- blue, Pre-Elzevirian- black.
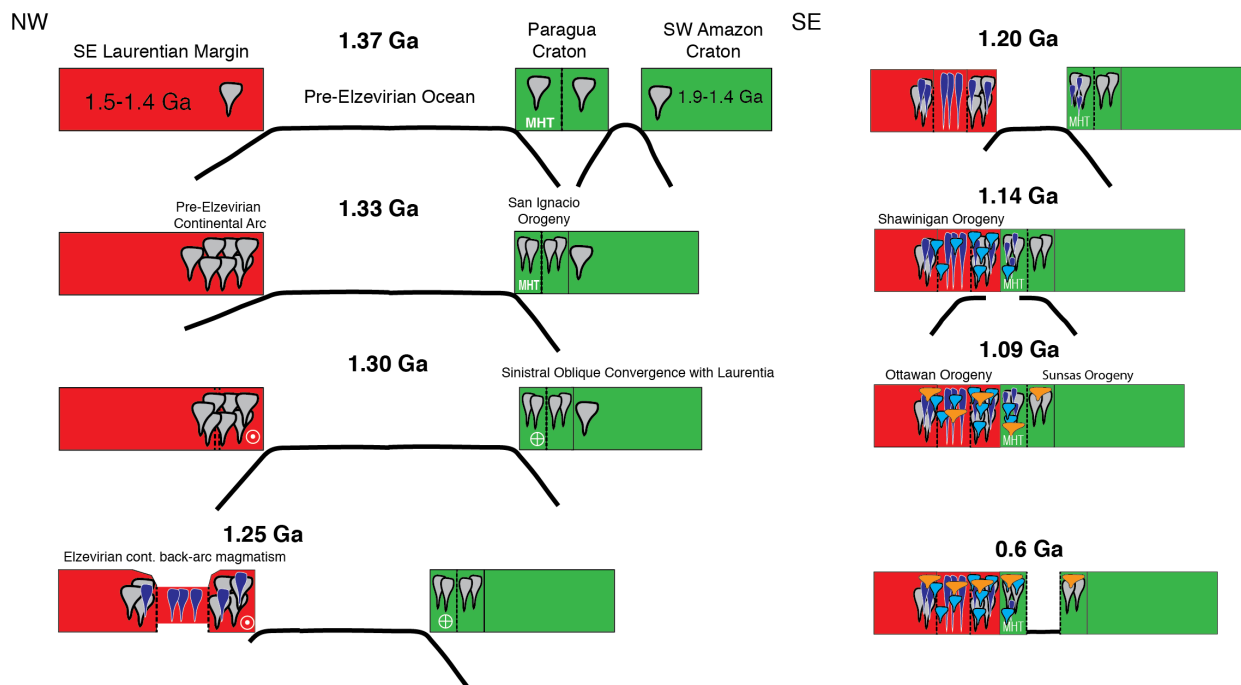
Fig. 8. Conceptual tectonic reconstruction of the evolving Laurentian-Amazonian margin during the mid- to late-Mesoproterozoic. This model considers the results of many previous Pb and Nd isotope studies along with the new zircon U-Pb and Hf data presented in this study. See section 6.4 for further discussion.

Chapter 3: Characterization of Zircon Inheritance and Thermometry Informs the Potential Origin of High-Zr Grenville Granitoids

In preparation for submission to:

Contributions to Mineralogy and Petrology

Abstract

The origin of granites produced during the Grenville orogeny (1.3-1.0 Ga) containing extraordinarily high concentrations of zirconium (Zr) is explored. Previous workers hypothesized that one mechanism responsible for their enrichment is by the significant incorporation of zircon xenocrysts. We measured U-Pb in approximately 200 zircon grains per igneous sample to test this hypothesis. Results indicate that Grenville high-Zr granites contain less than <10% xenocrysts, with several being xenocryst-free. Thus, xenocryst incorporation into these melts to produce Zr-enriched magmas is not the likely mechanism. Instead, zircon extracted from high-Zr granites (>500 ppm) record unusually high-temperature magmatic conditions during their formation, allowing for increased zircon solubility at the melt source.   Temperatures as high as 1045 °C were determined using the Ti-in-zircon thermometer and as high as 1050 °C with the zircon saturation thermometer. To explore how this compares to granites with mid- to low-Zr concentrations (<300 ppm), several plutons of both Grenville and non-Grenville age were sampled. Non-Grenville age samples studied here contain a significant xenocryst budget (>28%) and were determined to have formed in lower-temperature magmatic conditions, evidenced by Ti-in-zircon and zircon saturation thermometer temperatures between 605 and 780 °C.

Chemical priming of the crust prior to Grenville Orogenesis (1.08-0.98 Ga) coupled with high-temperature conditions prevailing during the Ottawan (1.08-1.01 Ga) and possibly the Rigolet (1.0-0.98 Ga) phases of the Grenville Orogeny acted together to create the conditions necessary for high-Zr granitoid production. Concentration of restitic zircon at low- to mid-crustal levels during the Pre-Elzevirian, Elzevirian, and

Shawinigan orogenies acted as the mechanism to enrich these crustal levels in zircon. Previous workers have used zircon Hf-O from the same rock units as this study to show they are not juvenile and instead record the recycling of 1.5-2.0 Ga crust.

1. Introduction

The Grenville Orogeny (1.2-0.9 Ga) has been interpreted to be the zenith of mountain building events in Earth's history, forming a mountain belt nearly 20,000 km long by 800 km wide (Van Kranendonk and Kirkland, 2013). Igneous rocks of the Grenville orogen in North America extend from Newfoundland, Canada to sparse segments of granitoid rocks in Mexico (Whitmeyer and Karlstrom, 2007; McLelland et al., 2013; Van Kranendonk and Kirkland, 2013). Granitoid rocks produced during this orogeny contain extraordinarily high concentrations of zirconium (Zr), in some cases exceeding 10x that of the upper crustal average of 190 ppm (Fig. 1; Taylor and McLennon, 1985; Moecher and Samson, 2006; Dickinson, 2008; Moecher et al., 2014; Samson et al., 2018). In this study we explore two potential mechanisms by which they could have been enriched.

Determining accurate temperatures of felsic magmas that crystallized to form granitic plutons is important to a wide variety of studies, including mechanisms of magma extraction and ascent, constraining potential heat sources, assessing degrees of fractional crystallization, and providing insights into potential temporal changes in thermal conditions of magmatic systems. Despite the importance of ascertaining accurate temperatures for these applications, doing so has remained a difficult task.

The landmark study of Watson and Harrison (1983) demonstrated that zircon crystallization is dependent on the temperature, chemistry, and bulk Zr content of the melt from which they crystallize (i.e., the zircon saturation thermometer; $^{zrc}T_{sat}$). For an accurate maximum temperature using the $^{zrc}T_{sat}$ thermometer, one must consider the effects of Zr content of melt source material, the degree of melting of that source, and whether or not the melt produced was saturated in zircon upon melting (i.e., entrainment of xenocrystic zircon). Miller et al. (2003) defined important constraints of the meaning of temperatures calculated using the $^{zrc}T_{sat}$ thermometer. In xenocryst rich plutons, the temperature calculated is the initial temperature of the melt whereas in xenocryst poor/free plutons the temperature calculated is likely an underestimate of their initial temperature. However, Moecher et al. (2014) found the best estimate of the initial temperature in xenocryst-free melts using the $^{zrc}T_{sat}$ thermometer was achieved using high-Zr granites because zircon reaches saturation earlier in the crystallization sequence.

Titanium (Ti) uptake into the zircon structure is temperature dependent, thereby providing another useful measure of zircon crystallization temperatures (i.e., the Ti-in-zircon thermometer; $^{zrc}T_{Ti}$; Watson et al., 2006; Ferry and Watson, 2007). To properly obtain meaningful crystallization temperatures, however, one must consider several potential pitfalls. The limitations purportedly inherent to the present Ti-in-zirconsolubility model and their bearing on the geologic meaningfulness of the Ti-in-zircon thermometer are beyond the scope of this paper, but it is acknowledged that a refined model incorporating a potential pressure correction would undoubtably solidify the validity of the current model. It has been demonstrated that the diffusion of Ti in zircon is

extremely slow, even in grains that have experienced protracted high temperature conditions (Cherniak and Watson, 2007). One potential limitation considered in this study is the degree to which the measured Ti-concentration via SIMS or LA-ICP techniques is the result of ablating Ti-bearing inclusions (e.g., Fu et al., 2008). The way in which this was evaluated is discussed further in the methods section. Lastly, determining the activity of TiO_2, a requirement for determining accurate Ti-in-zircon temperatures, in granitoids this is often difficult because rutile does not occur as a primary mineral in granitoids. Despite the potential pitfalls, the Ti-in-zircon thermometer has been used in several petrological studies with success (e.g., Watson and Harrison, 2005; Claiborne et al., 2010; Moecher et al., 2014; Schiller and Finger, 2019). We use this thermometer to estimate the temperatures at which Grenville granitoids crystallized.

Samson et al. (2018) presented several hypotheses to explain the origins of Grenville high-Zr granitoids. Data produced for this study allows for the detailed testing of two of their five hypotheses- 1) They contain a large number of inherited (xenocrystic) grains, thereby elevating their measured Zr-contents and 2) high magmatic temperatures increased the ability to incorporate Zircon at the source before the melt was saturated in zircon. Additionally, the hypothesis that copious amounts of continental crustal recycling, in the form of sediment delivery to subduction zones (and hence detrital zircon), may account for the high-Zr contents in Grenville granitoids will also be discussed in light of the new zircon Hf-O data set given in Chapter 2.

An important aspect of this study involves the analysis of large-*n* (i.e., >30 analyses per samples) zircon U-Pb and Ti-in-zircon measurements of non-Grenville granite samples with modest to low Zr values, collected from locations near the Grenville

granitoids, for comparison to the Grenville-aged samples. This was done as a form of "control" samples to compare more typical granites to the unusual Grenville granitoids. It also provides a unique opportunity to discuss how xenocrysts may (or may not) affect the measured Zr concentration in a pluton. Lastly, the ages of the measured xenocrysts in the non-Grenville samples provides useful information to the sources of the material incorporated into these granitoids which intruded the same crustal regions as those of the Grenville granitoids.

2. Previous work/sample descriptions

Samples for this study come from Mesoproterozoic Grenville-aged igneous or meta-igneous rocks exposed in the Appalachian Inliers of the New Jersey-Hudson Highlands, Shenandoah massif in Virginia, and the French Broad massif in western North Carolina. For all of the samples from the French Broad massif (Great Smoky augen gneiss NC17-1; Fines Creek gneiss NC17-2; Fines Creek gneiss NC17-3; Max Patch granite NC17-5; Earlies gap granitoid gneiss NC17-6; Toxaway gneiss NC17-10, Doggett Gap granitoid gneiss NC19-7; Earlies Gap charnockite NC19-9), the U-Pb data are taken from Chapter 1. For samples from the New Jersey-Hudson Highlands and the Shenandoah/Pedlar River massifs (Mt. Eve granite NJ15-1; Stage Road Suite charnockite VA12-1; Low Silica charnockite VA12-2; Stage Road biotite granite VA15-1; Pedlar River leuco-charnockite VA15-2) the U-Pb data were taken from Moecher et al. (2014), Burk (2017), Samson et al. (2018), and Chapter 2. As was mentioned above several non-Grenville age plutons were sampled for comparison. Of those, the Rabun granite (sample GA17-1), Looking Glass granite (sample NC17-8), Henderson gneiss

(Sample NC17-9), and the Whiteside granite (sample NC17-11) all come from the eastern Blue Ridge province of south-central North Carolina. These were originally dated by Miller et al. (2000) by ion-probe techniques but were re-dated here by LA-ICPS-MS techniques for the purposes of establishing the xenocrystic component. Three additional samples from the North Carolina Piedmont, which include the Danburg, Wise, and Wyatt granites, were analyzed for their whole-rock chemistry and Ti-in-zircon contents

3. Methods

Whole-rock and trace element analyses were conducted for use in Rhyolite-MELTS modeling and to utilize the zircon saturation thermometer. For sample preparation techniques and results see Chapters 1 and 2. For new samples of this study (GA17-1, NC17-8, NC17-9, and NC17-11) measurements were made using the Thermo ARL Perform'X X-ray fluorescence (XRF) spectrometer at the Hamilton Analytical Laboratory (Hamilton College, NY). Analytical conditions are described by Johnson et al. (1999) and Table 1 presents the results of the analyses and calculated M values (molar $[(K+Na+2*Ca)/(Al*Si)]$; Watson and Harrison, 1983; Hanchar and Watson, 2003).

To establish the potential xenocrystic component of a pluton, the analyses of an extremely larger number of zircon crystals than would normally be determined for the purposes of dating a pluton was completed. For details on sample preparation and zircon textural characterization by backscattered electron (BSE) and cathodoluminescence (CL) imaging see Chapters 1 and 2. Backscattered electron and CL images for new samples presented in this study (GA17-1, NC17-8, NC17-9, and

NC17-11) are given in the supplementary material. U-Pb isotopic data were collected using the Thermo Element2 laser ablation inductively coupled plasma mass spectrometer at the LaserChron laboratory at the University of Arizona following the methods of Pullen et al. (2018). Standards measured during the analytical session were FC1, SL, and R33. To confirm the spot locations used for measuring Ti contents were in Grenville-aged domains, U-Pb measurements were simultaneously measured following Coble et al. (2018) and Spencer et al. (2019), respectively. Age standards used at Stanford University were Temora-1, 91500, MAD and MADDER. The primary age standards used at Curtin University were FC1, GJ1, Plesovice, R33, and 91500. The age data for both samples and standards are presented in Chapters 1 and 2 but are briefly mentioned here.

Titanium contents were measured by two techniques, via the SHRIMP-RG at Stanford university and the SS-LA-ICPMS at Curtin University in Perth, Western Australia. Trace element standards measured at Stanford include 91500, MAD, MADDER, and Temora-1. Trace element standards measured at Curtin University include FC1, MUN, 530, GJ1, MUD, OGC, Plesovice, P1, R33, and 91500. Rare-earth elements (REE) were measured at both institutions simultaneous to the measurement of the Ti-concentrations. Iron (Fe) was also measured with the SHRIMP-RG to identify analytical spots ablating non-zircon material. The measurements of Fe and REE were evaluated in both real-time (to stop analysis and pick a new analytical spot) and post-session analysis of the raw data (for automated runs) to determine if the analytical spot ablated either Fe(Ti)-rich micro-inclusions or other inclusions (e.g., apatite, feldspar, etc). If an analyzed zircon contained more than 25 ppm Fe it was not used for Ti-in-

zircon temperature calculations. Chondrite normalized REE patterns from the

remaining analyses were then generated. A typical zircon REE pattern from figure 1 in

Hoskin and Schaltegger (2003) was used as a guide. If an analyzed zircon contained a

lanthanum (La) value (chondrite normalized) greater than 10 then it was not used in Ti-

in-zircon temperature calculations.

   To better constrain the activity of TiO_2 ($a_{TiO_2}^{rutile-melt}$, referenced to rutile at standard

state conditions, i.e., 1 bar and 25 ºC) in the magmatic system, Rhyolite-MELTS

modeling was employed (Gualda et al., 2012; Ghiorso and Gualda, 2013; 2015).

Results were produced using the following protocol- 1) Major elements are entered into

the graphical user interface 2) H_2O-contents of each sample are assumed to be the

measured loss on ignition (LOI) values determined during XRF sample preparation 3)

model conditions were set to run at an isobaric pressure of 5 kbar 4) oxygen-fugacity is

buffered using the quartz-fayalite-magnetite (QFM) buffer 5) the resulting compositions

are normalized to 100% 6) the liquidus was determined 7) the system was allowed to

cool in 25 ºC increments until completely crystallized (or less than 2% liquid remained)

8) rutile affinity was determined, and final temperature recorded from results of model

run. Affinity is related to the chemical equilibrium of a particular phase within a well-

defined chemical system (Ghiorso and Gualda, 2013). If a phase (e.g., SiO_2) is part of

an equilibrium assemblage, then its affinity is zero. The further from equilibrium a

phase is, the higher its affinity value becomes. Rutile affinity was converted to activity

using the following equation (Ghiorso and Gualda, 2013; Schiller and Finger, 2019):

$$aTiO_2 = e^{\frac{-A}{RT}}$$

where A is the determined rutile affinity, R is the gas constant, and T is the last temperature step in Kelvin run in the model. The results of the model runs and calculated rutile affinities are presented in Table 2.

The majority of Zr in a rock is contained in the mineral zircon (500,000 ppm; Samson et al., 2018). Thus, identifying the percent of xenocrysts in a rock allows for a calculation of a new, corrected whole-rock Zr concentration. This in turn can be re-entered into the equation for the zircon saturation thermometer to obtain a more robust determination of the melt temperature at the time zircon reached saturation. A xenocryst is here characterized by whether an individual analyses lies within error of the interpreted age of the unit. For example, if a rock had an interpreted crystallization age of 100 ± 1 Ma, then any individual analysis with a date greater than 101 Ma could be considered a xenocryst. However, given the large uncertainty on any single measurement (i.e. 1-4%) a more realistic cutoff in this example would be greater than 104 Ma. The results of this analysis and the resulting corrected whole-rock Zr-concentrations and $^{zrc}T_{sat}$ are given in Table 3.

4. Results

4.1. U-Pb results

Rabun granite (GA17-1)

A total of 147 zircon U-Pb measurements were performed on the Rabun granite. Textures revealed by CL imaging are complex for this sample. Cores are often bright and oscillatory zoned surrounded by very dark, yet faintly oscillatory zoned mantles. Almost every grain has a bright, texture-less rim domain. A cluster of 94 grains produce

a ^{206}Pb/^{238}U weighted mean date of 339 $\pm$ 0.42 Ma (MSWD = 31) which is interpreted as the best estimate of the crystallization age of this unit (Fig. 2a). Miller et al. (1998) interpreted the age of the Rabun granite to be 374 $\pm$ 4 Ma. The remaining 53 analyses are generally spread between 800 and 1200 Ma, the upper end of which (i.e., 1000-1200 Ma) is within a spread of ages commonly seen in crystalline basement rocks ~100 km to the north (see Chapter 1). The younger end of this spread (800-900 Ma) is likely the result of the analytical spot hitting mixed growth zones, as 800-900 Ma age material is not a common age seen in the area. Three analyses have ^{207}Pb/^{206}Pb dates of c.a. 1350 Ma and the oldest analysis has a ^{207}Pb/^{206}Pb date of 1874 Ma, suggesting the melt that went on to crystallize the Rabun granite intruded and incorporated crust of significantly older age.

Looking Glass granite (NC17-8)

A total of 77 zircon U-Pb analyses were performed on the Looking Glass granite. Textures revealed by CL imaging are complex. Most grains contain bright cores, displaying either oscillatory zoning or are featureless. Core boundaries are distinct and are either rounded or subhedral. Cores are surrounded by zones with very low CL intensity and are also featureless. A cluster of 15 grains yield a concordia date of 352 $\pm$ 0.9 Ma (MSWD = 2500) which is interpreted as the best estimate of the crystallization age of this unit (Fig. 2b). Miller et al. (2000) interpreted the age of the Looking Glass granite to be 380 Ma. The remaining 62 analyses are spread along concordia, most with individual dates ranging from 800-1400 Ma. Similar to the Rabun granite, and in conjunction with post-analyses CL verification, the lower range of this spread (i.e., 800-900 Ma) is likely the result of the analytical spot intersecting two distinct growth zones,

producing mixed dates. However, analyses with dates ranging from 1000 to ~1380 Ma are not exotic dates for this region, as Moecher et al. (2020) identified orthogneisses with similar interpreted crystallization ages. The five oldest grains analyzed within this sample have individual ^{207}Pb/^{206}Pb dates of 1410, 1457, 1459, 1735, and 1960 Ma, significantly older than any known exposed crust in the southern Appalachians, yet evidence of material incorporated into the Looking Glass granite.

Henderson gneiss (NC17-9)

A total of 129 zircon U-Pb analyses were performed on the Henderson gneiss. Textural characteristics evinced by CL imaging are simple. Most grains have oscillatory or sector zoned cores with variable CL intensities. Cores grade smoothly into outer core and rim domains with little to no sharp boundaries separating different zones. A ^{206}Pb/^{238}U weighted mean date of 443 ± 0.43 Ma (Fig. 2c; MSWD = 14) is defined by all analyses and is interpreted to represent the best estimate of the crystallization age of the Henderson gneiss.

Whiteside granite (NC17-11)

A total of 129 zircon U-Pb analyses were performed on the Whiteside granite. Textural characterization via CL reveals a complex growth history for grains within this sample. Textures within cores range from dark and featureless to bright with clear oscillatory zoning. Some grains also display a mottled texture with light CL intensity. Core domains typically have sharp boundaries and the edges range from rounded to subhedral. The complexity of the textures manifests itself in the complexity of the U-Pb results. A cluster of 76 analyses yields a ^{206}Pb/^{238}U weighted mean date of 452 ± 0.62 Ma (MSWD = 41) and provide the best estimate for the crystallization age of this unit.

Miller et al. (2020) obtained an age of 465 Ma for this unit. Similar to both the Rabun

and Looking Glass granites, the Whiteside granite contains grains with dates with a very

large spread (Fig. 2d). Dates range from ~750 to 2565 Ma, with the majority within the

range of 1000-1200 Ma. The five oldest grains analyzed in this sample have individual

^{207}Pb/^{206}Pb dates of 1536, 1604, 1790, 1857, and 2565 Ma. These dates are

significantly older than any known exposed crust in the southern Appalachians.

4.2 Xenocrystic component

   A large number of grains were analyzed for each sample to establish the potential

xenocrystic component within each sample, which in turn allows for testing of the

hypothesis that Grenville high-Zr granites were enriched by this mechanism. The

method used to determine a xenocryst was outlined above in the methods section and

the results of this analysis are presented in Table 3. The resulting change to the

measured whole-rock Zr concentration vs xenocryst-corrected whole-rock Zr

concentrations is illustrated in figure 3. To summarize the results, all non-Grenville

aged samples except one (NC17-9) contained a very high percentage of xencocrysts,

ranging from 27 to 82%. The Henderson gneiss does not contain any xenocrysts, at

least for the grains measured and the methods used to distinguish xenocrysts from non-

xenocrysts. The significance of this will be addressed in the discussion section. All

Grenville aged samples except one (NC17-1) contained a very low xenocryst budget,

with most less than 5% (Table 3).

4.3 Zircon thermometry

4.3.1 Zircon Saturation

Zircon saturation thermometry is an easy-to-implement tool allowing for rapid determination of magmatic temperatures at the time of zircon crystallization. Temperatures for the Rabun, Looking Glass, Henderson, and Whiteside only are considered here because they are the non-Grenville age samples for which zircon U-Pb, and therefore xenocrystic components, were determined. From these, the measured zircon saturation temperatures are 761, 721, 859, and 753 °C, respectively. When considering the determined xenocrystic component for these samples, zircon saturation temperatures become 736, 605, 859, and 726 °C, also respectively. The difference between the measured Zr-concentration and the xenocryst corrected Zr-concentration for Grenville samples (and therefore corrected $^{zrc}T_{sat}$) is negligible because of their extremely low xenocrystic components. Thus, only the Great Smoky Mountains augen gneiss is presented here, refer to Table 3 for all others. For this sample, it was determined it contained 28% xenocrysts, changing its calculated $^{zrc}T_{sat}$ value from 830 to 800 °C.

4.3.2 Ti-in-zircon

After filtration of the data as outlined above in the methods section, a total of 202 out of 734 analyses were rejected and not used for Ti-in-zircon temperature calculations, leaving 532 suitable analyses. See the supplementary files for all Ti and REE data. Refer to Table 2 for the Rhyolite-MELTS and resulting calculated TiO_2 activities. Table 3 provides a summary of the resulting Ti-in-zircon temperatures.

5. Discussion

The results of this study allow for a comprehensive evaluation of the hypothesis set forth by Samson et al. (2018) that one mechanism by which Grenville granitoids have high measured Zr concentrations is due to the incorporation of xenocrystic grains. In so doing, an approach to potentially determine more meaningful zircon saturation temperatures is discussed. Using this approach and Ti-in-zircon thermometry, the high-temperature hypothesis of Moecher et al. (2014) and Samson et al. (2018) for Grenville granites is tested.

The tectonic conditions that produced high-Zr granites will also be discussed. Samson et al. (2018) suggested that chemical priming of the continental crust prior to the onset of high-temperature melting during the Grenville could produce high-Zr granitoids. The thermometry results from this study and the results of zircon Hf-O results presented in Chapter 2 from the central and southern Appalachians allow for the evaluation of this hypothesis.

5.1 Xenocrysts do not contribute to the high-Zr nature of Grenville granitoids

The zircon U-Pb results from this study, those from Samson et al. (2018), and those presented in Chapters 1 and 2 do not support the hypothesis that Grenville high-Zr granites were enriched in Zr due to xenocryst incorporation. Of the 13 samples between the above mentioned studies, only one has a xenocryst budget over 8%, that being the Great Smoky Mountains augen gneiss (NC17-1; Table 3). In fact, outside of this sample only 28 xenocrysts were identified from a total of 1026 analyses, accounting for only 2.7% of the total grains analyzed.

A rock containing a large population of xenocrysts will not necessarily have an elevated Zr concentration. For example, three of the four non-Grenville aged samples studied here contain a minimum of 27% xenocrysts yet the maximum Zr concentration between them is 125 ppm, 65 ppm below an estimate of the upper continental crustal average of 190 ppm (Taylor and McLennon, 1985).   Our study does not preclude all high Zr granitoids from containing a significant xenocryst population, nor does it imply that most low Zr granitoids will contain abundant xenocrysts. However, our study does show that the high Zr content of many Grenville granitoids is not controlled by an abundant xenocryst population. Furthermore, it shows that geographically proximal low-Zr granitoids do not have a low abundance of zirconium due to a lack of xenocrysts.

5.2 High-temperature magmatic conditions

The rocks studied here with extremely elevated whole-rock Zr concentrations are otherwise geochemically "normal", begging the question how did they become so enriched? The zircon Ti data from this study strongly supports the conclusions of Moecher et al. (2014) and Samson et al. (2018) that Grenville high-Zr granites were formed under unusually hot magmatic conditions. Average measured zircon Ti-concentrations are among some of the highest recorded in natural samples, with sample VA15-1 (Stage Road Suite biotite granite) having an average concentration of 54 ppm (Fig. 4). Only one sample (NC17-10, Toxaway gneiss) has an average Ti concentration below 10 ppm. Comparing these to the non-Grenville "control" samples further highlights the unusual nature of the Grenville samples. All of these samples have zircon Ti concentrations below 10 ppm, and four out of five are below 5 ppm. The

difference of the average values for each sample between the Grenville and non-Grenville samples is 18 ppm, again highlighting the extreme difference between these two subsets of granitoids. To further highlight the high-Ti nature of the Grenville zircon measured here, Ti-contents in zircon were compiled from the geochemical data base EarthChem (Fig. 5) and from Fu et al. (2008). The Grenville zircon analyzed in this study have a mean of 28 ppm (n = 532) whereas zircon in the EarthChem data base have a mean of 9.3 ppm (n = 3,798; Fig. 5), further demonstrating the high-Ti nature of our samples. Fu et al. (2008) produced a large data set of zircon Ti-concentrations from intermediate-felsic rocks from the Sierra Nevada batholith. Comparing the results of our Ti-in-zircon thermometry to their data set again clearly demonstrates the high-temperature nature of our sampled units (Fig. 7).

In some samples the measured zircon Ti concentrations were higher in those produced by laser ablation than by ion probe (Fig. 4). Datum produced by both techniques were scrutinized using the same filters outlined in the methods section. No appreciable differences in either chondrite-normalized REE abundances or REE curve shapes were observed between the two techniques. Though hard to quantify, it is possible that coincidentally the spots chosen for analysis by laser ablation were in growth zones containing high Ti concentrations. Alternatively, the differences can be reconciled by the different procedures used to correct for potential isobaric interferences between the two laboratories. Apparent elevated Ti concentrations was observed for samples VA12-1, VA15-1, VA15-2, NC17-1, and NC17-3, although it was not observed in NC17-5 or NC17-10. In samples where it was observed, the values were within a

range that is interpreted to be geologically plausible (i.e., 10-25 ppm). Hence, they are retained here for use in determining temperatures.

Translating Ti data to temperatures can be difficult as it is necessary to constrain the activity of TiO_2 in igneous systems. Early workers estimated $aTiO_2$ in granitoids to be near sub-unity values of 0.6-0.9, based primarily on the presence of minerals within the rock unit containing Ti as a stoichiometric component of its structure (Watson and Harrison, 2005; Moecher et al., 2014). However, more recent studies estimate $aTiO_2$ to be closer to 0.1-0.6, based on equilibrium thermodynamic modelling using rhyolite-MELTS (Schiller and Finger, 2019). Rhyolite-MELTS modelling was used to estimate titania activity and our results are similar to those of Schiller and Finger (2019) in that all samples have sub-unity values between 0.37-0.59 (Table 2). Using this method, it is apparent the Grenville zircon from our samples crystallized at higher temperatures than the non-Grenville granites used for comparison (Fig. 6). There is one notable exception to this, and that is the Henderson Gneiss (sample NC17-9). It has the highest measured whole-rock Zr concentration of the non-Grenville aged samples (395 ppm). Additionally, no xenocrysts were identified from any of the 126 analyses (Table 3). Finally, it has the highest measured zircon Ti values of all the non-Grenville aged samples (13 ppm). It is no surprise then the Henderson gneiss demonstrates characteristics similar to those seen for our Grenville samples. This result is promising because it demonstrates these characteristics are transferrable to any pluton that contains an elevated whole-rock Zr content and a limited xenocryst budget.

Harrison et al. (2007) recognized that the spread often seen in Ti-in-zircon temperatures is likely due to continued zircon crystallization starting at the beginning of

zircon saturation down to complete solidification of the magma, what they call the Ti-in-zircon temperature spectra. They also recognize that if $aTiO_2$ is not at unity (i.e., $aTiO_2$ = 1) at the time zircon is crystallizing, then the resulting calculated temperature is an estimated minimum (Harrison et al., 2007). This phenomena is well documented by the spread in measured Ti concentrations (and subsequent calculated temperatures) for most of our samples (Fig. 4). Two observations can be made when comparing the 3rd quartile Ti-in-zircon temperatures against the calculated xenocryst-corrected whole-rock zircon saturation temperatures (Fig. 6). For the control samples, most of which contain a significant xenocryst budget, the corrected whole-rock zircon saturation temperature is greater than the 3rd quartile Ti-in-zircon temperature. Conversely, for the Grenville samples, the corrected whole-rock zircon saturation temperature is less than the 3rd quartile Ti-in-zircon temperature. These observations corroborate the conclusion made by Miller et al. (2003) that the geologic utility of the zircon saturation thermometer is dictated by the presence of inherited zircon in a plutonic rock. That is, zircon saturation temperatures from plutons containing a high budget of inherited zircon represent the maximum temperature possible by that method, and zircon saturation temperatures from plutons with minimal to no inherited zircon represent minimum temperatures by that method. Thus, for the latter scenario, employing multiple thermometery methods together aid in constraining the initial magmatic temperatures. This subsequently allows for better constraints on the mechanisms responsible for magma extraction and ascent, as well as potential heat sources. Furthermore, the degree to which the zircon saturation thermometer may underestimate the initial magmatic temperatures for plutons with little to no inherited zircon is illustrated in figure 6. Several Grenville

samples have similar 1st quartile and xenocryst corrected temperatures. This may

provide evidence that zircon saturation temperatures from xenocryst-poor plutons can

be interpreted as the conditions prevailing towards the later stages of magma

crystallization. Although, this method may underestimate the initial magmatic conditions

by as much as 100 °C.

5.3 Tectonic considerations

5.3.1 Chemically primed crust prior to Grenville orogenesis

The southeastern Laurentian margin was tectonically active during the

Mesoproterozoic (McLelland et al., 2013; Tollo et al., 2017; Moecher et al., 2020; see

Chapter 1; plus many others). A protracted history of continental arc magmatism and

accretion of island arc terranes is well documented. It is also well established that

zircon is a refractory mineral and will typically be left behind in the restitic material

during low-temperature melting conditions (Watson and Harrison, 1983; Miller et al.,

2003; Boehnke et al., 2013). Because of this, Samson et al. (2018) hypothesized that

one possible mechanism to enrich the continental crust in zircon is by low temperature

melting. In the case of the Laurentian margin during the Mesoproterozoic, several

tectonic events may have served to enrich the crust by this process. For example, prior

to the onset of the Grenville Orogeny (*sensu stricto*; 1080-980 Ma; Gowers and Krogh,

2002) the Pre-Elzevirian (1380-1330 Ma), Elzevirian (1290-1250 Ma) and Shawinigan

Orogenies (1190-1140 Ma) all may have served to enrich the crust in zircon by

production of mostly moderate temperature granites at the Laurentian margin.

Subsequent continent-continent collision between Laurentia and Amazonia during the

Ottawan (1080-1010 Ma) and Rigolettan (1000-980 Ma) phases of the Grenville

Orogeny was evidently a high temperature event. This is not only evident by pervasive

high-temperature metamorphism on an orogen-wide scale but is also recorded by high

temperature magmatism (Rivers et al., 2012; Moecher et al., 2014; Burk, 2017; this

study). The geochemistry of high-Zr granitoids offers additional context into their high-

temperature origin. For example, all rocks studied here with high whole-rock Zr

concentrations are A-type granites, often associated with low-H_2O magmatic conditions

(Pearce et al., 1984; see Chapters 1 and 2). This is verified by anhydrous mineral

assemblages and measured LOI for XRF analyses (Moecher et al., 2014; Burk, 2017;

this study). Hence, several lines of evidence now exist from multiple studies leading to

the interpretation that Grenville granites are most likely the product of high temperature

melting of potentially chemically primed crust (i.e., zircon fertile).

5.3.2 Implications of old xenocrysts in Paleozoic southern Appalachian granites

Xenocrysts analyzed from the Whiteside, Looking Glass, and Rabun granites

offer additional insight into the age of the crust into which they were intruded. Crustal

material of significantly older age than any known to exist at the current level of

exposure was incorporated into these magmas, with dates ranging from 1400-2565 Ma.

Similar dates were identified by Miller et al. (2000) and they speculated either the

configuration of Paleoproterozoic and Archean crust was complex or that they are from

a terrane not of Laurentian affinity. A myriad of isotopic studies have been conducted

since their publication documenting the likelihood that the Mesoproterozoic crust in the

southern Appalachians is not of Laurentian affinity (Sinha et al., 1996; Sinha and

McLelland, 1999; Carrigan et al., 2003; Ownby et al., 2004; Fisher et al., 2010; Moecher et al., 2020; Chapter 2). Most recently, my study presented in Chapter 2 used zircon Hf isotopes from the same rocks as this study (Shenandoah and French Broad massifs) and found that zircon Hf model ages for these rocks range from 1390-2070 Ma (Table 3). The dates of the measured xenocrysts from these samples corresponds well to the Hf model ages calculated in Chapter 2 and corroborate their claim that Mesoproterozoic crust in the southern Appalachians is not of Laurentian affinity and instead is most likely of Amazonian affinity.

5.3.3 Role of crustal recycling in high-Zr granitoid production

To strengthen the argument made herein that chemical priming of the continental crust prior to Grenvillian magmatism is the most likely mechanism by which high-Zr granitoids were produced, a brief examination of the zircon Hf-O data presented in Chapter 2 is considered. The rocks used in this study are identical to those used for that study, at least those within the Shenandoah/Pedlar River and French Broad massifs. They found that most of their samples had zircon $\delta^{18}O$ values between 6.0 and 8.0‰ (Table 3, Chapter 2). In addition, initial εHf values were mildly positive, with most values between -0.5 and +4 εHf units (Table 3). These two lines of evidence suggest that there was a significant degree of crustal recycling involved in the petrogenesis of the units they studied. Indeed, the interpretation that chemical priming of the continental crust prior to high-Zr magma production necessitates that a significant degree of crustal recycling occurred. Thus, the results presented in Chapter 2 coupled with the results of this study support the notion that chemical priming of the crust by

prior low-temperature magmatism with subsequent high-temperature magmatism during the Ottawan phase of the Grenville Orogeny acted together to produce some of Earth's most zircon fertile magmas.

6. Conclusions

Several studies over the last decade have been undertaken to better understand the origin of the Grenville high-Zr granitoids (Moecher et al., 2014; Burk, 2017; Samson et al., 2018; this study). Compelling evidence is now available to reasonably conclude that the high-Zr nature of Grenville granitoids is likely the result of unusually high magmatic temperatures for granitic compositions. This evidence includes 1) zircon xenocryst populations appear to be very minimal in Grenville high-Zr granitoids, typically less than 10% 2) zircon saturation temperatures, corrected for xenocryst components, demonstrate that zircon began crystallizing in these granitoid compositions at temperatures as high as 1050 °C 3) Ti-contents in zircon include some of the highest yet measured in natural samples, where the Stage Road Suite biotite granite (sample VA15-1) contains an average zircon Ti concentration of 62 ppm 4) Ti-in-zircon thermometry indicates that zircon was crystallizing at temperatures as high as 1045 °C.

The tectonic history of the Laurentian margin prior to Grenville orogenesis allowed for the production of high-Zr granitoids. Repeated amalgamation of material to the Laurentian margin coupled with magmatism associated with the Pre-Elzevirian, Elzevirian, and Shawinigan orogenies acted to enrich the restitic continental crust in zircon. The temperature conditions prevailing at the Laurentian margin related to the assembly of Rodinia during the Ottawan and Rigoletan phases were sufficiently high to

melt the restitic zircon and incorporate them into undersaturated magmas. Zircon Hf-O evidence supports the interpretation that the petrogenesis of Grenville high-Zr magmas included both juvenile and evolved components (see Chapter 2).

Protocols were developed to maximize the geologic utility of the zircon saturation and Ti-in-zircon thermometers. To provide more robust geologic interpretations of magmatic temperatures using zircon saturation thermometry, it is recommended that one account for the contribution of xenocrysts to the measured whole-rock Zr concentration. This is especially important in units that contain a significant population of xenocrysts as uncorrected zircon saturation temperatures will be geologically erroneous. It is also recommended that Rhyolite-MELTS be used to model the TiO_2 activity to be used in the Ti-in-zircon thermometer. The Ti-in-zircon thermometer is also believed to be more useful for estimating initial magmatic temperatures in rocks with greater than 500 ppm Zr, since the zircon saturation thermometer is a minimum under these conditions (assuming an insignificant xenocryst population can be established) whereas the Ti-in-zircon thermometer is more likely to capture temperatures nearer the initial magmatic conditions.

Table 1. Whole-rock major and trace element geochemistry. For samples NC17-1 thru NC19-9, see Chapter 1.

Sample	Harbison	Danburg	Wise	Wyatt	GA17-1	NC17-8	NC17-9	NC17-11	NJ15-1	VA12-1	VA12-2	VA15-1	VA15-2
M value	1.6	1.6	1.3	1.4	1.4	1.4	1.5	1.5	1.9	1.4	2.1	2.0	2.3
SiO2	66.72	69.74	74.90	72.49	71.81	72.18	68.55	70.83	66.81	67.18	60.06	61.34	58.42
TiO2	0.62	0.52	0.11	0.31	0.24	0.22	0.62	0.19	0.76	0.84	1.84	1.63	2.16
Al2O3	15.78	14.44	13.80	14.55	14.89	15.19	15.01	16.42	13.68	13.96	14.11	13.28	14.45
FeO*	3.35	2.53	0.61	1.64	1.47	1.36	3.33	1.38	4.60	4.96	8.18	9.48	9.41
MnO	0.06	0.05	0.01	0.03	0.02	0.03	0.07	0.03	0.11	0.15	0.12	0.15	0.14
MgO	1.35	0.77	0.20	0.34	0.60	0.62	0.83	0.68	0.78	0.53	1.30	1.01	1.74
CaO	2.71	2.13	0.80	1.25	2.36	1.53	2.01	3.28	2.77	1.27	4.56	3.93	5.59
Na2O	4.32	3.49	3.86	3.32	4.25	4.94	3.46	5.10	3.29	2.60	2.73	2.98	3.03
K2O	3.83	4.84	4.72	5.34	3.07	3.18	5.18	1.35	5.64	5.96	4.30	3.48	3.32
P2O5	0.24	0.15	0.02	0.09	0.09	0.07	0.19	0.07	0.19	0.23	0.94	0.73	1.00
Ni	11.4	3.3	2.6	n.a.	3.4	3.2	3.5	7.2	7.7	5.2	4.5	6.1	7.8
Cr	16.0	8.9	8.4	n.a.	11.5	9.7	8.0	15.8	196.1	7.0	9.0	65.5	91.7
V	55.2	41.0	5.7	n.a.	24.8	18.9	38.2	21.7	12.9	13.2	59.3	43.1	91.4
Sc	5.6	5.1	1.0	n.a.	3.0	2.8	9.1	3.0	8.8	12.2	18.4	22.0	23.3
Cu	10.0	5.6	2.9	n.a.	2.4	5.1	7.2	2.6	17.7	2.3	7.9	9.0	10.4
Zn	58.4	56.2	27.6	n.a.	35.6	47.1	60.9	24.9	137.8	118.7	196.4	228.9	213.2
Ga	19.2	19.1	20.7	n.a.	17.6	21.2	20.2	19.2	24.3	22.3	27.5	28.9	28.1
Ba	968.3	968.3	299.2	n.a.	796.8	753.2	958.2	359.0	1998.0	2648.0	2510.7	2553.5	1794.6
Rb	125.5	159.3	123.8	n.a.	73.6	94.4	163.0	41.5	137.6	148.7	118.2	95.0	76.7
Cs	0.7	0.0	2.5	n.a.	0.6	3.0	4.9	0.0	1.8	0.0	1.2	1.2	1.0
Sr	781.7	324.6	101.8	n.a.	485.1	459.8	186.1	725.5	377.7	225.5	560.8	353.0	576.7
Y	14.5	22.9	3.0	n.a.	5.0	4.9	38.0	1.9	158.3	24.8	67.3	71.2	81.2

Sample	Harbison	Danburg	Wise	Wyatt	GA17-1	NC17-8	NC17-9	NC17-11	NJ15-1	VA12-1	VA12-2	VA15-1	VA15-2
Zr	199.7	270.6	63.5	219.0	124.5	73.0	395.0	112.7	1306.2	1297.8	866.1	2374.8	974.4
Hf	4.0	7.1	0.8	n.a	2.2	1.1	10.0	1.3	34.3	28.8	20.6	53.9	23.7
Nb	15.9	22.7	1.7	n.a	1.1	2.2	25.6	2.4	71.9	13.7	30.0	43.9	35.2
Ta	1.0	0.2	0.0	n.a	0.0	2.1	2.9	1.0	3.8	3.7	3.9	5.9	4.9
Mo	0.0	0.0	0.0	n.a	0.0	0.0	0.4	0.0	2.4	1.6	3.4	3.9	2.8
La	41.6	61.2	9.6	n.a	28.3	8.1	74.8	7.3	116.5	32.8	98.9	95.1	104.0
Ce	76.4	137.9	21.4	n.a	56.6	14.7	154.2	27.7	316.5	64.0	212.8	210.5	241.0
Nd	28.8	56.8	8.0	n.a	19.8	4.7	59.2	7.3	202.5	38.1	117.7	126.9	131.3
Sm	4.6	9.3	0.4	n.a	3.1	0.8	10.1	0.8	34.7	6.4	19.3	21.2	21.7
Dy	2.6	3.9	0.4	n.a	0.9	0.7	6.3	0.3	25.0	4.2	12.6	12.6	15.1
Yb	2.3	1.4	1.9	n.a	0.6	0.0	5.2	1.4	14.9	0.7	4.0	8.0	3.1
Th	15.3	25.6	12.7	n.a	6.9	4.1	15.6	5.1	8.5	1.0	4.7	1.9	3.7
U	5.8	4.2	0.5	n.a	0.7	2.3	3.1	3.2	3.5	1.1	0.0	0.0	0.0
Tl	0.0	0.9	0.0	n.a	0.3	0.0	0.5	0.0	0.6	0.0	3.3	0.6	2.2
Pb	26.4	24.5	27.5	n.a	20.8	24.2	20.5	15.7	11.9	25.5	32.0	33.2	22.1
Bi	1.0	0.8	0.3	n.a	0.8	0.0	0.0	0.0	n.d.	n.d.	n.d.	n.d.	n.d.

Table 2. Calculated TiO$_2$ activities from Rhyolite-MELTS model runs.

	Arutile	R	T (°C) solidus	T (K)	aTiO2
Harbison	6811	8.31446618	718	991.15	0.44
Danburg	6139	8.31446618	725	998.15	0.48
Wise	4331	8.31446618	707	980.15	0.59
Wyatt	5205	8.31446618	712	985.15	0.53
Rabun	5123	8.31446618	704	977.15	0.53
Henderson	6104	8.31446618	707	980.15	0.47
Mt Eve	7356	8.31446618	713	986.15	0.41
VA12-1	4557	8.31446618	679	952.15	0.56
VA12-2	6394	8.31446618	701	974.15	0.45
VA15-1	7111	8.31446618	702	975.15	0.42
VA15-2	8978	8.31446618	1000	1273.15	0.43
NC17-1	6460	8.31446618	719	992.15	0.46
NC17-2	6120	8.31446618	703	976.15	0.47
NC17-3	7241	8.31446618	710	983.15	0.41
NC17-5	6130	8.31446618	711	984.15	0.47
NC17-6	8054	8.31446618	707	980.15	0.37
NC17-10	7316	8.31446618	723	996.15	0.41
NC19-7	5731	8.31446618	714	987.15	0.5
NC19-9	7553	8.31446618	721	994.15	0.4

Table 3. Summary of corrected whole-rock Zr-concentrations, percent xenocrysts, zircon saturation temperatures, and Ti-in-zircon temperatures. References- 1) this study; 2) Coler et al. (1997); 3) Samson et al. (2018); 4) Chapter 2; 5) Burk (2017); 6 Chapter 1.

Sample	Zircon U-Pb age (Ma)	Uncorr. whole-rock [Zr] (ppm)	Tzirc sat (˚C)	% Xeno	Corrected whole-rock [Zr] (ppm)	Corrected Tzirc sat (˚C)	Avg zircon [Ti] (ppm)	Avg Ti-in-zircon temp (˚C)	$\delta^{18}O$	ϵHf(i)	Zircon Hf model age (Ma)	Reference
Harbison	n.d.	200	787	n.a.	200	787	2	690	n.d.	n.d.	n.d.	1
Danburg	n.d.	271	821	n.a.	271	821	3	701	n.d.	n.d.	n.d.	1
Wise	n.d.	63	716	n.a.	63	716	2	666	n.d.	n.d.	n.d.	1
Wyatt	n.d.	219	817	n.a.	219	817	8	780	n.d.	n.d.	n.d.	2
GA17-1	340 ± 0.40	125	761	27	91	736	4	699	n.d.	n.d.	n.d.	1
NC17-8	352 ± 0.90	73	721	82	13	605	n.d.	n.d.	n.d.	n.d.	n.d.	1
NC17-9	443 ± 0.43	395	859	0	395	859	13	837	n.d.	n.d.	n.d.	1
NC17-11	451 ± 0.62	113	753	28	81	726	n.d.	n.d.	n.d.	n.d.	n.d.	1
NJ15-1	1011 ± 4	1306	954	0	1306	954	17	880	8	n.d.	n.d.	1,3,4
VA12-1	1009 ± 7.7	1298	1001	0	1298	1001	42	966	7.4	-0.4	1.74-1.97	1,3,4
VA12-2	1029 ± 5	866	894	4	849	886	13	852	7.7	n.d.	n.d.	1,3,4
VA15-1	1012 ± 7.8	2375	1019	0	2375	1019	62	1045	7.6	0.1	1.70-1.95	1,4,5
VA15-2	1034 ± 2.9	974	883	0	974	883	23	920	8	0.9	1.73-1.92	1,4,5
NC17-1	1142 ± 1.0	337	830	28	242	800	13	778	8	0.3	1.79-2.03	1,4,6
NC17-2	1139 ± 11	309	805	4	296	802	19	869	7.5	0.5	1.62-2.07	1,4,6

| Sample	Zircon U-Pb age (Ma)	Uncorr. whole-rock [Zr] (ppm)	Tzirc sat (˚C)	% Xeno	Corrected whole-rock [Zr] (ppm)	Corrected Tzirc sat (˚C)	Avg zircon [Ti] (ppm)	Avg Ti-in-zircon temp (˚C)	δ^{18}O	εHf(i)	Zircon Hf model age (Ma)	Reference
NC17-3	1175 ± 29	346	802	1	342	801	25	876	7.5	1.5	1.72-2.05	1,4,6
NC17-5	1034 ± 0.9	573	864	8	527	855	26	917	7.8	3.1	1.50-1.83	1,4,6
NC17-6	1283 ± 9.4	147	728	8	135	721	12	869	6.9	6.7	1.39-1.84	1,4,6
NC17-10	1159 ± 28	273	824	1	271	823	9	791	6.5	3.6	1.58-1.81	1,4,6
NC19-7	1191 ± 8.1; 1034 ± 5.7	179	795	2	175	793	17	791	cores-7.4; rims-7.2	cores -0.3; rims -3.5	1.76-2.32	1,4,6
NC19-9	1250 ± 54; 1126 ± 23	19	577	0	19	577	12	859	Bright cores-6.0; Dark cores-6.1	Bright cores 0.4; Dark cores -0.8	1.78-2.11	1,4,6
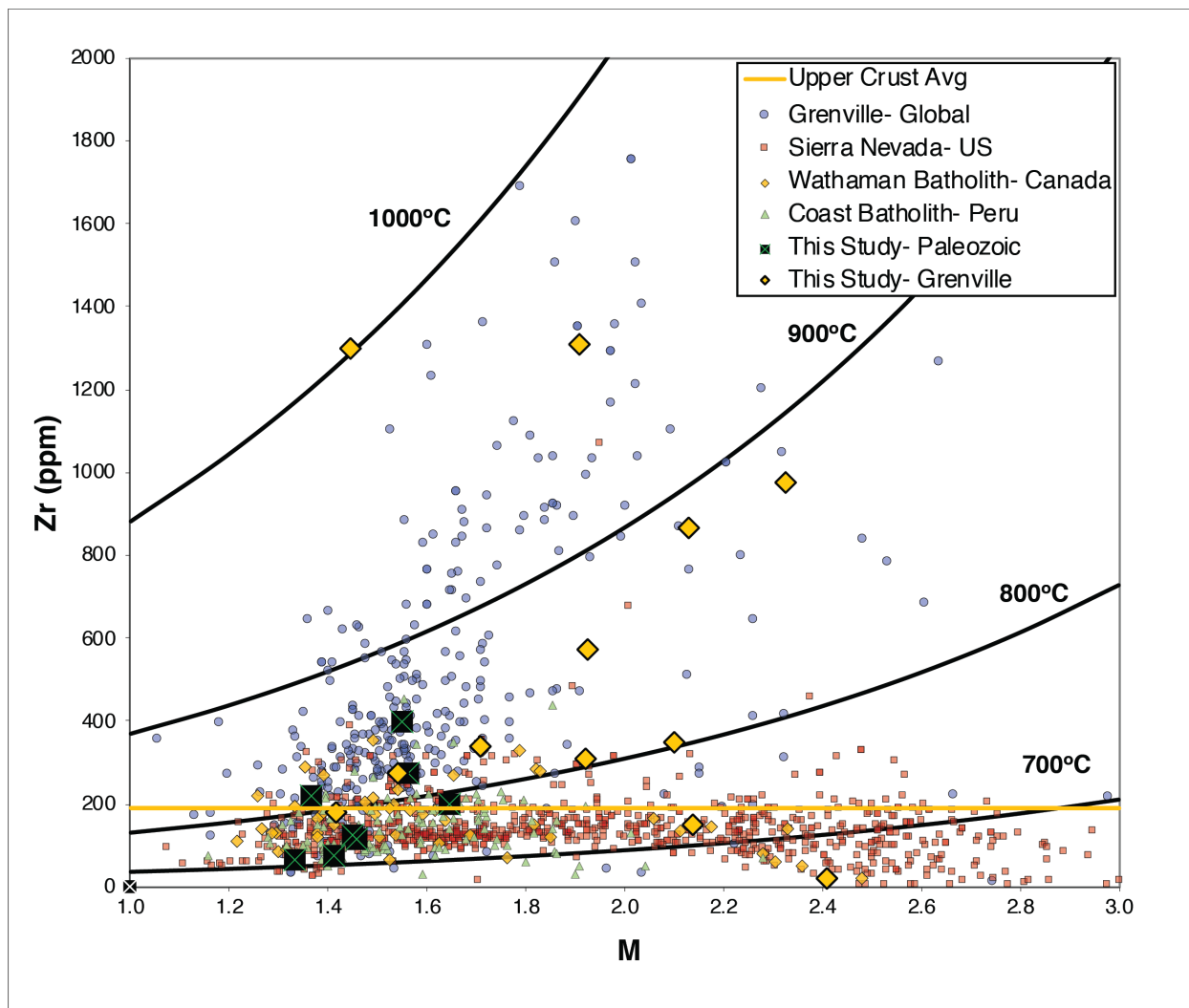
Fig 1. Zr vs M [(K+Na+2Ca)/Al*Si] (Watson and Harrison, 1983) for granitoids from other major batholiths of age younger and older than the Grenville Orogeny. Thick black lines represent the calculated zircon saturation thermometer temps for a given Zr concentration and M value. Solid yellow line represents upper crustal [Zr] of 190 ppm (Taylor and McLennon, 1985). Modified from Samson et al. (2018).
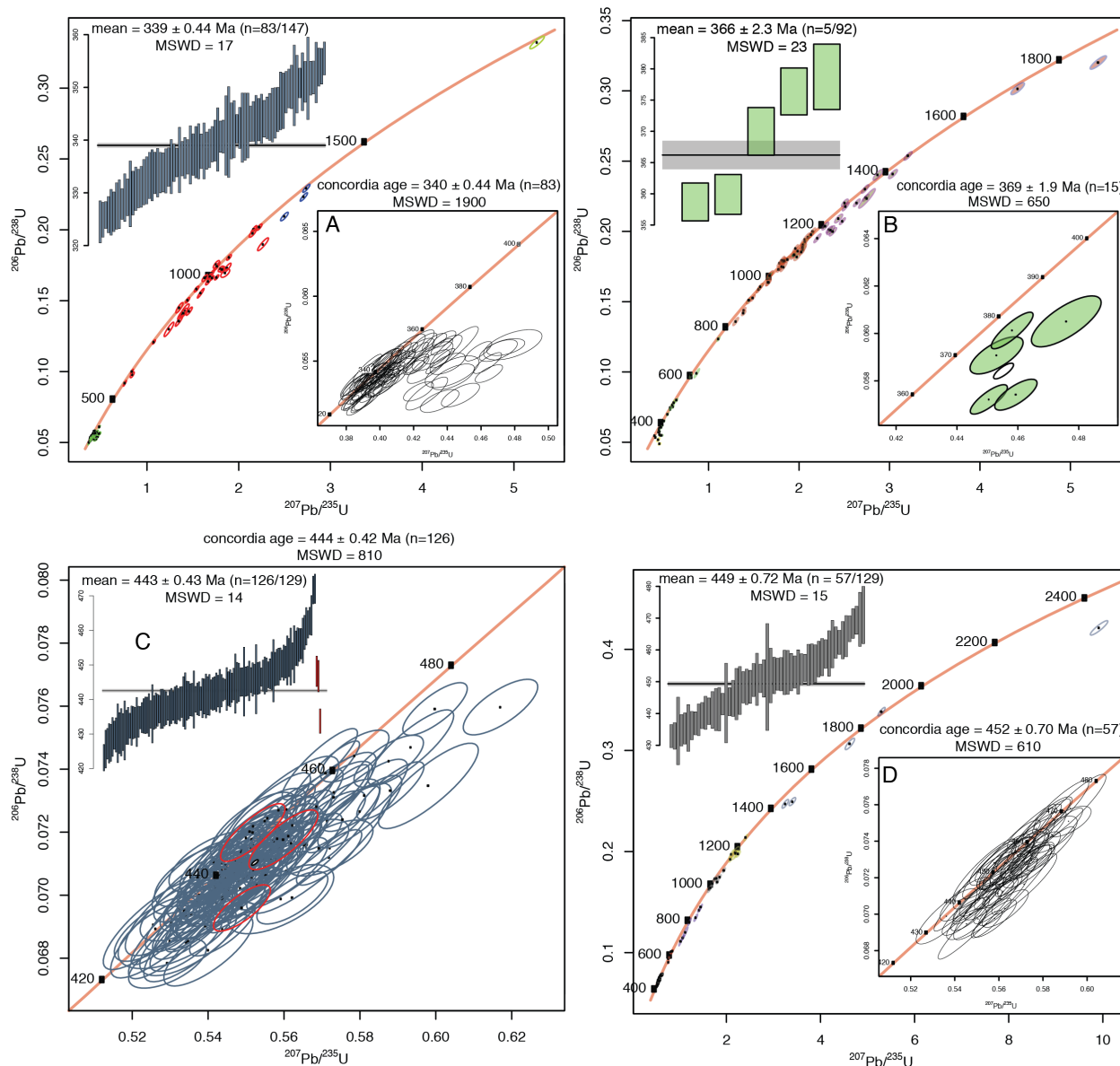
Fig 2. Concordia diagrams for non-Grenville samples for this study. A) Rabun granite (sample GA17-1) B) Looking Glass granite (sample NC17-8) C) Henderson gneiss (sample NC17-9) D) Whiteside granite (sample NC17-11). Inset figures show weighted mean and a close-up of the cluster of samples used to make the age interpretation. Red circles on C are analyses made in rim zones identified by CL. Figures made in IsoPlotR (Vermeesch, 2019).
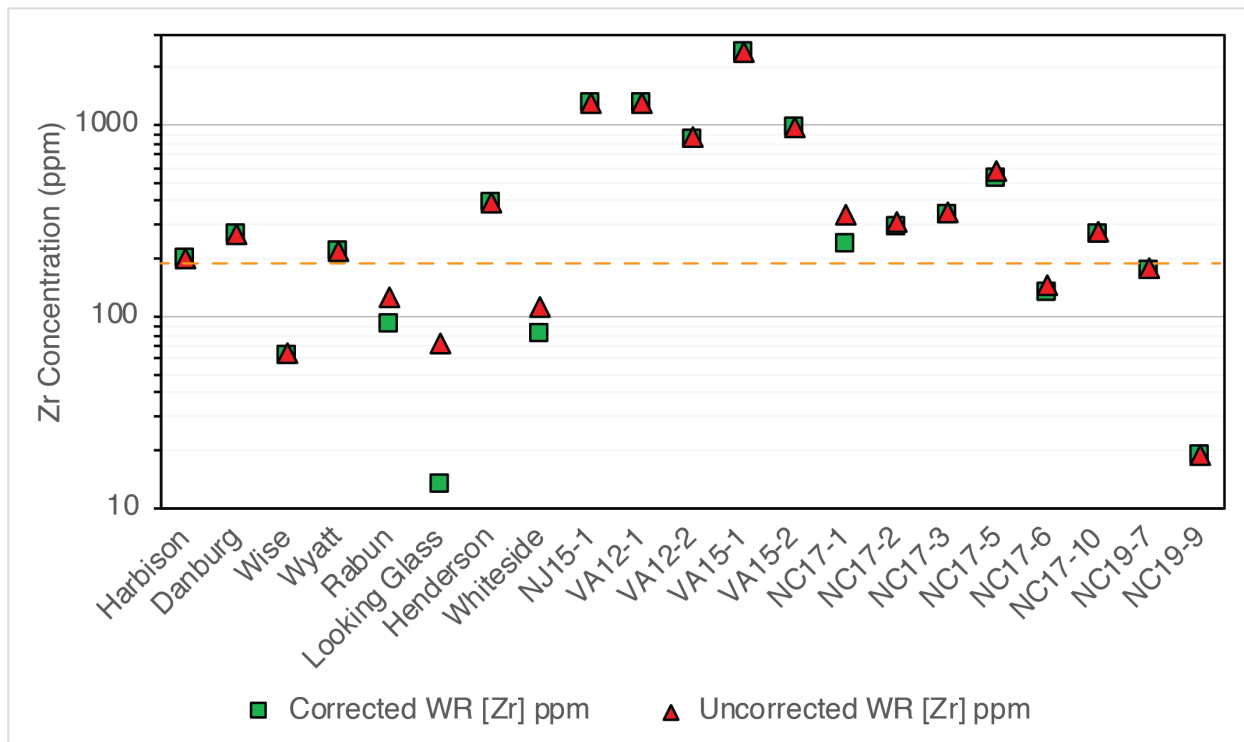
Fig 3. Graph showing the measured and xenocryst corrected whole-rock [Zr] for each sample. Orange dashed line represents average upper crustal average [Zr] of 190 ppm (Taylor and McLennon, 1985).
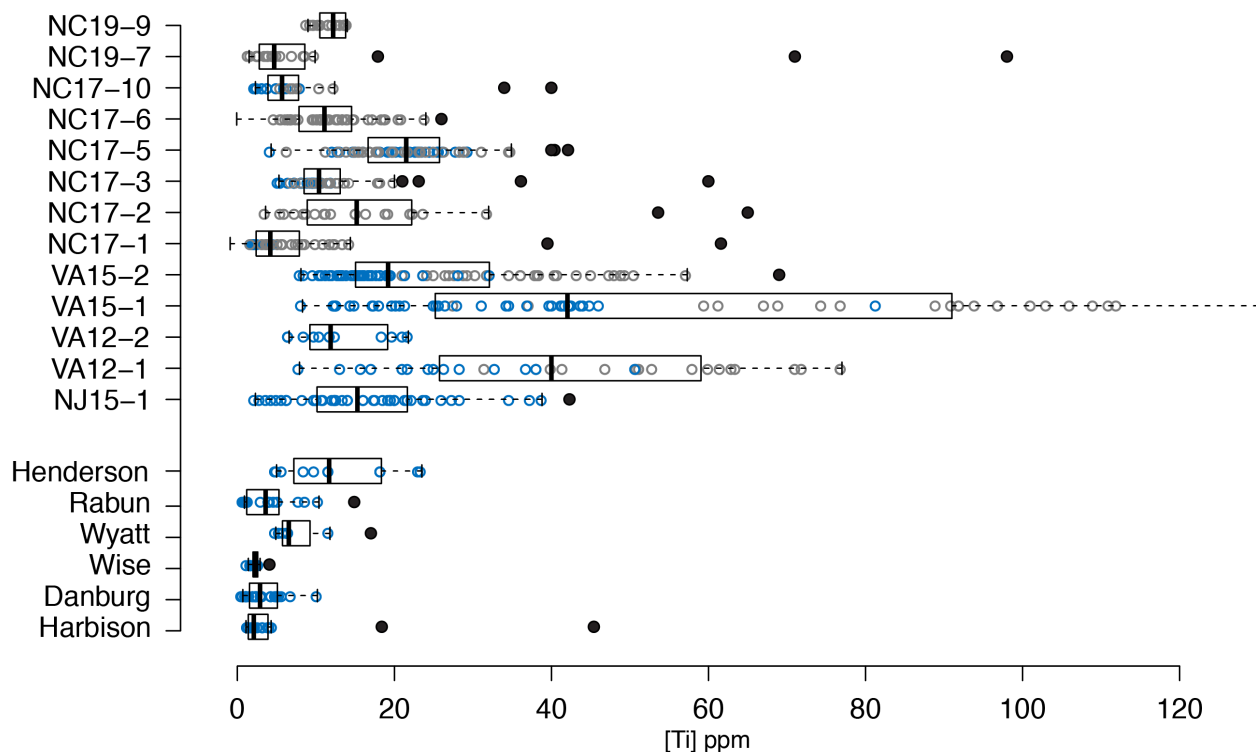
Fig 4. Box plots showing Ti-contents in zircon after filtering of data as outlined in the methods section. Gray circles represent data produced by laser ablation methods, blue circles from data produced by either SHRIMP-RG or ion probe methods. Whiskers are calculated by 1.5 x IQR (Tukey method; inter-quartile range). Solid black circles represent analyses exceeding 1.5 x IQR. Solid vertical lines within boxes are the median values. Box plots made using BoxPlotR online (http://shiny.chemgrid.org/boxplotr/). Ion probe data for VA12-1 and VA12-2 from Moecher et al. (2014), SHRIMP-RG data for VA15-1; VA15-2; and NJ15-1 from Burk (2017).
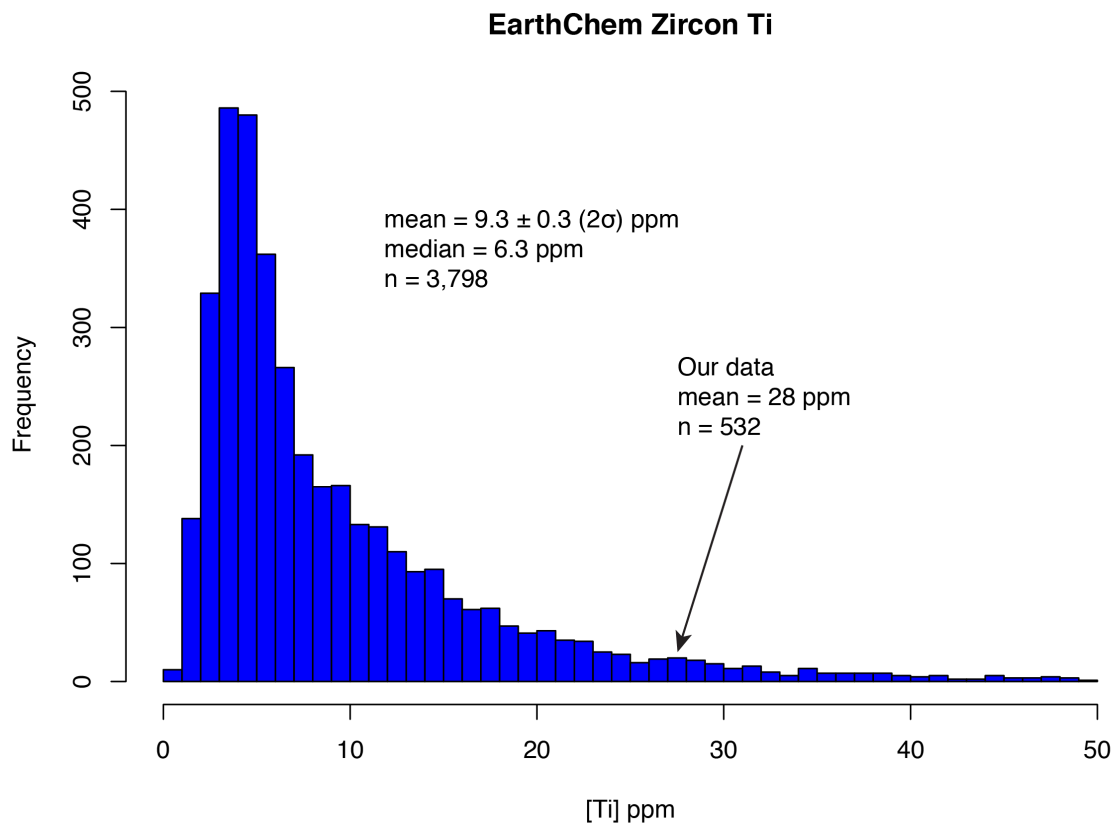
Fig 5. Ti-contents of plutonic and volcanic zircon measured by SIMS or LA-ICP-MS

from the EarthChem data base (https://www.earthchem.org). This figure illustrates the

significant difference in Ti-contents for most igneous zircon relative to the high-Ti

content from our Grenville samples.
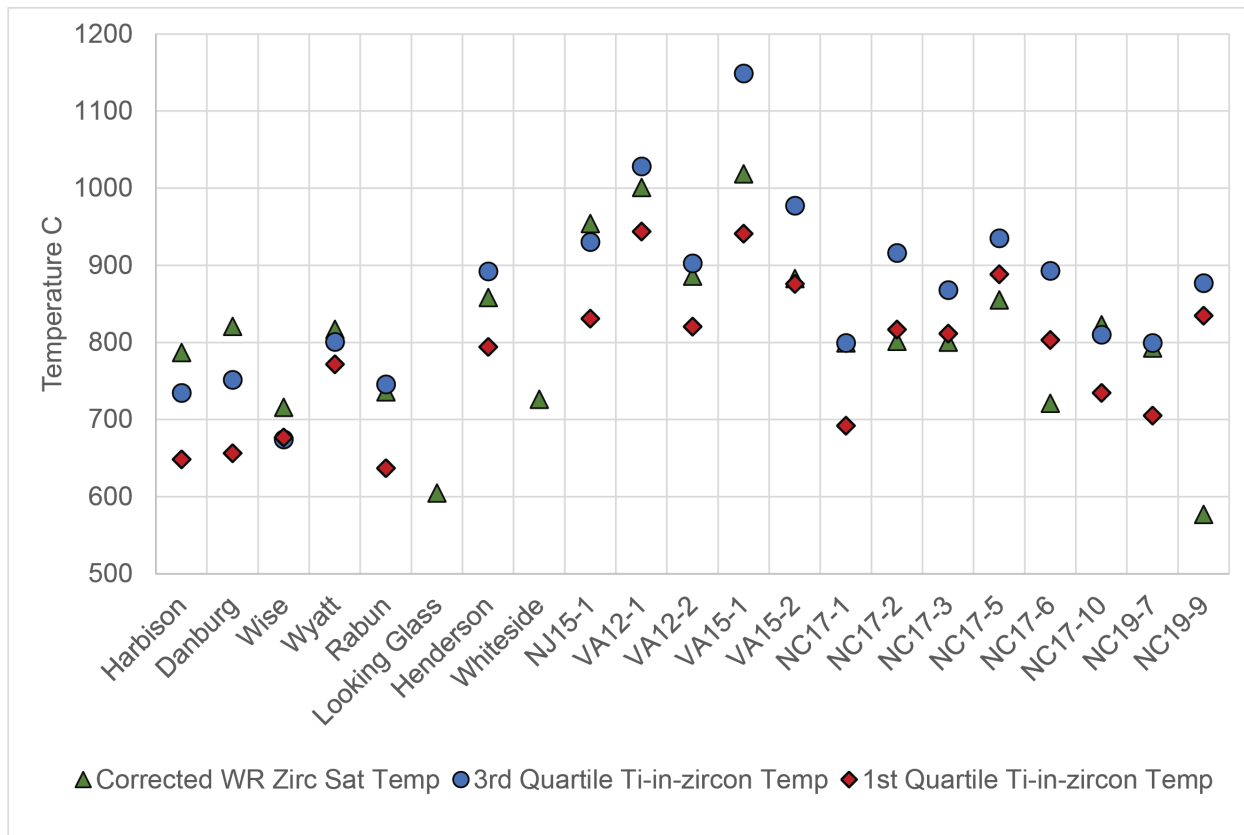
Fig 6. Graph showing the 1st quartile Ti-in-zircon temperatures (red diamonds), 3rd quartile Ti-in-zircon temperatures (blue circles), and whole-rock [Zr] corrected zircon saturation thermometry results (green triangles). See text for further discussion.
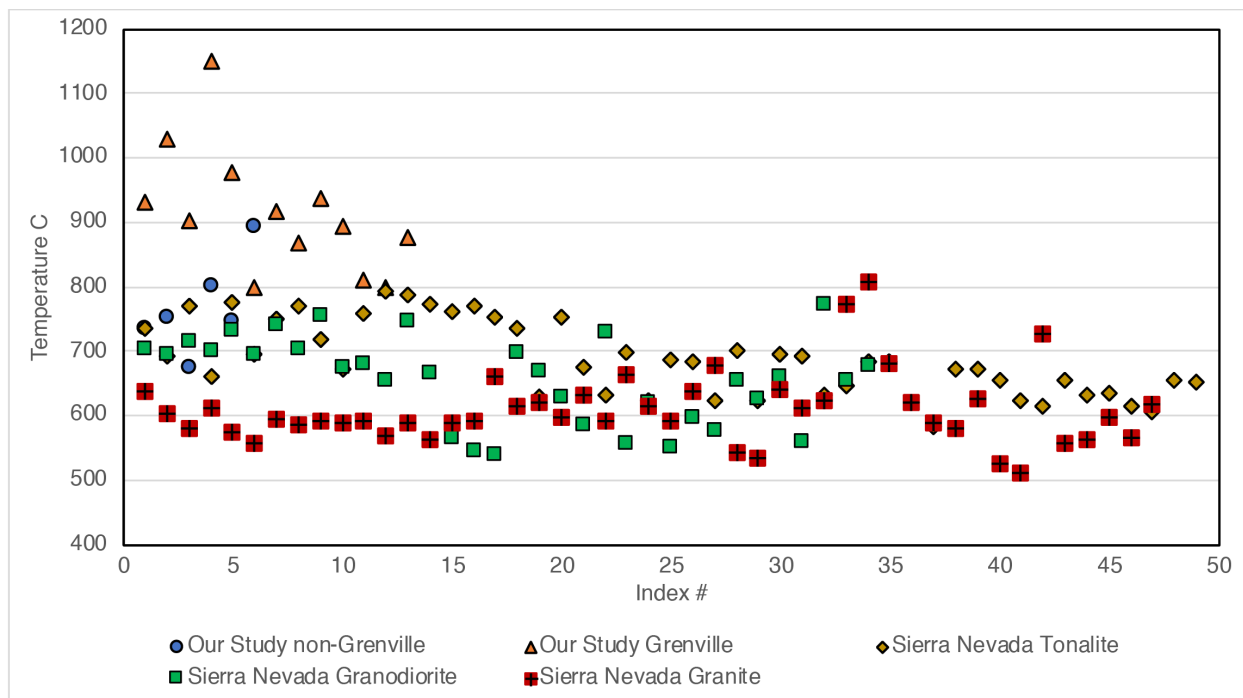
Fig. 7. Results of Ti-in-zircon thermometry for all samples using aTiO$_2$ determined by Rhyolite-MELTS modeling. Temperatures are calculated for our non-Grenville (blue circles) and Grenville samples (orange triangles) using the 3rd quartile Ti value. All other values are those reported by Fu et al. (2008) for Sierra Nevada tonalites (amber diamonds), granodiorites (green squares), and granites (red boxes with black pluses).

References

Aleinikoff, J., Jr, J.W., Jr, A.A. Wintsch., R., Fanning, C., Yi, K. 2004. Deciphering multiple Mesoproterozoic and Paleozoic events recorded in zircon and titanite from the Baltimore Gneiss, Maryland: SEM imaging, SHRIMP U-Pb geochronology, and EMP analysis. In Tollo, R.P., Corriveau, L., McLelland, J., and Bartholomew, M.J., eds., Proterozoic tectonic evolution of the Grenville orogeny in North America. Boulder, Colorado, Geological Society of America Memoir 197, p. 411-434. DOI: 10.1130/0-8137-1197-5.411.

Aleinikoff, J., Ratcliffe, N., Walsh, G. 2011. Provisional Zircon and Monazite Uranium-Lead Geochronology for Selected Rocks from Vermont. Unites State Geological Survey Open-File Report 2011-1309. 46 p., available only online at http://pubs.usgs.gov/of/2011/1309/.

Bea, F. 1996. Residence of REE, Y, Th, and U in Granites and Crustal Protoliths; Implications for the Chemistry of Crustal Melts. Journal of Petrology. v. 37. p. 521-552.

Belousova, E., Griffin, W., O'Reilly, S. Zircon Crystal Morphology, Trace Element Signatures and Hf Isotope Composition as a Tool for Petrogenetic Modelling: Examples from Eastern Australian Granitoids. 2006. Journal of Petrology. v. 47. no. 2. p. 329-353. DOI: 10.1093/petrology/egi077.

Beumont, C., Nguyen, M., Jamieson, R., Ellis, S. 2006. Crustal Flow Modes in Large
   Hot Orogens. In Law, R., Searle, M., Godin, L., (eds) Channel Flow, Ductile
   Extrusion, and Exhumation in Continental Collision Zones. Geological Society,
   London. v. 288. p. 91-145.

Bickford, M., Soegaard, K., Nielson, K., McLelland, J. 2000. Geology and
   Geochronology of Grenville-Age Rocks in the Van Horn and Franklin Mountains
   Area, West Texas: Implications for the Tectonic Evolution of Laurentia During the
   Grenville. Geological Society of America Bulletin. v. 112. no. 7. p. 1134-1148.
   DOI: 10.1130/0016-7606(2000)112.

Bickford, M., McLelland, J., Mueller, P., Kamenov, G., Neadle, M. 2010. Hafnium
   Isotopic Compositions of Zircon from Adirondack AMCG Suites: Implications for the
   Petrogenesis of Anorthosites, Gabbros, and Granitic Members of the Suites. The
   Canadian Mineralogist. v. 48. p. 751-761. DOI: 10.3749/canmin.48.2.751.

Bickford, M., Van Schmus, W., Karlstrom, K., Mueller, P., Kamenov, G. 2015.
   Mesoproterozoic-trans-Laurentian Magmatism: A Synthesis of Continent-Wide Age
   Distributions, New SIMS U-Pb Ages, Zircon Saturation Temperatures, and Hf and
   Nd Isotopic Compositions. Precambrian Research. v. 265. p. 286-312. DOI:
   10.1016/j.precamres.2014.11.024.

Black, L., Kamo, S., Allen, C., Aleinikoff, J., Davis, D., Korsh, R., Foudoulis, C. 2003.

   TEMORA-1: A New Zircon Standard for Phanerozoic U-Pb Geochronology.

   Chemical Geology. v. 200. p. 155-170.

Boehnke, P., Watson, E.B., Trail, D., Harrison, T.M., Schmitt, A. 2013. Zircon

   Saturation Re-Revisited. Chemical Geology. v. 351. p. 324-334.

Bouvier, A., Vervoort, J., Patchett, J. 2008. The Lu-Hf and Sm-Nd Isotopic

   Composition of CHUR: Constraints from Unequilibrated Chondrites and Implications

   for the Bulk Composition of Terrestrial Planes. Earth and Planetary Science Letters.

   v. 273. p. 48-57. DOI: 10.1016/j.epsl.2008.06.010.

Burk, S.R. 2017. Zircon as a Proxy for "Taking the Temperature" of Granites: An

   Example Using Zircon Thermometry Applied to Grenvillian Mid-Crustal Magmas in

   the Blue Ridge Province, Virginia. Masters Thesis. University of Kentucky.

   Lexington, Kentucky, USA. DOI: 10.13023/ETD.2017.118. 84 pp.

Cardona, A., Chew, D., Valencia, V., Bayona, G., Mišković, A., Ibañez-Meija. 2010.

   Grenvillian remnants in the Northern Andes: Rodinian and Phanerozoic

   Paleogeographic Perspectives. Journal of South American Earth Sciences. v. 29.

   p. 92-104. DOI: 10.1016/j.jsames.2009.07.011.

Carr, M., Gazel, E. 2017. Igpet Software for Modeling Igneous Processes: Examples of Application Using the Open Educational Version. Contributions to Mineralogy and Petrology. v. 111. p. 283-289. DOI: 10.1007/s00710-016-0473-z.

Carrigan, C., Miller, C., Fullagar, P., Bream, B., Hatcher, R., Jr., Coath, C. 2003. Ion Microprobe Age and Geochemistry of Southern Appalachian Basement, with Implications for Proterozoic and Paleozoic Reconstructions. Precambrian Research. v. 120. p. 1-36.

Cartwright, S., West, D., Amidon, W. 2019. Depositional Constraints from Detrital Zircon Geochronology of Strata from Multiple Lithotectonic Belts in South-Central Maine, USA. Atlantic Geology. v. 55. p. 93-136. DOI: 10.4138/atlgeol.2019.003.

Cherniak, D., Watson, E.B. 2007. Ti Diffusion in Zircon. Chemical Geology. v. 242. p. 470-483. DOI: 10.1016/j.chemgeo.2007.05.005.

Chew, D., Cardona, A., Mišković, A. 2011. Tectonic Evolution of Western Amazonia from the Assembly of Rodinia to its Break-up. International Geology Review. v. 53. no. 11-12. p. 1280-1296. DOI: 10.1080/00206814.2010.527630.

Claiborne, L., Miller, C., Wooden, J. 2010. Trace Element Composition of Igneous

    Zircon: A Thermal and Compositional Record of the Accumulation and Evolution of

    a Large Silicic Batholith, Spirit Mountain, Nevada. Contributions to Mineralogy and

    Petrology. v. 160. p. 511-531. DOI: 10.1007/s00410-010-0491-5.

Coble, M., Vazquez, J., Barth, A., Wooden, J., Burns, D., Kylander-Clark, A., Jackson,

    S., Vennari, C. 2018. Trace Element Characterisation of MAD-559 Zircon Reference

    Material for Ion Microprobe Analysis. Geostandards and Geoanalytical Research.

    DOI: 10.1111/ggr.12238.

Conrey, R., Bailey, D., Singer, J., Wagoner, L., Parfitt, B., Hay, J., Keh, O. 2019.

    Combined Use of Multiple Internal and External Standards in LA-ICPMS Analysis of

    Geologic Samples Using Lithium Borate Fused Glass. American Geophysical Union

    Fall Meeting. v. V11D-0106.

Cordani, U., Teixeira, W. 2007. Proterozoic Accretionary Belts in the Amazonian

    Craton. *In* Hatcher, R. Jr., Carlson, M., McBride, J., and Martinez, C., eds. 4-D

    Framework of Continental Crust. Geological Society of America Memoir 200. p.

    297-320. DOI: 10.1130/2007.1200(14).

Cordani, U., Teixeira, W., D'Agrella-Filho, M., Trindade, R. 2009. The Position of the Amazonian Craton in Supercontinent. Gondwana Research. v. 15. p. 396-407. DOI: 10.1016/j.gr.2008.12.005.

Crowley, W., Cleaves, E. 1974. Geologic Map of the Towson Quadrangle, Maryland. Maryland Geological Survey, Geologic Map QA-2. 1:24,000 scale.

Daly, J., McLelland, J. 1991. Juvenile Middle Proterozoic Crust in the Adirondack Highlands Grenville Province, Northeastern North America. Geology. v. 19. p. 119-122.

Davidson, J., McMillan, N., Moorbath, S., Worner, G., Harmon, R., Lopez-Escobar, L. 1990. The Nevados de Payachata Region (18° S/ 69° W, N. Chile) II. Evidence for Widespread Crustal Involvement in Andean Magmatism. Contributions to Mineralogy and Petrology. v. 105. No. 4. p. 412-432. DOI: 10.1007/BF00286829.

Dickin, A., McNutt, R. 2003. An Application of Nd Isotopic Mapping in Structural Geology: Delineating an Allochthonous Grenvillian Terrane at North Bay, Ontario. Geological Magazine. v. 140. no. 5. p. 539-548. DOI: 10.1017/S0016756803008070.

Dickinson, W. 2008. Impact of Differential Zircon Fertility of Granitoid Basement Rocks

    in North America on Age Populations of Detrital Zircons and Implications for Granite

    Petrogenesis. Earth and Planetary Science Letters. v. 275. p. 80-92. DOI:

    10.1016/j.epsl.2008.08.003.

Drake, A. Jr., Volkert, R. 1991. The Lake Hopatcong Intrusive Suite (Middle

    Proterozoic) of the New Jersey Highlands. *In* Contributions to New Jersey Geology:

    U.S. Geological Survey Bulletin 1952. 1952-A. p. A1-A9.

Farmer, G., Bowring, S., Matzel, J., Maldonado, G., Fedo, C., Wooden, J.

    Paleoproterozoic Mojave Province in Northwestern Mexico? Isotopic and U-Pb

    Zircon Geochronologic Studies of Precambrian and Cambrian Crystalline and

    Sedimentary Rocks, Caborca, Sonora. 2005. *In* Anderson, T., Nourse, J., McKee,

    J., Steiner, M. eds. The Mojave-Sonora Megashear Hypothesis: Development,

    Assessment, and Alternatives. Geological Society of America Special Paper 393. p.

    183-198. DOI: 10.1130/2005.2393(05).

Ferry, J.M., Watson, E.B. 2007. New Thermodynamic Models and Revised

    Calibrations for the Ti-in-zircon and Zr-in-rutile Thermometers. Contribution to

    Mineralogy and Petrology. v. 154. p. 429-437.

Fisher, C., Loewy, S., Miller, C., Berquist, P., Van Schmus, W., Hatcher, R., Jr.,
   Wooden, J., Fullagar, P. 2010. Whole-Rock Pb and Sm-Nd Isotopic Constraints on
   the Growth of Southeastern Laurentia during Grenville Orogenesis. Geological
   Society of America Bulletin. v. 122. no. 9/10. p. 1646-1659. DOI:
   10.1130/B30116.1.

Fu, B., Page, F.Z., Cavosie, A.J., Fournelle, J., Kita, N.K., Lackey, J.S., Wilde, S.A.,
   Valley, J.W. 2008. Ti-in-zircon Thermometry: Applications and Limitations:
   Contribution to Mineralogy and Petrology. v. 156. p. 197-215.

Ghiorso, M., Gualda, G. 2013. A Method for Estimating the Activity of Titania in
   Magmatic Liquids from the Compositions of Coexisting Rhombohedral and Cubic
   Iron-Titanium Oxides. Contributions to Mineralogy and Petrology. v. 165. p. 73-81.
   DOI: 10.1007/s00410-012-0792-y.

Ghiorso, M., Gualda, G. 2015. An H20-C02 Mixed Fluid Saturation Model Compatible
   with Rhyolite-MELTS. Contributions to Mineralogy and Petrology. v. 169. no. 53.
   DOI: 10.1007/s00410-015-1141-08.

Gorring, M., Estelle, T., Volkert, R. 2004. Geochemistry of the Late Mesoproterozoic
     Mount Eve Granitic Suite: Implications for Late to Post-Ottawan Tectonics in the
     New Jersey-Hudson Highlands. *In* Tollo, R., Corriveau, L., McLelland, J., and
     Bartholomew, M. eds. Proterozoic Tectonic Evolution of the Grenville Orogen in
     North America. Geological Society of America Memoir 197. p. 505-523.

Gower, C., Krogh, T. 2002. A U-Pb Geochronological Review of the Proterozoic
     History of the Eastern Grenville Province. Canadian Journal of Earth Sciences. v.
     39. no. 5. p. 795-829.

Gualda, G.A.R., Ghiorso, M.S., Lemons, R.V., Carley, T.L. 2012. Rhyolite-MELTS: A
     Modified Calibration of MELTS Optimized for Silica-Rich, Fluid Bearing Magmatic
     Systems.   Journal of Petrology. v. 53. p. 875-890.

Hadley, J., Goldsmith, R. 1963. Geology of the Eastern Great Smoky Mountains, North
     Carolina and Tennessee. Geological Survey Professional Paper 349-B, A Study of
     Stratigraphy, Structure, and Metamorphism in the Southern Appalachian Region.
     118 pp.

Halpin, J., Daczko, N., Milan, L., Clarke, G. 2012. Decoding Near-Concordant U-Pb
     Zircon Ages Spanning Several Hundred Million Years: Recrystallization,
     Metamictisation or Diffusion? Contributions to Mineralogy and Petrology. v. 163. p.
     67-85. DOI: 10.1007/s00410-011-0659-7.

Hanchar, J., Watson, E.B. 2003. Zircon Saturation Thermometry. *In* Zircon, Hanchar,

    J., Hoskin, P. (eds). Reviews in Mineralogy and Geochemistry. v. 53. p. 89-112.

    ISBN 0-93995060-X. 500 pp.

Harrison, T.M., Watson, E.B., Aikman, A.B. 2007. Temperature Spectra of Zircon

    Crystallization in Plutonic Rocks. Geology. v. 35. p. 635-638.

Hatcher, Jr., R. 1987. Tectonics of the Southern and Central Appalachian Internides.

    Annual Review of Earth and Planetary Sciences. v. 15. p. 337-362. DOI:

    10.1146/annurev.ea.15.050187.002005.

Hildreth, W., Moorbath, S. 1988. Crustal Contributions to Arc Magmatism in the Andes

    of Central Chile. Contributions to Mineralogy and Petrology. v. 98. No. 4. p. 455-

    499. DOI: 10.1007/BF00372365.

Hoskin, P., Schaltegger, U. 2003. The Composition of Zircon and Igneous and

    Metamorphic Petrogenesis. *In* Zircon, Hanchar, J., Hoskin, P. (eds). Reviews in

    Mineralogy and Geochemistry. v. 53. p. 89-112. ISBN 0-93995060-X. 500 pp.

Howard, A., Farmer, G., Amato, J., Fedo, C. 2015. Zircon U-Pb Ages and Hf Isotopic

    Compositions Indicate Multiple Sources for Grenvillian Detrital Zircon Deposited in

    Western Laurentia. Earth and Planetary Science Letters. v. 432. p. 300-310. DOI:

    10.1016/j.epsl.2015.10.018.

Hughes, S., Lewis, S., Bartholomew, M., Sinha, K., Herz, N. Geology and

    Geochemistry of Granitic and Charnockitic Rocks in the Central Lovingston Massif of

    the Grenvillian Blue Ridge Terrane. 2004. *In* Tollo, R., Corriveau, L., McLelland, J.,

    and Bartholomew, M. eds. Proterozoic Tectonic Evolution of the Grenville Orogen in

    North America. Geological Society of America Memoir 197. p. 549-569.

Ibanez-Meija, M., Ruiz, J., Valencia, V., Cardona, A., Gehrels, G., Mora, A. 2011. The

    Putumayo Orogen of Amazonia and its Implications for Rodinia Reconstructions:

    New U-Pb Geochronological Insights into the Proterozoic Tectonic Evolution of

    Northwestern South America. Precambrian Research. v. 191. p. 58-77. DOI:

    10.1016/j.precamres.2011.09.005.

Ibanez-Meija, M., Pullen, A., Arenstein, J., Gehrels, G., Valley, J., Ducea, M., Mora, A.,

    Precha, M., Ruiz, J. 2015. Unraveling Crustal Growth and Reworking Processes in

    Complex Zircons from Orogenic Lower-Crust: The Proterozoic Putumayo Orogen of

    Amazonia. Precambrian Research. v. 267. p. 285-310. DOI:

    10.1016/j.precamres.2015.06.014.

Ibanez-Meija. 2020. The Putumayo Orogen of Amazonia: A Synthesis. *In* Gómez, J.

    and Mateus-Zabala, D. eds. The Geology of Colombia, Volume 1 Proterozoic-

    Paleozoic. Servicio Geológico Colombiano, Publicaciones Geológicas Especiales.

    v. 35. p. 101-131. DOI: 10.32685/pub.esp.35.2019.06.

Kristoffersen, A., Elburg, M. 2018. Visualizing, Interpreting, and Comparing Detrital Zircon Age and Hf Isotope Data in Basin Analysis- A Graphical Approach. Basin Research. v. 30. p. 132-147.

Loewy, S., Connelly, J., Dalziel, I., Gower, C. 2003. Eastern Laurentia in Rodinia: Constraints from Whole-Rock Pb and U/Pb Geochronology. Tectonophysics. p. 169-197. DOI: 10.1016/S0040-1951(03)00338-X.

Ludwig, K. 1998. ISOPLOT for MS-DOS, A Plotting and Regression Program for Radiogenic Isotope Data for IBM-PC Compatible Computers, Version 1.00. USGS Open-File Report OF-88-0557.

MacLachlan, D., Buckwalter, T., McLaughlin, D. 1975. Geology and Mineral Resources of the Sinking Spring Quadrangle. Pennsylvania Geological Survey Atlas 177d. 1:24000 scale.

Marquez, L. 2005. Map of the Bedrock Geology, Wagontown Quadrangle, Chester County, Pennsylvania. Pennsylvania Geological Survey Open-File Report OFBM 05-05.0. 1:24000 scale.

McDonough, W., and Sun, S. 1995. The Composition of the Earth. Chemical Geology. v. 67. No. 5. p. 1050-1056.

McLelland, J., Daly, J.S., McLelland, J.M. 1996. The Grenville Orogenic Cycle (ca. 1350-1000 Ma): An Adirondack Perspective. Tectonophysics. v. 265. p. 1-28.

McLelland, J.M., Selleck, B.W., and Bickford, M.E. 2010. Review of the Proterozoic Evolution of the Grenville Province, its Adirondack Outlier, and the Mesoproterozoic Inliers of the Appalachians, *in* Tollo, R.P., Bartholomew, M.J., Hibbard, J.P., and Karabinos, P.M. (eds.). From Rodinia to Pangea: The Lithotectonic Record of the Appalachian Region: Geological Society of America Memoir 206, p. 1–29, doi: 10.1130/2010.1206(02).

McLelland, J., Selleck, B., Bickford, M. 2013. Tectonic Evolution of the Adirondack Mountains and Grenville Orogen Inliers within the USA. Geoscience Canada. v. 40. p. 318-352. DOI: 10.12789/geocanj.2013.40.022.

Merschat, C., Cattanach, B. 2008. Bedrock Geologic Map of the Western Half of the Asheville 1:100,000-Scale Quadrangle, North Carolina and Tennessee. North Carolina Geological Survey. Geologic Map Series GMS-13. 1:100k scale.

Miller, C., Hatcher, R., Jr., Harrison, T.M., Coath, C., Gorisch, E. 1998. Cryptic Crustal Events Elucidated through Zone Imaging and Ion Microprobe Studies of Zircon, Southern Appalachian Blue Ridge, North Carolina- Georgia. Geology. v. 26. no. 5. p. 419-422.

Miller, C., Hatcher, R., Jr., Ayers, J., Coath, C., Harrison, T.M. 2000. Age and Zircon Inheritance of Eastern Blue Ridge Plutons, Southwestern North Carolina and Northeastern Georgia, with Implications for Magma History and Evolution of the Southern Appalachian Orogen. American Journal of Science. v. 300. p. 142-172.

Miller, C., McDowell, S., Mapes, R. 2003. Hot and Cold Granites? Implications of Zircon Saturation Temperatures and Preservation of Inheritance. Geology. v. 31. no. 6. p. 529-532.

Moecher, D., Samson, S. 2006. Differential Zircon Fertility of Source Terranes and Natural Bias in the Detrital Zircon Record: Implication for Sedimentary Provenance Analysis. Earth and Planetary Science Letters. v. 247. p. 252-266. DOI: 10.1016/j.epsl.2006.04.035.

Moecher, D., Hietpas, J., Samson, S., Chakraborty, S. 2011. Insights into Southern Appalachian Tectonics from Ages of Detrital Monazite and Zircon in Modern Alluvium. Geosphere. v. 7. no. 2. p. 494-512. DOI: 10.1130/GES00615.1.

Moecher, D.P., McDowell, S.M., Samson, S.D., and Miller, C.F. 2014. Ti-in-Zircon Thermometry and Crystallization Modeling Support "Hot" Grenville Granite Hypothesis. Geology. v. 42. p. 267-270.

Moecher, D., Harris, F., Larking, E., Quinn, R., Walsh, K., Loughry, Jr., D., Anderson, E., Samson, S., Satkoski, A., Tohver, E. 2020. Zircon U-Pb Geochronology and Nd-Pb Isotope Geochemistry of Blue Ridge Basement in the Eastern Great Smoky Mountains, USA: Implications for the Proterozoic Tectonic Evolution of the Southeastern Laurentian Margin. American Journal of Science. v. 320. p. 677-729. DOI: 10.2475/10.2020.02.

Mosher, S., Hoh, A., Zumbro, J., Reese, J. 2004. Tectonic Evolution of the Eastern Llano Uplift, Central Texas: A Record of Grenville Orogenesis Along the Southern Laurentian Margin. In Tollo, R., Corriveau, L., McLelland, J., and Bartholomew, M. eds. Proterozoic Tectonic Evolution of the Grenville Orogen in North America. Geological Society of America Memoir 197. p. 783-798.

Nagasawa, H. 1970. Rare Earth Concentrations in Zircon and Apatites and their Host Dacites and Granites. Earth and Planetary Science Letters. v. 9. p. 359-364.

Owens, B., Tucker, R. 2003. Geochronology of the Mesoproterozoic State Farm Gneiss and Associated Neoproterozoic Granitoids, Goochland Terrane, Virginia. Geological Society of America Bulletin. v. 115. no. 8. p. 972-982.

Owens, B., Samson, S. 2004. Nd Isotopic Constraints on the Magmatic History of the

  Goochland Terrane, Easternmost Grenvillian Crust in the Southern Appalachians. *In*

  Tollo, R., Corriveau, L., McLelland, J., and Bartholomew, M. eds. Proterozoic

  Tectonic Evolution of the Grenville Orogen in North America. Geological Society of

  America Memoir 197. p. 601-608.

Owens, B., Dymek, R. 2016. Comparitive Petrology of the Montpelier and Roseland

  Potassic Anorthosites, Virginia. The Canadian Mineralogist. v. 54. No. 6. p. 1563-

  1593. DOI: 10.3749/canmin.1600002.

Ownby, S., Miller, C., Berquist, P., Carrigan, C., Wooden, J., Fullager, P. 2004. U-Pb

  Geochronology and Geochemistry of a Portion of the Mars Hill Terrane, North

  Carolina and Tennessee: Constraints on Orogin, History, and Tectonic Assembly. In

  Tollo, R.P., Corriveau, L., McLelland, J., and Bartholomew, M.J., eds., Proterozoic

  tectonic evolution of the Grenville orogeny in North America. Boulder, Colorado,

  Geological Society of America Memoir 197, p. 609-632. DOI: 10.1130/0-8137-1197-

  5.609.

Paces, J., Miller, Jr., J. 1993. Precise U-Pb Ages of Duluth Complex and Related Mafic

  Intrusions, Northeastern Minnesota: Geochronological Insights to Physical,

  Petrogenetic, Paleomagnetic, and Tectonometamorphic Process Associated with the

  1.1 Ga Midcontinent Rift System. Journal of Geophysical Research- Solid Earth. v.

  98. No. B8. p. 13997-14013. DOI: 10.1029/93JB01159.

Payne, J., McInerney, D., Barovich, K., Kirkland, C., Pearson, N., Hand, M. 2016. Strengths and Limitations of Zircon Lu-Hf and O Isotopes in Modelling Crustal Growth. Lithos. p. 175-192. DOI: 10.1016/j.lithos.2015.12.015.

Pearce, J., Harris, N., Tindle, A. 1984. Trace Element Discrimination Diagrams for the Tectonic Interpretation of Granitic Rocks. Journal of Petrology. v. 25. Part 4. p. 956-983.

Peck, W., Valley, J. 2000. Large Crustal Input to High δ^{18}O Anorthosite Massifs of the Southern Grenville Province: New Evidence from the Morin Complex, Quebec. Contributions to Mineralogy and Petrology. v. 139. p. 402-417.

Pepper, M., Gehrels, G., Pullen, A., Ibanez-Meija, M., Ward, K., Kapp, P. 2016. Magmatic History and Crustal Genesis of Western South America: Constraints from U-Pb Ages and Hf Isotopes of Detrital Zircons in Modern Rivers. Geosphere. v. 12. no. 5. p. 1532-1555. DOI: 10.1130/GES01315.1.

Peterssen, A., Schersten, A., Andersson, J., Whitehouse, M., Baranoski, M. 2015. Zircon U-Pb, Hf and O Isotope Constraints on Growth versus Reworking of Continental Crust in the Subsurface Grenville Orogen, Ohio, USA. Precambrian Research. v. 265. p. 313-327. DOI: 10.1016/j.precamres.2015.02.016.

Pullen, A., Ibanez-Mejia, M., Gehrels, G., Giesler, D., Pecha, M. 2018. Optimization of

   a Laser Ablation-Single Collector-Inductively Coupled Plasma-Mass Spectrometer

   (Thermo Element 2) for Accurate, Precise, and Efficient Zircon U-Th-Pb

   Geochronology. Geochemistry, Geophysics, Geosystems. v. 19. p. 1-17. DOI:

   10.1029/2018GC007889.

Ratcliffe, N., Aleinikoff, J., Burton, W., Karabinos, P. 1991. Trondhjemitic, 1.35-1.31 Ga

   Gneisses of the Mount Holly Complex of Vermont: Evidence for an Elzeverian Event

   in the Grenville Basement of the United States Appalachians. Canadian Journal of

   Earth Sciences. v. 28. p. 77-93.

Rivers, T. 1997. Lithotectonic Elements of the Grenville Province: Review and

   Tectonic Implications. Precambrian Research. v. 86. No. 3-4. p. 117-154. DOI:

   10.1016/S0301-9268(97)00038-7.

Rivers, T. 2008. Assembly and Preservation of Lower, Mid, and Upper Orogenic Crust

   in the Grenville Province- Implications for the Evolution of Large Hot Long-Duration

   Orogens. Precambrian Research. v. 167. p. 237-259. DOI:

   10.1016/j.precamres.2008.08.005.

Rivers, T. 2009. The Grenville Province as a Large Hot Long-Duration Collisional

    Orogeny- Insights from the Spatial and Thermal Evolution of its Orogenic Fronts. In

    Ancient Orogens and Modern Analogues. Murphy, J., Keppie, J., Hynes, A. (eds).

    Geological Society Special Publication 327. p. 405-444. DOI: 10.1144/SP327.17.

Rivers, T., Culshaw, N., Hynes, A., Indares, A., Jamieson, R., Martignole, J. 2012.

    Chapter 3- The Grenville Orogen- a Post LITHOPROBE Perspective. In Percival, J.,

    Cook, F., Clowes, R (eds) Tectonic Styles in Canada: The LITHOPROBE

    Perspective. Geological Association of Canada Special Paper 49. p. 97-236.

Rivers, T. 2015. Tectonic Setting and Evolution of the Grenville Orogen: An

    Assessment of Progress Over the Last 40 Years. Geoscience Canada Harold

    Williams Series. v. 42. p. 77-124. DOI: 10.12789/geocanj.2014.41.057.

Roback, R. 1996. Characterization and Tectonic Evolution of a Mesoproterozoic Island

    Arc in the Southern Grenville Orogen, Llano Uplift, Central Texas. Tectonophysics.

    v. 265. p. 29-52.

Robinson, G., Jr., Lesure, F., 2nd, Marlow, J., Foley, N., Clark, S. 1979. Bedrock

    Geology and Mineral Resources of the Knoxville 1° x 2° Quadrangle, Tennessee,

    North Carolina, and South Carolina. U.S. Geological Survey Bulletin 1979. 73 pp.

Rodríguez, G., Zapata, G., Velásquez, M. E., Cossio, U., & Londoño, A. C. 2003.
 Geología de las planchas 367 Gigante, 368 San Vicente del Caguán, 389 Timaná,
 390 Puerto Rico, 391 Lusitania (parte noroccidental) y 414 El
 Doncello. *INGEOMINAS, Mapa, escala*, *1*(100.000).

Samson, S., Moecher, D., Satkoski, A. 2018. Inherited, Enriched, Heated, or
 Recycled? Examining Potential Causes of Earth's Most Zircon Fertile Magmatic
 Episode. Lithos. v. 314-315. p. 350-359. DOI: 10.1016/j.lithos.2018.06.015.

Schiller, D., Finger, F. 2019. Application of Ti-in-zircon Thermometery to Granite
 Studies: Problems and Possible Solutions. Contributions to Mineralogy and
 Petrology. v. 174. no. 51. 16 pp. DOI: 10.1007/s00410-019-1585-3.

Schmitz, M., Bowring, S., Ireland, T. 2003. Evaluation of the Duluth Complex
 Anorthositic Series (AS3) Zircon as a U-Pb Geochronological Standard: New High-
 Precision Isotope Dilution Thermal Ionizing Mass Spectrometry Results. Geochimica
 et Cosmochimica Acta. v. 67. No. 19. p. 3665-3672. DOI: 10.1016/S0016-
 7037(03)00200-X.

Schulz, K., Cannon, W. 2007. The Penokean Orogeny in the Lake Superior Region.
 Precambrian Research. v. 157. p. 4-25. DOI: 10.1016/j.precamres.2007.02.022.

Sinha, A., Hogan, J., Parks, J. 1996. Lead Isotope Mapping of Crustal Reservoirs Within the Grenville Superterrane: 1. Central and Southern Appalachians. Earth Processes: Reading the Isotopic Code. Geophysical Monograph 95.

Sinha, A., McLelland, J. 1999. Lead Isotope Mapping of Crustal Reservoirs within the Grenville Superterrane: 2. Adirondack Massif, New York. Basement Tectonics. v. 13. p. 297-312.

Soderlund, U., Patchett, J., Vervoort, J., Isachsen, C. 2004. The ^{176}Lu Decay Constant Determined by Lu-Hf and U-Pb Isotope Systematics of Precambrian Mafic Intrusions. Earth and Planetary Science Letters. v. 219. p. 311-324. DOI: 10.1016/S0012-821X(04)00012-3.

Southworth, S., Aleinikoff, J., Tollo, R., Bailey, C., Burton, W., Hackley, P., Fanning, M. 2010. Mesoproterozoic Magmatism and Deformation in the Northern Blue Ridge, Virginia and Maryland: Application of SHRIMP U-Pb Geochronology and Integrated Field Studies in the Definition of Grenvillian Tectonic History. In Tollo, R., Bartholomew, M., Hibbard, J., Karabinos, P. (eds). From Rodinia to Pangea: The Lithotectonic Record of the Appalachian Regions. Geological Society of America Memoir. v. 206. p. 795-836. DOI: 10.1130/2010.1206(31).

Spencer, C., Kirkland, C., Roberts, N., Evans, N., Liebmann, J. 2019. Strategies

Towards Robust Interpretations of in situ Zircon Lu-Hf Isotope Analyses. Geoscience

Frontiers. v. 11. No. 3. p. 843-853. DOI: 10.1016/j.gsf.2019.09.004.

Streckeison, A., Le Maitre, R. 1979. A Chemical Approximation to the Modal QAPF

Classification of the Igneous Rocks. Neues Jahrbuch fur Mineralogie, Abhandlungen.

v. 136. p. 169-206.

Taylor, S., McLennon, S. 1985. The Continental Crust: Its Composition and Evolution,

An Examination of the Geochemical Record Preserved in Sedimentary Rocks.

Hallam, A., (ed). Geoscience Texts. Blackwell Scientific Publication. Oxford. 312

pp.

Teixeira, W., Geraldes, M., Ruiz, A., Saes, G., Vargas-Mattos, G. 2010. A Review of

the Tectonic Evolution of the Sunsás Belt, SW Amazonian Craton. Journal of South

American Earth Sciences. v. 29. p. 47-60. DOI: 10.1016/j.jsames.2009.09.007.

Thompson, R. 1982. Magmatism of the British Tertiary Volcanic Province. Scottish

Journal of Geology. v. 18. p. 49-107.

Tohver, E., Bettencourt, J., Tosdal, R., Mezger, K., Leite, W., Payolla, B. 2004. Terrane Transfer During the Grenville Orogeny: Tracing the Amazonian Ancestry of Southern Appalachian Basement Through Pb and Nd Isotopes. Earth and Planetary Science Letters. v. 228. p. 161-176. DOI: 10.1016/j.epsl.2004.09.029.

Tollo, R., Corriveau, L., McLelland, J., Bartholomew, M. 2004. Proterozoic Tectonic Evolution of the Grenville Orogen in North America: An Introduction. *In* Tollo, R.P., Corriveau, L., McLelland, J., and Bartholomew, M.J., eds., Proterozoic tectonic evolution of the Grenville orogeny in North America. Boulder, Colorado, Geological Society of America Memoir 197, p. 1-18.

Tollo, R.P., Aleinikoff, J.N., Borduas, E.A., Dickin, A.P., McNutt, R.H. 2006. Grenvillian Magmatism in the Northern Virginia Blue Ridge: Petrologic Implications of Episodic Granitic Magma Production and the Significance of Postorogenic A-type Charnockite. Precambrian Research. v. 151. p. 224-264.

Tollo, R., Aleinikoff, J., Wooden, J., Mazdab, F., Southworth, S., Fanning, M. 2010. Thermomagmatic Evolution of Mesoproterozoic Crust in the Blue Ridge of SW Virginia and NW North Carolina: Evidence from U-Pb Geochronology and Zircon Geothermometry. In Tollo, R., Bartholomew, M., Hibbard, J., Karabinos, P., (eds). From Rodinia to Pangea: The Lithotectonic Record of the Appalachian Region. Geological Society of America Memoir. v. 206. p. 859-896. DOI: 10.1130/2010.1206(33).

Tollo, R., Aleinikoff, J., Dickin, A., Radwany, M., Southworth, S., Fanning, M. 2017.
Petrology and Geochemistry of Mesoproterozoic Basement of the Mount Rogers
Area of Southwestern Virginia and Northwestern North Carolina: Implications for the
Precambrian Tectonic Evolution of the Southern Blue Ridge Province. American
Journal of Science. v. 317. p. 251-337. DOI: 10.2478/03.2017.01.

Tosdal, R. 1996. The Amazonian-Laurentian Connection as Viewed from the Middle
Proterozoic Rocks in the Central Andes, Western Bolivia and Northern Chile.
Tectonics. v. 15. no. 4. p. 827-842.

Trail, D., Mojzsis, S., Harrison, T., Schmitt, A., Watson E., Young, E. 2007. Constraints
on Hadean Zircon Protoliths from Oxygen Isotopes, Ti-Thermometry, and Rare Earth
Elements. Geochemistry Geophysics Geosystems. v. 8. p. Q06014.

Valley, J., Chiarenzelli, J., McLelland, J. 1994. Oxygen Isotope Geochemistry of
Zircon. Earth and Planetary Science Letters. v. 126. p. 187-206.

Valley, J., Chiarenzelli, J., McLelland, J. 1994. Oxygen Isotope Geochemistry of
Zircon. Earth and Planetary Science Letters. v. 126. p. 187-206.

Valley, J., Kinny, P., Schulze, D., Spicuzza, M. 1998. Zircon Megacrysts from

Kimberlite: Oxygen Isotope Heterogeneity Among Mantle Melts. Contributions to

Mineralogy and Petrology. v. 133. p. 1-11.

Valley, J. 2003. Oxygen Isotopes in Zircon. *In* Zircon, Hanchar, J., Hoskin, P. (eds).

Reviews in Mineralogy and Geochemistry. v. 53. p. 89-112. ISBN 0-93995060-X.

500 pp.

Valley, J., Lackey, J., Cavosie, A., Clechenko, C., Spicuzza, M., Basei, M., Bindeman,

I., Ferreira, V., Sial, A., King, E., Peck, W., Sinha, A., Wei, C. 2005. 4.4 Billion

Years of Crustal Maturation: Oxygen Isotope Ratios of Magmatic Zircon.

Contributions to Mineralogy and Petrology. v. 150. p. 561-580. DOI:

10.1007/s00410-005-0025-8.

Valley, J., Kita, N. 2009. Mineralogical Association of Canada Short Course. v. 41.

No. 9.

Valley, P., Fisher, C., Hanchar, J., Lam, R., Tubrett, M. 2010. Hafnium Isotopes in

Zircon: A Tracer of Fluid-Rock Interaction During Magnetite-Apatite ("Kiruna-Type")

Mineralizationa. Chemical Geology. v. 275. p. 208-220. DOI:

10.1016/j.chemgeo.2010.05.011.

Valley, P., Hanchar, J., Whitehouse, M. 2011. New Insights on the Evolution of the Lyon Mountain Granite and Associated Kiruna-Type Magnetite-Apatite Deposits, Adirondack Mountains, New York State. Geosphere. v. 7. No. 2. p. 357-389. DOI: 10.1130/GES00624.1.

Van Kranendonk, M., Kirkland, C.L. 2013. Orogenic Climax of Earth: The 1.2-1.1 Ga Grenvillian Superevent. Geology. v. 41. no. 7. p. 735-738. DOI: 10.1130/G34243.1.

Vermeesch, P. 2018. IsopotR: A Free and Open Toolbox for Geochronology. Geoscience Frontiers. v. 9. p. 1479-1493. DOI: 10.1016/j.gsf.2018.04.001.

Volkert, R., Aleinikoff, J., Fanning, C. 2010. Tectonic, Magmatic, and Metamorphic History of the New Jersey Highlands: New Insights from SHRIMP U-Pb Geochronology. *In* Tollo, R., Bartholomew, M., Hibbard, J., Karabinos, P., eds. From Rodinia to Pangea: The Lithotectonic Record of the Appalachian Region. Geological Society of America Memoir 206. p. 307-346. DOI: 10.1130/2010.1206(14).

Walsh, G., Aleinikoff, J., Fanning, C. 2004. U-Pb Geochronology and Evolution of

Mesoproterozoic Basement Rocks, Western Connecticut. *In* Tollo, R.P., Corriveau,

L., McLelland, J., and Bartholomew, M.J., eds., Proterozoic tectonic evolution of the

Grenville orogeny in North America. Boulder, Colorado, Geological Society of

America Memoir 197, p. 729-753.

Watson, B. 1980. Some Experimentally Determined Zircon/Liquid Partition Coefficients

for the Rare Earth Elements. Geochimica et Cosmochimica Acta. v. 44. p. 895-897.

Watson, B., Harrison, T.M. 1983. Zircon Saturation Revisited: Temperature and

Composition Effects in a Variety of Crustal Magma Types. Earth and Planetary

Science Letters. v. 64. p. 295-304.

Watson, E.B., Harrison, T.M. 2005. Zircon Thermometer Reveals Minimum Melting

Conditions on Earliest Earth. Science. v. 308. p. 841-844.

Watson, E.B., Wark, D.A., Thomas, J.B. 2006. Crystallization Thermometers for Zircon

and Rutile. Earth and Planetary Science Letters. v. 151. p. 413-433.

Whalen, J., Currie, K., Chappell, B. 1987. A-Type Granites: Geochemical

Characteristics, Discrimination and Petrogenesis. Contributions to Mineralogy and

Petrology. v. 95. p. 407-419.

Whitmeyer, S., Karlstrom, K. 2007. Tectonic Model for the Proterozoic Growth of North

America. Geosphere. v. 3. no. 4. p. 220-259. DOI: 10.1130/GES00055.1.

Biographical Data

Name of Author: Kyle Aaron Makovsky

Place of Birth: Windom, Minnesota

Date of Birth: March 23, 1987

Graduate and Undergraduate Schools Attended:

Minnesota State University, Mankato, Mankato, MN

Boise State University, Boise, ID

Degrees Awarded:

Master of Science, 2013, Boise State University

Bachelor of Science, 2010, Minnesota State University, Mankato

Awards and Honors:

Syracuse University Research Excellence Doctoral Fellowship

Syracuse University Department of Earth Science Chair's Award

Geological Society of America Graduate Student Research Award

John Prucha Award

Nelson Field Award

Mineralogy, Geochemistry, Petrology, and Volcanology Award

Best Student Poster Award, Institute on Lake Superior Geology

Professional Experience:

Teaching Assistant. Department of Earth Sciences, Syracuse University, Syracuse, NY.

    2016-2017; 2018-2019; Fall 2021

Research Assistant. Department of Earth Sciences, Syracuse University, Syracuse, NY.

    2017-2018

Research Fellow. Department of Earth Sciences, Syracuse University, Syracuse, NY.

    2019-2020

Geology Consultant. Self-Employed.

    2013-2016

Teaching Assistant. Department of Geosciences, Boise State University, Boise, ID.

    2010-2013